# Dominant Slip Systems of Naturally Deformed Quartz under the Mid-Crustal Conditions: Implications for Rheology of the Continental Crust

**Wang Qi**

September, 2024

Department of Biology and Geosciences, Graduate School of Science

Osaka City University

## Acknowledgements

Completing this doctoral thesis has been a long and challenging journey, one that would not have been possible without the support and encouragement of many individuals and institutions. I am deeply grateful to all those who have contributed to my academic and personal growth during this time.

First and foremost, I would like to express my deepest gratitude to my academic supervisor, Professor Takamoto Okudaira. His meticulous guidance and unwavering support both academically and personally have been fundamental to my growth as a researcher. His expertise, patience, and encouragement have not only shaped the course of my research but also profoundly impacted my personal development. I am deeply grateful for his insightful feedback, constructive criticism, and the countless hours he dedicated to mentoring me.

I would also like to extend my heartfelt thanks to Dr. Norio Shigematsu from AIST. His support and assistance in my research experiments and the writing of this thesis have been invaluable, particularly with EBSD operation and analysis. Dr. Shigematsu's willingness to share his knowledge and his guidance during critical moments of my research have significantly contributed to the successful completion of this work.

I would also like to express my deep appreciation to the professors who have supported and guided me throughout my doctoral studies. Their expertise, advice, and encouragement have been invaluable in shaping my academic journey. I am especially thankful for the insightful lectures, constructive feedback, and the opportunities they provided for intellectual growth. Their support and concern have greatly enriched my

research experience and academic development.

I am deeply indebted to fellow students in the Okudaira Lab. Their unwavering support, encouragement, and understanding have made my doctoral journey enriching and rewarding. The collaborative environment and the friendships I have formed here have been a source of motivation and inspiration. I am particularly thankful for the stimulating discussions, the collaborative efforts in our research projects, and the camaraderie that has made my time in the lab enjoyable and productive.

My sincere appreciation goes to Osaka City University for providing an excellent research environment and the necessary resources that were essential to my work. The facilities and academic resources available at the university have been instrumental in advancing my research. Additionally, I am grateful to the SPRING program for their generous financial support, and to the Nishimura Scholarship Foundation. The funding and scholarships I received allowed me to focus entirely on my research and writing without financial concerns, ultimately enabling the successful completion of this dissertation.

Furthermore, I would like to express my heartfelt gratitude to my friends in Japan. Your steadfast support and encouragement have been a pillar of strength during my stay here. The mental challenges posed by the three-year COVID-19 pandemic were alleviated by your constant companionship and support. I am truly fortunate to have you by my side during these challenging times.

Lastly, I extend my deepest thanks to my family and my wife. Despite the physical distance and the inability to meet during the three-year COVID-19 pandemic, your unconditional support and love have been my greatest source of strength. Your unwavering belief in me and your constant encouragement have given me the courage to persevere through the toughest times. Your support made it easier to face challenges, and your love has made my accomplishments all the more meaningful and joyous. I am profoundly grateful for your sacrifices and for being my anchor throughout this endeavor.

## Abstract

Quartz is the most dominant constitutive mineral in the continental crust, and thus, the deformation mechanism of quartz is essential for understanding the continental crust rheology. Under the mid-crustal conditions, dislocation creep of quartz is the dominant deformation mechanism. Based on the previously proposed flow laws, the flow strength of quartz aggregates with a dominant basal <*a*> slip system differs from that with a dominant prism <*a*> slip system by tens of megapascals under mid-crustal conditions, where crustal strength is at its maximum. Thus, identifying the dominant slip systems in naturally deformed quartz is crucial for understanding the continental crust rheology. Although the basal <*a*> slip system is considered dominant in quartz under mid-crustal conditions, its activity is controversial because some microstructural observations support an oriented nucleation growth model for *c*-axis distribution near the minimum strain axis. This study examined the crystallographic orientation and shape of quartz phenocrysts in a deformed granitic porphyry in the Ryoke belt, SW Japan, to clarify the dominant slip systems in the naturally deformed quartz at temperature conditions of ~400–500 °C utilizing optical and electron backscatter diffraction (EBSD) observations. Identified active slip systems include prism <*a*>, basal <*a*>, prism [*c*], and rhomb <*a*> through misorientation analyses via EBSD data. The aspect ratios of phenocrysts with dominant prism <*a*> and basal <*a*> slip systems are higher than prism [*c*] and rhomb <*a*> slip systems, indicating similar strengths between prism <*a*> and basal <*a*> slip systems, which are weaker than prism [*c*] and rhomb <*a*> slip systems under the mid-crustal conditions. Misorientation analysis showed *c*-axis orientations of basal <*a*> phenocrysts distributed at pole figures peripheries, indicating basal <*a*> activation over the proposed oriented nucleation and growth model. Consequently, this study provided robust evidence for the basal <*a*> and prism <*a*> slip systems as the dominant slip systems in the middle crustal conditions. We proposed a proportional model of the combination of basal <*a*> and prism <*a*> slip systems, suggesting that crustal strength would be controlled by the increasing ratio from prism <*a*> to basal <*a*> with decreasing depth in the continental middle crust.

## Contents

# 1. Introduction

## *1.1. Quartz as an important mineral in the crustal rheology*

Quartz is a dominant mineral in the continental upper to middle crust, and thus the rheological properties of quartz are important in the deformation of the continental crust (e.g., Kohlstedt et al., 1995; Scholz, 1998; Tokle et al., 2019; Tokle and Hirth, 2021). The inference of deformation processes, conditions, and rheology at depth in active tectonic settings is of fundamental importance to a quantitative geodynamic understanding of deformation in the Earth (Prior et al., 2011). Several researchers estimated the upper limit for the strength of the lithosphere as a function of depth based on the results of laboratory measurements on the mechanical properties of rocks, noting that the strength of Earth cannot be greater than the strength of the rocks of which it is composed (Kohlstedt et al., 1995 and references therein). Quartz, feldspar, and olivine are particularly common minerals in the lithosphere, and their rheological properties play a significant role to the continental crust rheology. **Figure 1.1** shows that the lithosphere is divided into three layers, each with strength controlled by different dominant minerals. A simple strength profile model for continental lithosphere is composed of a strength profile predicted by a constitutive equation for rock strength determined through experiments (**Fig. 1.1**). This model subdivides the lithosphere into three layers where brittle deformation mechanisms in an upper part and a lower part where plastic flow dominates, referred to as rheological stratification. The notably abundant minerals quartz and feldspar dominate the rheological properties of the crust, while olivine controls the rheological characteristics of the upper mantle. Although the crust is not monomineralic, it is generally assumed that there is enough quartz in the continental crust to control its rheology. This means that even if feldspar is still brittle at 15–20 km, quartz is sufficiently represented and distributed that the crust is predominantly deforming plastically even at 10–12 km. Therefore, several experimental studies focused on establishing plastic flow laws of quartz (Ashby, 1972; Kohlstedt et al., 1995; Stipp and Tullis, 2003; Evans, 2005).

The paramount influence of quartz on the mechanical properties of the middle crust underscores the importance of a detailed understanding and development of its deformation flow laws. Various independent deformation mechanisms, such as dislocation creep, diffusion creep, and defect-free flow, each characterized by distinct constitutive equations, contribute to the plastic deformation of rocks (Ashby, 1972). Microstructures observed in many deformed quartzites indicate that dislocation creep is a prevalent deformation mechanism under upper to middle crustal conditions, providing robust constraints on rheological behavior (Hirth and Tullis, 1992). **Figure 1.2** shows the changes in quartz CPO along depth and stress, as well as the extrapolated strength profile based on the quartz dislocation creep flow laws with different quartz CPOs. Based on the flow laws proposed in a recent study by Tokle et al. (2019), the flow strength of quartz aggregates with a dominant basal <*a*> slip system is higher than that with a dominant prism <*a*> slip system by tens of megapascals under mid-crustal conditions, where crustal strength is at its maximum (**Fig. 1.2**). This suggests that the transition in flow laws results from a simultaneous shift in the dominant slip system or the slip system that rate-limits deformation. Therefore, clarifying the dominant slip system under mid-crustal conditions is crucial for assessing the strength of the Earth crust.

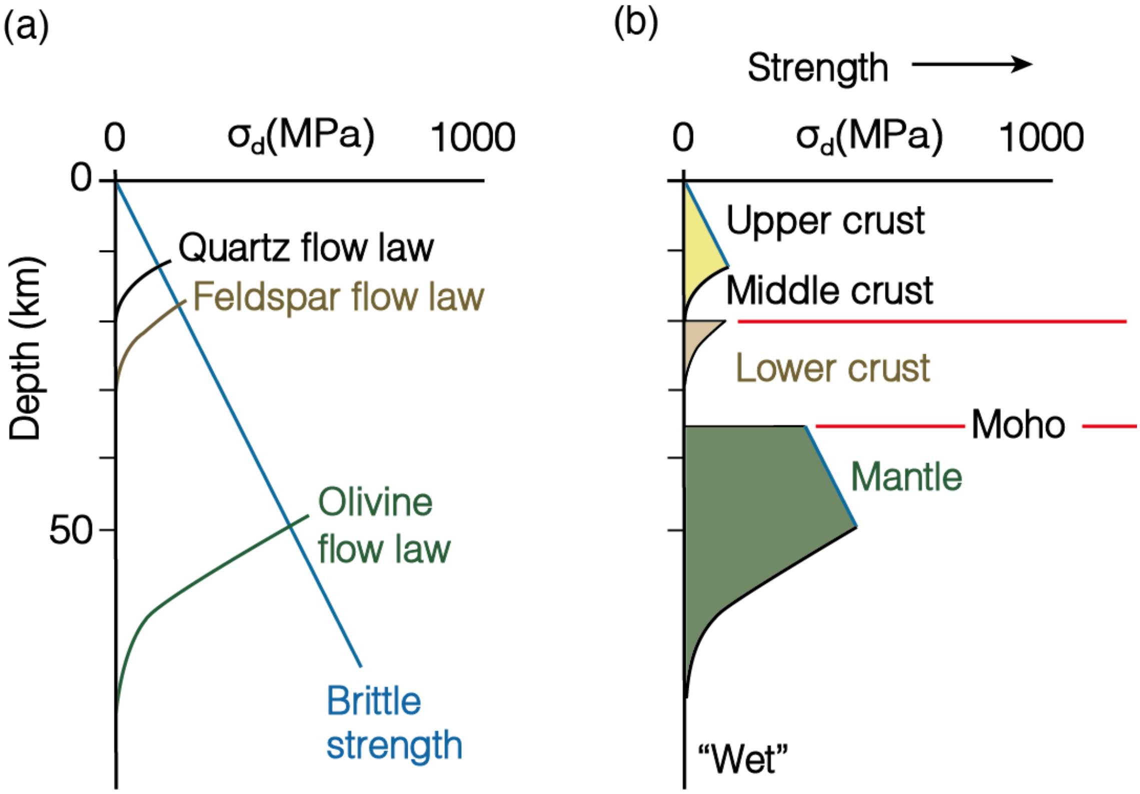

**Fig. 1.1.** Rheological stratification of continental lithosphere based on a combination of the brittle friction law and the plastic flow law derived experimentally for quartz, feldspar and olivine (modified from Fossen, 2010). **(a)** Brittle–plastic transitions occur where the brittle (frictional) and plastic flow laws intersect. **(b)** The strength profile depends on mineralogy and lithologic stratification.

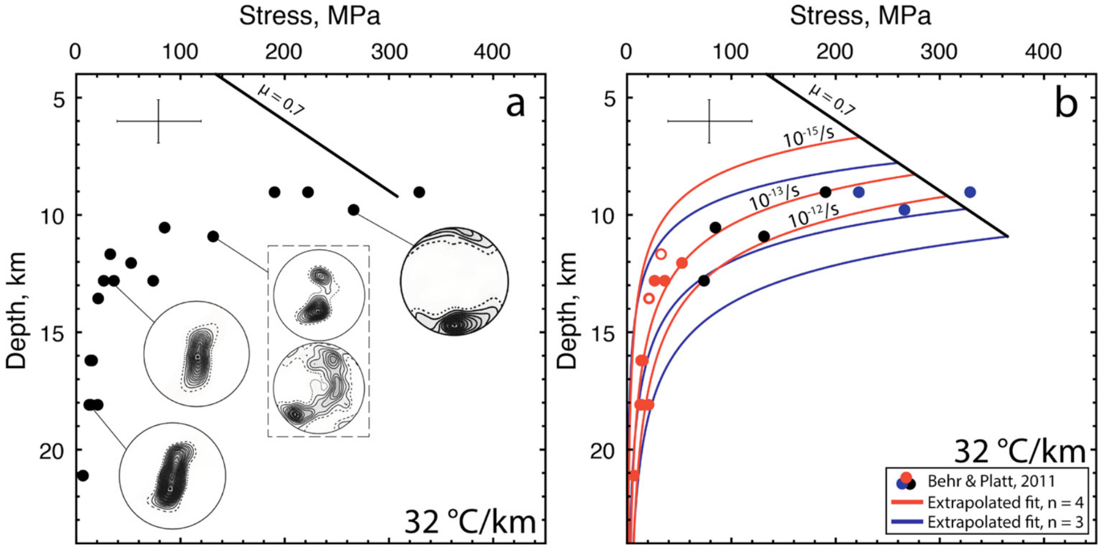

**Fig. 1.2.** Plots of stress versus depth with the constrained natural and experimental data (Tokle et al., 2019). (**a**) Plot of stress versus depth with the constrained Whipple Mountains core complex (WMCC) samples from Behr and Platt (2011). Representative error bars for the WMCC data are shown by the black bars. The shear plane for the *c*-axis pole figures is horizontal with a dextral sense of shear. The black line is the frictional stress for a strike-slip boundary assuming the effective normal stress equals the lithostatic normal stress (i.e., $\alpha = 0$) and $\mu = 0.7$. (**b**) Plot of stress versus depth with the extrapolated fit end-member flow laws for strain rates of $10^{-12}$, $10^{-13}$, and $10^{-15}$ $s^{-1}$ plotted against the constrained WMCC samples from Behr and Platt (2011). The WMCC samples are color-coded to illustrate what flow law represents the sample based on the *c*-axis fabric. Black points represent samples with transitional *c*-axis fabrics. There is no fabric data for the points labeled with a white dot and therefore we infer the color coding.

### *1.2. Quartz slip system*

There are three equivalent crystallographic axes, referred to as the *a*-axes in quartz. Three *a*-axes lie in the basal plane and intersect at 120º angles with each other. The *c*-axis, serving as the principal axis, is perpendicular to the basal plane. **Figure 1.3** shows the Schematic figure of a quartz crystal and the main crystallographic axes and crystallographic planes. Additionally, the main crystallographic planes of quartz include the basal plane, denoted as (0001) and abbreviated as (*c*); the prismatic plane, denoted as $\{10\bar{1}0\}$ and abbreviated as {*m*}; the positive rhombohedral plane, denoted as $\{0\bar{1}11\}$ and abbreviated as {*r*}; and the negative rhombohedral plane, denoted as $\{01\bar{1}1\}$ and abbreviated as {*z*}(**Fig. 1.3**). Quartz slip systems are defined by the main slip crystallographic planes *c* (0001), *m* $\{10\bar{1}0\}$, *r* $\{0\bar{1}11\}$, *z* $\{01\bar{1}1\}$, *π* $\{0\bar{1}12\}$, and *π*' $\{01\bar{1}2\}$ and the main crystallographic directions *c* [0001] and *a* $<2\bar{1}\bar{1}0>$ of slip within the plane (e.g., Baëta and Ashbee, 1969). Single crystals of synthetic quartz deformed experiment and transmission electron microscopy (TEM) analyses were carried out to confirm (*c*)<*a*> (= basal <*a*>), {*m*}<*a*> (= prism <*a*>), {*m*}[*c*] (= prism [*c*]), {*r*}<*a*> (= positive rhomb <*a*>), and {*z*}<*a*> (= negative rhomb <*a*>) as the common slip systems in nature (e.g., Baëta and Ashbee, 1969; Neumann, 2000; Morales et al., 2011).

The activation of different slip systems within a crystal depends on both the orientation and intensity of the stress field present within the grain, in addition to the critical resolved shear stress (CRSS), denoted as $\tau_c$, associated with slip system. Dislocation movement is initiated only when the shear stress component acting in the direction of slip exceeds the CRSS of the slip system. The value of CRSS is predominantly influenced by temperature and, to a lesser extent, by other factors such as strain rate, differential stress, and the chemical activity of certain components, like water, which may alter the strength of particular bonds within the crystal structure (Passchier and Trouw, 2005). Therefore, the activity of the different slip systems in quartz mainly depends on temperature, where different slip system becomes dominant under different temperature conditions (e.g., Hobbs, 1985; Mainprice and Nicolas, 1989). **Figure 1.4** illustrates the relationship between different dominant slip systems and the temperature range in natural samples. Basal <*a*> and rhomb <*a*>, prism <*a*>, and prism [*c*] are dominant at low (~300–450 °C), medium (450–600 °C), and high (≥600 °C) temperatures, respectively (**Fig. 1.4**; e.g., Lister and Dornsiepen, 1982; Mainprice and Nicolas, 1989; Takeshita, 1996; Toy et al., 2008; Law, 2014; Wallis et al., 2019). Separately, the use of the opening angle of quartz crystallographic preferred orientation (CPO) as a deformation thermometer is increasingly validated (e.g., Kruhl, 1998; Law, 2014; Faleiros et al., 2016). However, the activity of slip systems at different temperatures could be influenced by other factors, e.g., strain, strain rate, water content, and stress (e.g., Muto et al., 2011; Law, 2014).

**Figure 1.5** shows the pole figure of *c*-axis projections in different domains, corresponding to the activation of different slip systems. In pole figures with the *X*-, *Y*- and *Z*-axes representing the maximum, intermediate and minimum strain axes, respectively, basal <*a*> and prism <*a*> slips may have a strong cluster of *c*-axes in the periphery near the *Z*-axis and the *Y*-axis of the pole figures, respectively (**Fig. 1.5**; e.g., Lister et al., 1978; Schmid and Casey, 1986; Takeshita and Wenk, 1988). Nevertheless, controversy surrounds the peripheral *c*-axis distribution near the *Z* axis in pole figures. The traditional view, based on numerical simulation studies, proposed that the peripheral *c*-axis fabrics result from the activity of the basal <*a*> slip system, with some rhomb slip systems, in low-temperature conditions (e.g., Hobbs, 1985; Lister et al., 1978; Morales et al., 2011, 2014). Recently, Kilian and Heilbronner (2017) have suggested that the textures with peripheral *c*-axis at high angles to shear plane in pole figures cannot be attributed to the activity of the basal <*a*> slip system, based on the microstructural analyses of experimentally sheared natural quartzite (**Fig. 1.6**; Heilbronner and Tullis, 2002, 2006). Instead, they proposed the model of initial oriented nucleation and growth of quartz. **Figure 1.6** shows the conceptual model of quartz CPO development through newly grown grains and dislocation glide involving multiple slip systems.

**Fig. 1.3.** Schematic figure of crystallographic axes and planes of quartz.

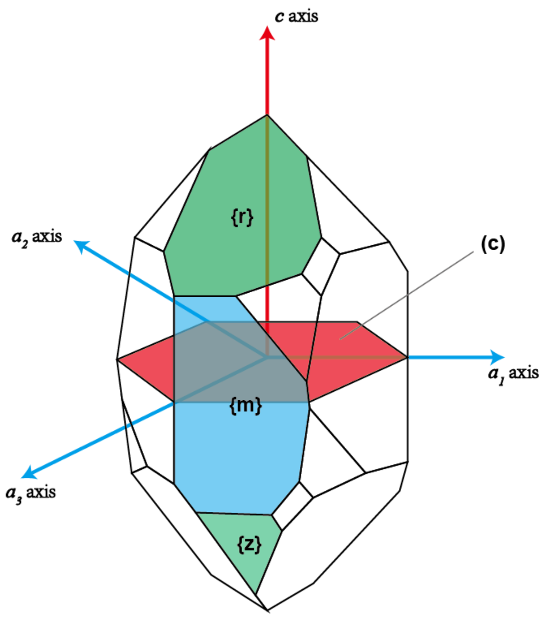

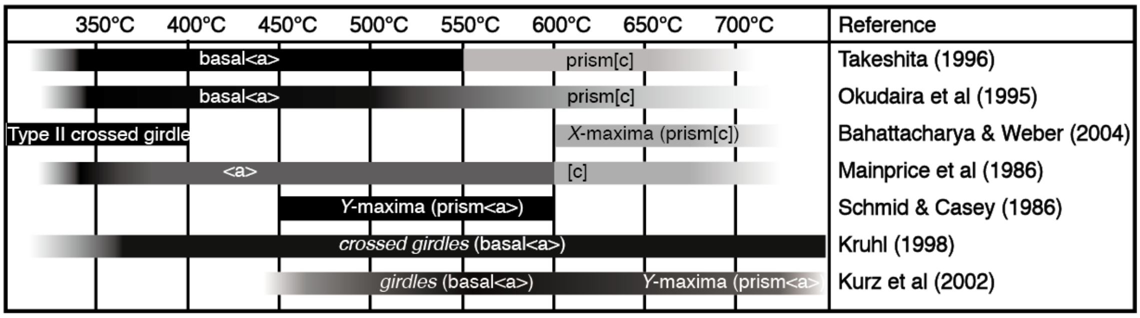

**Fig. 1.4.** Summary of the temperature ranges in which certain quartz slip systems have been found to operate or where CPO patterns characteristic of operation of certain slip systems have been measured (modified form Toy et al., 2008 and references therein).

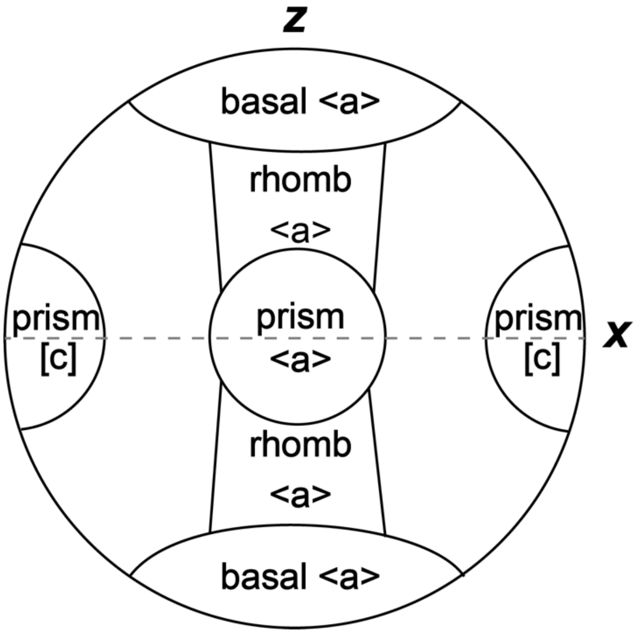

**Fig. 1.5.** Pole figure of *c*-axis distribution showing correlation between locations of *c*-axis peaks on CPO figures and the active slip systems in quartz (Toy et al., 2008). *X* is the lineation direction, *Z* the pole to foliation.

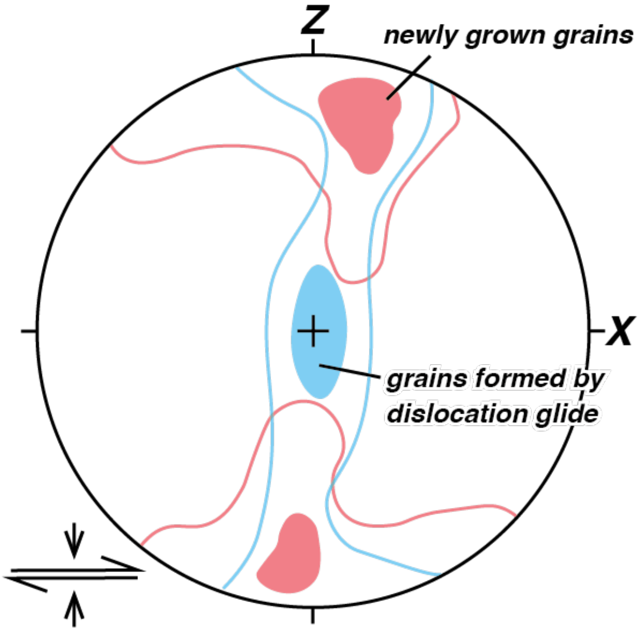

**Fig. 1.6.** Pole figure of *c*-axis orientation showing conceptual model of quartz CPO development (modified from Kilian and Heilbronner, 2017). The areas colored in red and blue represent *c*-axis positions of newly grown grains and *c*-axis positions formed during dislocation glide along multiple <*a*> slip systems, respectively. A combination of the two areas could form quartz CPO. Large contributions of dislocation glide lead to a high density of *c*-axes in the center of the pole figure, and only few newly grown grains from the periphery contribute to the peripheral part of the girdle.

### *1.3. The advantage and objective of the study*

The advantage of this study is the selection of granite porphyry sample instead of quartz aggregate. The evaluation of the dominant slip systems in equigranular monophase or polyphase aggregates, e.g., quartzite or granitoids, is usually difficult due to the von Mises criterion, which necessitates the activity of five independent slip systems to deform a crystal into any arbitrary shape. In the cases of equigranular aggregates, a grain can deform if its easy slip planes are favorably oriented and if the surrounding grains can also deform to the same degree; the orientation and presence of the surrounding other phases can affect quartz *c*-axis textures (e.g., Kilian et al., 2011). In contrast, relatively large particles (e.g., phenocrysts in porphyries) in fine-grained matrix can be deformed by a slip on easy-slip plane(s) accommodated by the flow of the matrix around the phenocryst. Since the fine-grained polyphase matrix would be weaker than the quartz phenocrysts (e.g., Bouchez and Duval, 1982; Ishii and Sawaguchi, 2002; Kilian et al., 2011; Ceccato et al., 2018), leading to the phenocrysts deformed by a slip on easy-slip plane. Thus, the active slip systems could be easily identified by the crystallographic orientations of deformed phenocrysts and through misorientation analysis. **Figure 1.7** shows the model of grains deformed and rotate with different glide plane in the matrix deforming by simple shear. **Figure 1.8** the grain with a glide plane at 90° in a matrix deformed by progressive deformation. The aspect ratio could also be controlled by the phenocryst's initial crystallographic orientation (**Figs. 1.7** and **1.8**; Etchecopar, 1977; Bouchez and Duval, 1982; Ishii and Sawaguchi, 2002), as shear deformation progresses, the aspect ratio of phenocrysts increases with easy slip planes parallel to the shear zone boundary (i.e., shear plane).

Ishii and Sawaguchi (2002) illustrate the deformation behavior of grains with different initial orientations of the glide plane in a simple shearing matrix. Grains with slip plane at different initial angles to the shear plane ($\theta_0$) deform differently under simple shear (**Fig. 1.7**). The grain with $\theta_0 = 0^\circ$ deformed only by simple shear without any rotation of glide plane; the grain with $\theta_0 = 90^\circ$ deformed with a shear sense opposite to matrix deformation with a clockwise rotation of glide plane; the grain with $\theta_0 = 50^\circ$ rotates clockwise with little deformation. **Fig. 1.8** details the progressive deformation of a grain with an initial glide plane orientation of $\theta_0 = 90^\circ$ under simple shear. Initially, the grain deforms with a shear sense opposite to the matrix deformation, gradually elongating. As the deformation continues, the grain transfers to deforming with the same shear sense as the matrix, with a concurrent clockwise rotation of the glide plane, causing the aspect ratio of the grain to decrease. As deformation progresses further, the aspect ratio of the grain increases again as the glide plane rotates to become parallel to the shear plane. This figure demonstrates that the aspect ratio ($R$) and the long-axis orientation ($\varphi$) of the grain change significantly with progressive shear deformation, where the aspect ratio of the grain increases as the glide plane gradually aligns parallel to the shear zone boundary (i.e., the shear plane) during progressive deformation. Therefore, we choose quartz phenocrysts in granitic porphyry to evaluate the dominant slip system of quartz (**Fig. 1.8**).

The objective of this study is to evaluate the relative activity of different slip systems under the lower amphibolite-facies conditions (i.e., ~400–500 °C) in the upper to middle crust through the analysis of the crystallographic orientation and shape of deformed quartz phenocrysts in the sheared granitic porphyry that occur in the Cretaceous Ryoke belt, Awaji Island, SW Japan (Kano and Takagi, 2013). Furthermore, this study also aims to find evidence for forming the peripheral *c*-axis in the pole figures, to evaluate the most plausible hypothesis for the formation of peripheral *c*-axes in the pole figures.

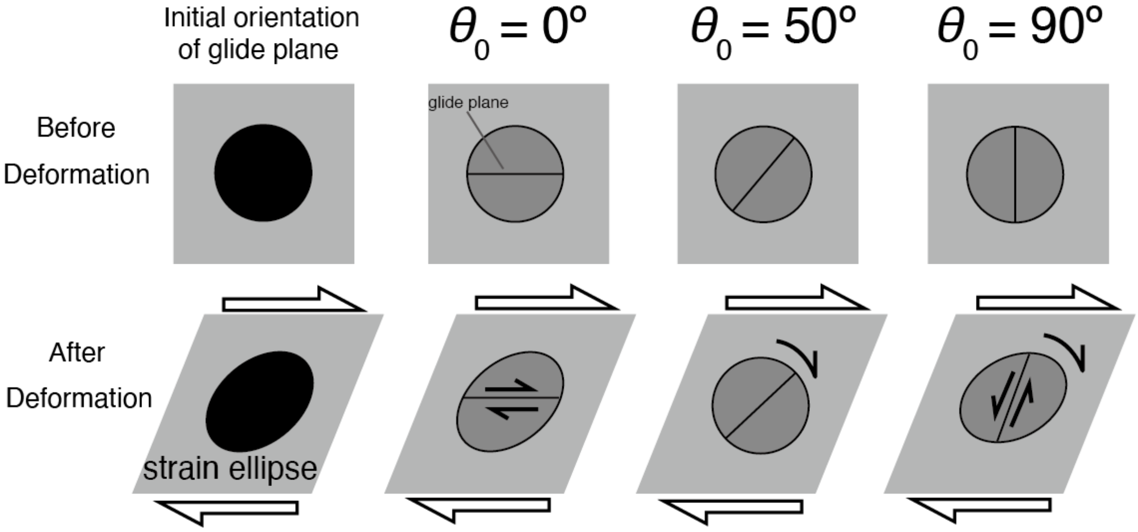

**Fig. 1.7.** Deformations and rotations of model circular grains with different glide-plane orientations $\theta_0$) in a matrix deforming by simple shear (modified from Ishii and Sawaguchi, 2002).

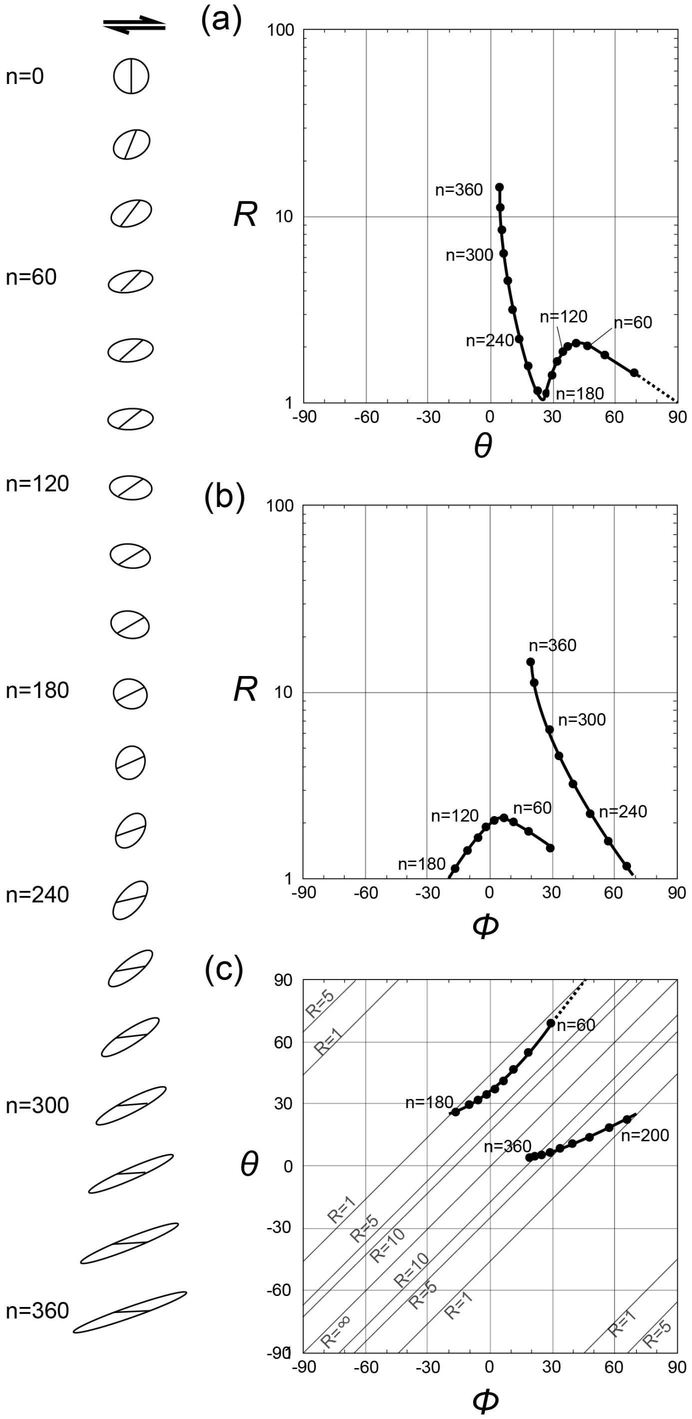

**Fig. 1.8.** A progressive deformation of a grain with $\theta_0 = 90°$ in a matrix deforming by progressive simple shear. *n* is the number of deformation increments. The deformation path of this grain is shown in *R*–*θ* (**a**), *R*–*φ* (**b**) and *θ*–*φ* (**c**) graphs (Ishii and Sawaguchi, 2002).

# 2. Samples

## *2.1. Geological background*

Awaji Island is located in the southern part of the Ryoke Belt, with the Median Tectonic Line (MTL) transecting its southern part (**Fig. 2.1**). **Figure 2.1** shows the geological map with the distribution of the locality of studied sample. Older Ryoke Granite with developed foliated structures are present on Awaji Island, but their distribution does not along the MTL. Massive granites, known as Younger Ryoke Granite, are interspersed within the acidic volcanic rocks of the Izumi Group located to the north of the MTL (Takahashi and Hattori, 1992). Kano and Takagi (2013) investigated of the granites on Awaji Island and performed a detailed study of the Older Ryoke Granite dikes.

In the Ryoke Belt of Awaji Island, Cretaceous Older and Younger Ryoke Granites are extensively distributed from the central to the northern parts of the island (**Fig. 2.1**). The granites of Awaji Island are classified into 11 different bodies based on lithology and their intrusive relationships. According to the sequence of formation, these granites can generally be divided into three main groups: Granite Types I, II, and III (Takahashi and Hattori, 1992). Granite type I is characterized by plastically deformed rocks that foliated structures, though with varying deformation degrees, and are equivalent to the Older Ryoke Granites. Granite type II is found to the north and south of Granite type I. It comprises blocky granodiorites that intrude into Granite type I, causing contact metamorphism in some areas, and is equivalent to the Younger Ryoke Granites. Granite type III, which intrudes into both Granite types I and II, consists of massive granites but does not cause contact metamorphism in Granite type II. In contrast to the granodiorites of Granite type II, Granite type III is primarily composed of granite.

Dikes that intrude into the granites are also classified into older and younger dike types (Takahashi and Hattori, 1992). The older dikes are composed of granitic porphyry and dioritic porphyry, which intrude into Granite type I, and foliated structures can be observed in the older dikes. The orientation of these dikes predominantly follows the NNW–WNW direction. The younger dikes, consisting of blocky and undeformed granitic porphyry and dioritic porphyry, intrudes into Granite types I, II, and III. Their intrusion orientation is predominantly in the NNW–NNE direction, intersecting obliquely with the direction of the older dikes.

Kano and Takagi (2013) identified 26 older dikes in the Shio region and across the central to the west coast of Awaji Island. The widths of the dikes vary from several tens of centimeters to several tens of meters. The dikes primarily consist of medium to coarse-grained quartz diorite-porphyry and granite-porphyry, though in some areas, fine-grained felsic porphyry is also present. The grain size of the matrix varies as well. Many of these dikes have been affected by mylonitization, developing foliated and linear structures. Evidence that the mylonite's protolith is granite-porphyry, rather than older granite, is the presence of quartz phenocrysts, with some showing signs of alteration. Plagioclase phenocrysts exhibit well-defined idiomorphic characteristics and develop zonal structures. During mylonitization, quartz phenocrysts can deform to varying degrees, forming polycrystalline aggregate phenocrysts, but in cases of intense mylonitization, these aggregates also assume a lenticular shape, allowing for their distinction from mylonitized of granite. However, if the protolith is fine-grained and strongly deformed, the quartz phenocrysts might also appear banded, thereby making it challenging to differentiate from mylonite derived from granite.

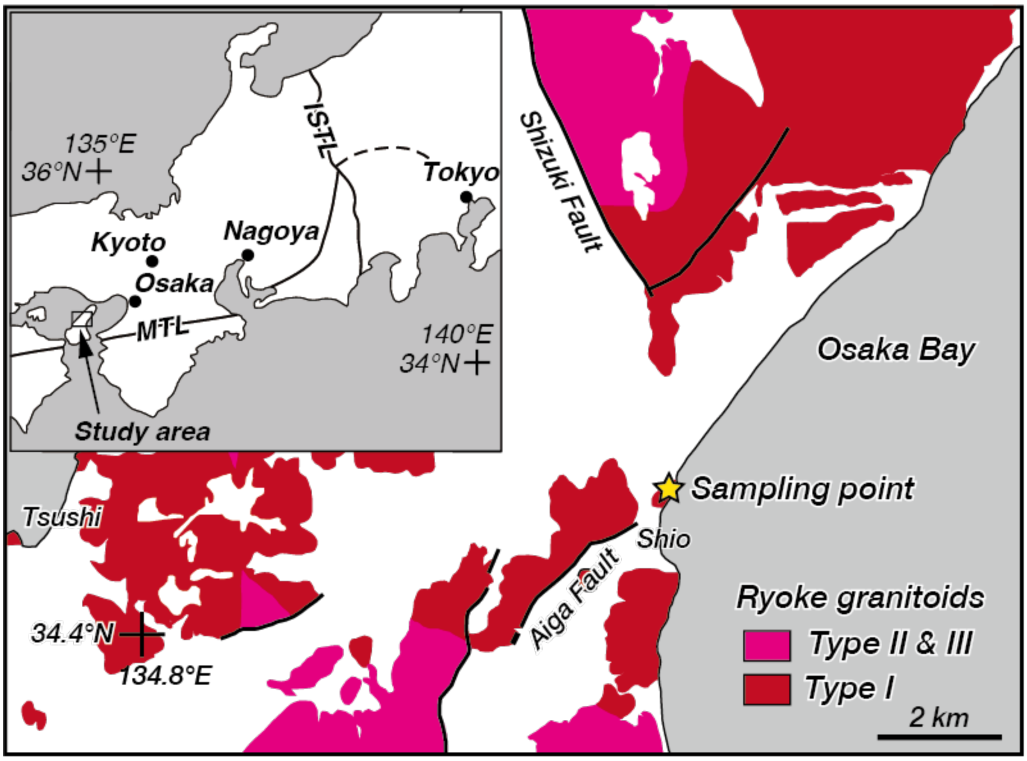

**Fig. 2.1.** Geological map showing the distribution of the Ryoke granitoids in the Awaji Island, SW Japan (modified from Kano and Takagi, 2013) and the locality of the studied sample. Inset: Location of the mapped area. MTL: Median Tectonic Line. ISTL: Itoigawa–Shizuoka Tectonic Line.

### *2.2. Sample descriptions*

The granitic porphyry samples used in this study were collected in the sheared granitic dike (dike 6 of Kano and Takagi, 2013) from northern Shio in Awaji Island (**Fig. 2.1**). In the samples, most quartz phenocrysts exhibit varying degrees of elongation (**Fig. 2.2**). The size of the quartz phenocrysts ranges from ~0.5 mm to ~3 mm. *C*- and *C′*-type shear bands (e.g., Passchier and Trouw, 2005) can be seen on the polished slab of hand specimen (**Fig. 2.2a**). Displacement along the *C′*-type shear bands indicates a top to the SW sense of shear (sense of shear referred to as dextral hereafter). An oblique foliation (i.e., *S*-plane) defined by the shape-preferred orientation of ellipsoidal quartz and mica (**Fig. 2.2b, c, f**) is transected by indistinct *C*-planes which are parallel to the bulk shear plane (*XY* plane of a finite strain ellipsoid). Under optical microscope, the elongated lenticular quartz phenocrysts exhibit undulose extinction, and recrystallized quartz grains are observed only distributed at the margins of some phenocrysts (**Fig. 2.2d, e**). Feldspars phenocrysts generally preserve their original euhedral shapes. Some biotite phenocrysts appear as mica fish (**Fig. 2.2f**). The asymmetric shapes of quartz (**Fig. 2.2c, e**) and mica fishes (**Fig. 2.2f**) also indicate a dextral sense of shear. The matrix mainly comprises fine-grained (up to ~50 μm) quartz, plagioclase, K-feldspar, and biotite. There is no chlorite in the sample, indicating that mylonitic deformation occurred under the temperature condition higher than the chlorite stability field (i.e., >~400–450 °C; Spear, 1993; Simpson et al., 2000). $TiO_2$ contents in the quartz phenocrysts are generally less than 0.008 wt.% (unpublished data of Liu Chenghan), suggesting that the deformation temperature at 300 MPa may be lower than

~530 °C, based on the TitaniQ thermometry of Thomas et al. (2010). The water content of the deformed quartz is ~100–300 wt. ppm (unpublished data of Junichi Fukuda).

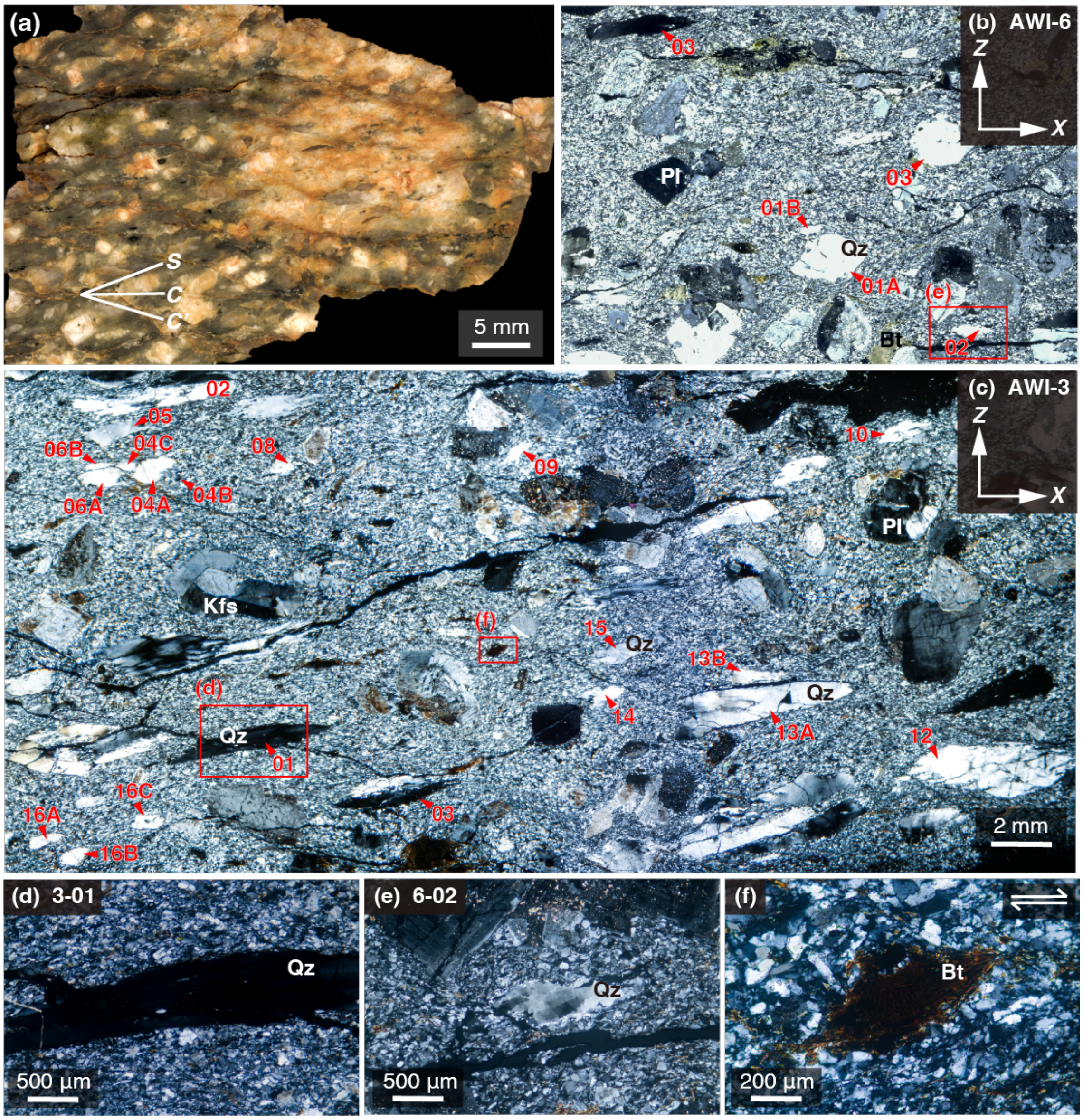

**Fig. 2.2.** Photographs of the deformed granite porphyry sample. (**a**) Photograph of the polished slabs of hand specimen. View from the northwest of the sample surface cut parallel to the lineation and normal to the foliation. (**b, c**) Photomicrographs of the thin section AWI-6 and AWI-3 under crossed-polarized light. (**d, e**) Photomicrographs of quartz phenocrysts 3-01 and 6-02. (**f**) Microstructure of mica fish. Qz: Quartz; Pl: Plagioclase; Kfs: K-feldspar; Bt: Biotite.

# 3. Methods

## *3.1. Shape preferred orientation*

To clarify the relationship between the strain magnitude and the dominant slip systems for each quartz phenocryst, the shape- and crystallographic orientation of quartz phenocrysts were measured for thin sections cut parallel to the lineation and normal to the foliation (referred to as *XZ* plane hereafter). Twenty-five quartz phenocrysts selected from two thin sections were analyzed in this study. The length of the long (*a*) and short (*b*) axis of the quartz phenocrysts and the angle ($\varphi$, anticlockwise positive) between the long axis and mylonitic lineation were analyzed by ImageJ software (Schneider et al., 2012). **Fig. 3.1** shows the method of measurement of the aspect ratio and $\varphi$ to the best-fit ellipse auto analyzed by ImageJ software. Here, the long (*a*) and short (*b*) axes of the phenocrysts are those of the fitted ellipse to the phenocryst by ImageJ. The aspect ratio (*R*) was obtained by *a*/*b* (**Fig. 3.1**).

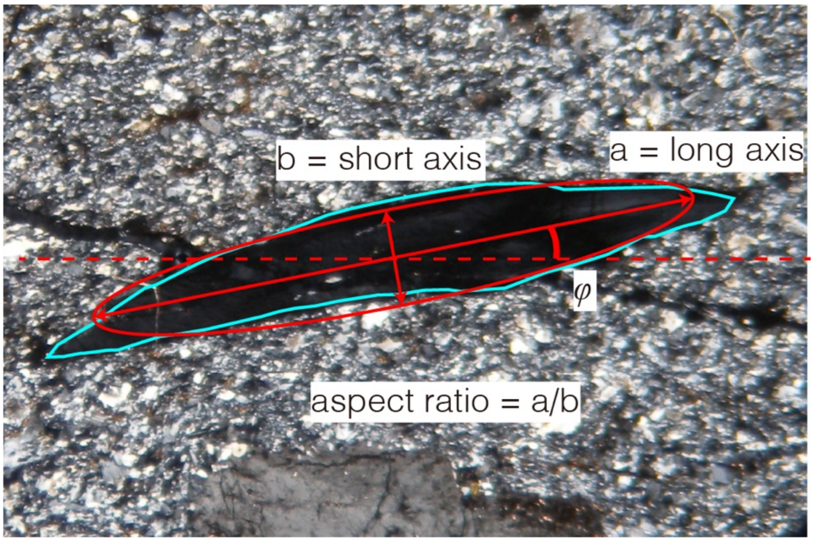

**Fig. 3.1.** Photomicrograph of the method of measurement of the aspect ratio and $\varphi$ of a deformed quartz phenocryst. The blue outline represents the phenocryst's outline boundary, while the red ellipse indicates the best-fit ellipse calculated using ImageJ software.

### *3.2. Electron Backscatter Diffraction (EBSD): Principles and measurement methods*

EBSD in recent years has become well-established to analyze rock microstructure (e.g., Prior et al., 1999). EBSD is a powerful microstructural characterization technique extensively used in materials science and geology. It provides valuable information about crystallographic orientations and the distribution of different mineral phases. EBSD is typically a detector attached to a Scanning Electron Microscope (SEM) that analyzes diffraction patterns from the sample surface to obtain crystallographic information.

The EBSD is the interaction between a focused high-energy electron beam and a tilted crystalline sample surface. Some of these incident electrons are backscattered and form a diffraction pattern (Kikuchi pattern) that contains crystallographic information about the sample. By capturing and analyzing the diffraction patterns, the crystallographic orientation and other related information of the sample can be determined (Schwartz et al., 2009). High-energy incident electrons interact with the sample surface, causing atomic scattering and producing backscattered electrons. These backscattered electrons diffracted by the crystal planes of the sample, forming distinct Kikuchi patterns. Kikuchi patterns are captured using a phosphor screen or other detectors installed in the SEM. Specialized software then analyzes these patterns to decode the crystallographic orientation information of the sample.

**Figure 3.2** is a schematic diagram showing the main components of an EBSD system. An EBSD system typically comprises a SEM, which provides the high-energy electron beam and allows the sample to be tilted at a specific angle (70°) to optimize the backscattered signal (Wilkinson et al., 2006). The detector, commonly a phosphor screen coupled with a CCD camera, captures the Kikuchi patterns. Proper sample preparation, including mechanical polishing and electro-polishing, is crucial to ensure a flat and clean sample surface for clear EBSD patterns (Humphreys, 2001). The analysis software decodes the Kikuchi patterns to generate crystallographic information.

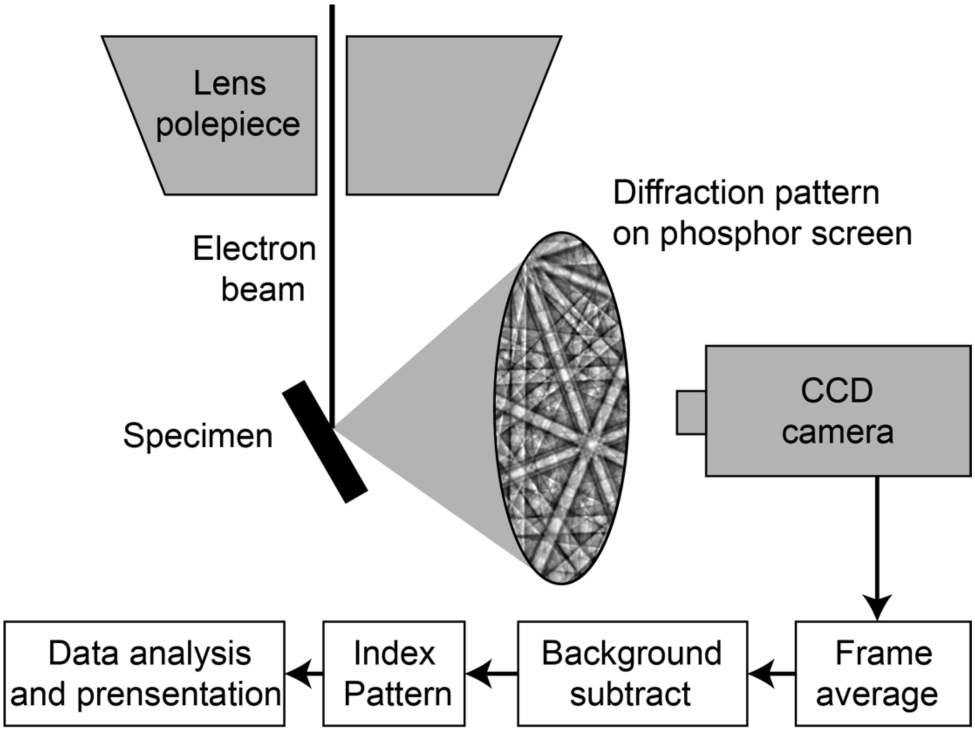

**Fig. 3.2.** Schematic diagram of the main components of an EBSD system (modified from Humphreys, 2001).

The measurement process begins with meticulous sample preparation to ensure the surface is free from scratches, contaminants, and oxidation layers, which are essential for obtaining high-quality EBSD patterns. In the SEM, parameters such as electron beam energy, beam current, and sample tilt angle (typically 70°) are optimized to enhance the backscattered signal. The sample is then placed in the SEM, and Kikuchi patterns are captured using the detector. These patterns are analyzed using specialized software to decode the crystallographic orientation, grain boundaries, and phase distribution information (Adams et al., 1993). The results are visualized as orientation maps, phase maps, and grain morphology maps, providing detailed insights into the sample's microstructure (Prior et al., 1999).

We analyzed the crystallographic orientations of quartz phenocrysts and matrix quartz grains using a Hitachi SU3500 scanning electron microscope (SEM) equipped with an electron backscatter diffraction (EBSD) system (HKL NordlysNano, Oxford Instruments) and AZtec Software at the GSJ Lab of the Geological Survey of Japan, AIST. Any surface damage was removed from the thin sections through treatment with a vibratory polisher (VibroMet2, Buehler) for 2 hours using colloidal silica before SEM analysis. EBSD measurements were conducted under an accelerating voltage of 15 kV, a working distance of 18 mm, and specimen tilting to 70° and under the low-vacuum mode. EBSD data were obtained using an automatic indexing system with a step size of 2–3 μm. For the acquisition of EBSD data, we used Oxford Instruments AZtec software. We used the MATLAB toolbox MTEX version 5.8 (Hielscher and Schaeben, 2008; Mainprice et al., 2014) to analyze the EBSD data (**Appendix**). All index data in this study represent points with a mean angular deviation (MAD) of <1°. In this study, grain boundaries are defined by a critical misorientation angle >10° because the transition from low to high angle boundaries has been suggested to occur in the range of 9°–14° (Shigematsu et al., 2006).

### *3.3. Geometrically necessary dislocation density analysis*

The portion of the dislocation density that contributes to lattice curvature at the scale of observation is classified as the geometrically necessary dislocation (GND) density. A Burgers circuit construction around an arbitrary group of dislocations reveals that only a fraction of them contribute to the net Burgers vector and thus correspond to the GND density. Dislocations are characterized by two types: edge dislocations and screw dislocations. For edge dislocation, the Burgers vector is normal to the dislocation line, while for screw dislocation, the Burgers vector is parallel the dislocation line. Geometrically necessary dislocations represent an extra storage of dislocations required to accommodate the lattice curvature (Gao and Huang, 2003) that arises whenever there is a non-uniform plastic deformation (**Fig. 3.3**). **Figure 3.3** shows the schematic view of geometrically necessary dislocations in a plastically bent lattice.

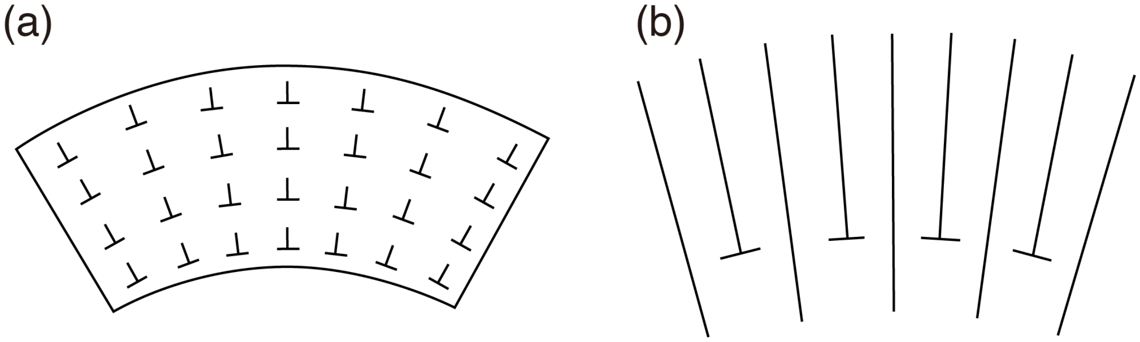

**Fig. 3.3.** Geometrically necessary dislocations in a plastically bent lattice. (**a**) A periodic array of dislocations with Burgers vector and spacing will generate a lattice curvature. (**b**) A schematic view of geometrically necessary dislocations in a plastically bent lattice (Gao and Huang, 2003).

We use conventional (Hough-transform based) EBSD to investigate geometrically necessary dislocation densities and various dislocation types. The approach primarily follows a novel method proposed by Wallis et al. (2019). This method uses high-angular resolution EBSD analysis for quantitatively characterize quartz subgrain structures through the estimation of types and densities of geometrically necessary dislocations. The method begins with an analysis of lattice curvature to derive a dislocation tensor $\alpha$, which is then utilized to compute the density of geometrically necessary dislocations using the Nye-Kröner method. The presence of dislocations introduces spatial gradients of lattice orientation (measured as rotations) and elastic strain, which contribute to the components $\alpha_{ij}$ of $\alpha$ by

$$\alpha_{ij} = \sum_{s=1}^{Smax} \rho^s b_i^s l_j^s \tag{3.1}$$

The components of $\alpha_{ij}$ relate to the densities, $\rho^s$, of $s_{\max}$ different types of dislocation, with Burgers vectors $b^s$ and line directions $l^s$.

In this study, the dislocation tensor $\alpha$ can be directly obtained from the EBSD data. When the number of dislocation types (S*max*) are fewer than 6, the GND density can be calculate directly using equation (3.1), .However, when the dislocation types exceed six, as in the case with quartz where we consider 19 types of dislocation types grouped into six families (i.e. (*c*) <*a*> edge; {*r/z*} <*a*> edge; {*m*} <*a*> edge; {*m*} [*c*] edge; <*a*> screw; and [*c*] screw), the system becomes under-constrained, and no unique solution exists the equation (3.1). An optimization scheme is employed as a solution to further minimize the total dislocation line energy (Wilkinson and Randman, 2010), which helps in determining the most suitable combination of dislocation types and densities. Notably, all dislocation types with <*a*> Burgers vectors contribute non-uniquely to specific components of the dislocation tensor. This implies that multiple dislocation types could potentially generate a specific component of lattice curvature. The frequent occurrence of the <*a*> screw type in the GND analysis can be attributed to the solution which aims to minimize the total dislocation line energy, defined as:

$$\frac{\mathrm{e}_{\mathrm{edge}}}{e_{screw}} = \frac{1}{1-\nu} \tag{3.2}$$

, where *v* is the Poisson's ratio. This could potentially explain the higher observed densities of <*a*> screw dislocations, as the method inherently favors configurations with lower total energy.

### *3.4. Misorientation axis and inferred slip system*

Misorientation is the difference in crystallographic orientation between two crystallites. For any two quartz lattices, there is a unique rotation axis and rotation angle that matches one lattice to the other (**Fig. 3.4**) and refer to these as the misorientation axis and the misorientation angle (Wheeler et al., 2001). The misorientation axis is a vector but it does not possess defined directional positive or negative ends. This characteristic stems from the equivalence of the rotational matching between adjacent grains: the rotation matching grain B to grain A is the inverse of that matching grain A to grain B. Consequently, the selection of the initial grain in the calculation bears no geometric significance, as the misorientation axis remains the same irrespective of the order in which the grains are considered.

In this study, we employ Electron Backscatter Diffraction (EBSD) to characterize the crystal orientations and misorientations between adjacent grains. We utilize the MTEX software to process the EBSD data, enabling the statistical analysis of the orientation of misorientation axes orientations and the misorientation angles. Based on the specific misorientation analysis, we identified the slip systems (**Fig. 3.4** and **3.5**). **Figure 3.4** shows the relationship between the misorientation axis, subgrain boundary and slip plane for tilt and twist boundaries. **Figure 3.5** shows the method of inferring slip systems from the relationship between misorientation axis and slip plane for tilt boundaries.

There are two distinct types of subgrain boundaries: tilt boundaries and twist boundaries. Tilt boundaries are formed by edge dislocations, whereas twist boundaries are formed by screw dislocations. During crystal deformation, different types of subgrain boundaries are formed, and their geometric relationships among the subgrain boundary, slip plane normal, and misorientation axis are different. **Figure 3.4** illustrates the different relationships between the subgrain boundary, slip plane, and misorientation axis. For tilt boundaries, the subgrain boundary is perpendicular to the slip plane, and the misorientation axis is parallel to both the subgrain boundary and the slip plane. Additionally, the misorientation axis is perpendicular to both the slip plane normal and the slip direction. For twist boundaries, the subgrain boundary is parallel to the slip plane, and the misorientation axis is perpendicular to both the subgrain boundary and the slip plane (Lloyd, 2004).

The concept of interpreting slip systems from misorientation axes at subgrain boundaries relates to the concepts of Lloyd and Freeman (1994), Lloyd et al. (1997) and Neumann (2000). It applies to slip due to edge dislocations resulting in a polygonized subgrain microstructure which dominantly consists of tilt boundaries. The activation of slip systems leads to the rotation of crystal orientations around the rotation axis defined by the slip system. For subgrain boundaries with tilt boundary characteristics, the misorientation axis is perpendicular to both the slip plane normal and the slip direction (e.g., Lloyd, 2004). Based on these concepts, the direction of the misorientation axis across subgrain boundaries formed by the activation of different slip systems varies within quartz crystals (**Fig. 3.5a**). By projecting these misorientation axes formed by different slip system activities into the quartz crystal coordinate, an inverse pole figure of the misorientation axes of tilt boundaries can be plotted (**Fig. 3.5b**; Neumann, 2000; Kilian and Heilbronner, 2017). We can reveal the dominant slip systems in quartz by comparing the misorientation axes of quartz phenocrysts across subgrain boundaries calculated from EBSD data with **Fig. 3.5b**.

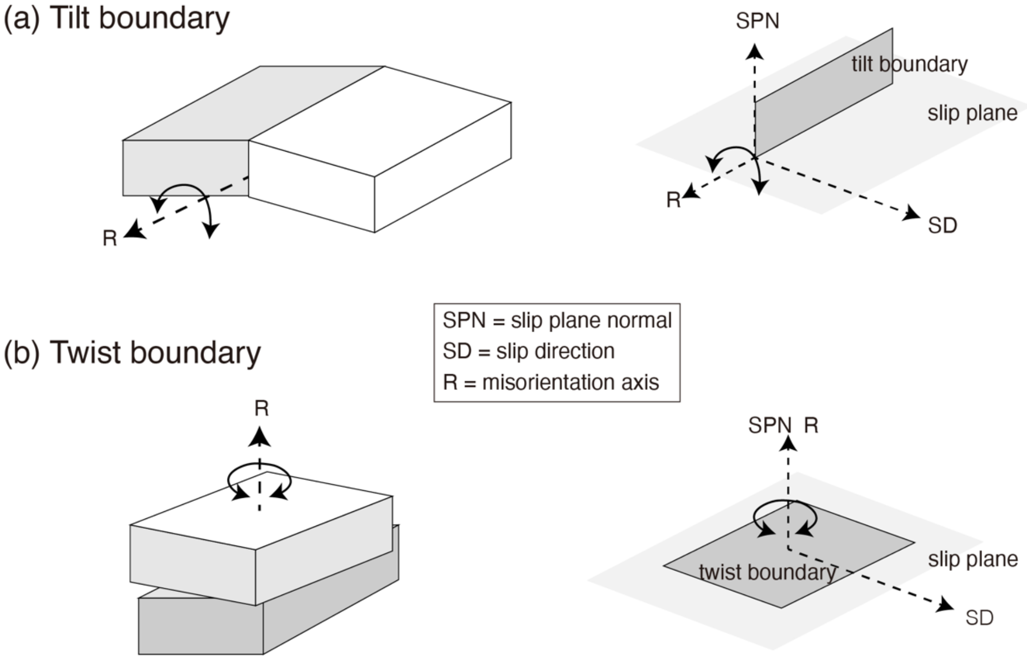

**Fig 3.4.** Relationship between the subgrain boundary, slip plane and misorientation axis. (**a**) General relationship of tilt boundary. (**b**) General relationship of twist boundary (modified from Lloyd, 2004).

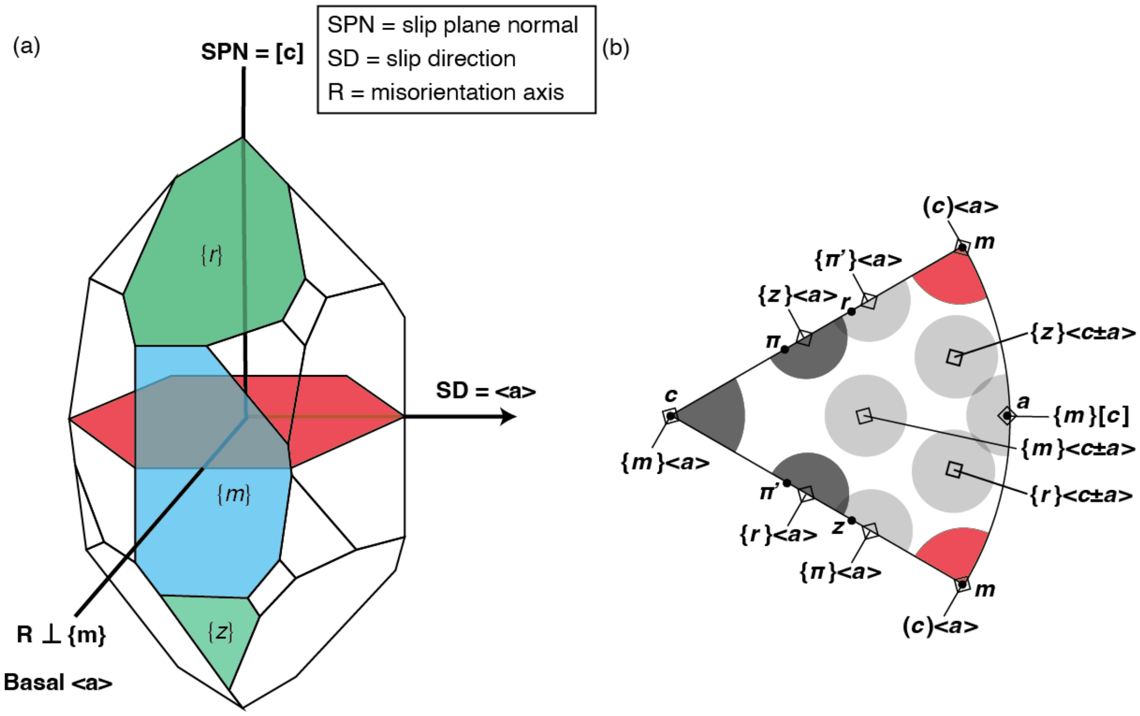

**Fig 3.5.** Concept of interpreting slip systems from misorientation axes at subgrain boundaries generated by simple slip (valid for tilt boundaries): (**a**) orientation of rotation axis of the basal <*a*> slip system of a quartz single crystal; (**b**) inverse pole figure with the rotation axes for common crystal slip systems in quartz, red area represents the rotation axis of basal <*a*> slip system (modified from Neumann, 2000 and Kilian and Heilbronner, 2017).

# 4. Results

## *4.1. Shape of phenocrysts*

The results of aspect ratio (*R*) and long-axis orientation $\varphi$ are listed in **Table 4.1**. The aspect ratios range between 1.5 and 6.3, whereas the $\varphi$ values range between –7° and 35° (**Fig. 4.1**). Almost all phenocrysts with aspect ratios above 2 are preferentially aligned and concentrated to $\varphi$ of 0° to 20°. The harmonic mean of the aspect ratios of the deformed phenocrysts for the *XZ* plane is 2.7. We also measured the aspect ratios for the *YZ* plane and found the harmonic mean to be 1.9, so Flinn (1962)'s *k* value, defined as $k = (R_{XY}–1)/(R_{YZ}–1)$, for the phenocrysts is estimated to be 0.4, indicating a general flattening.

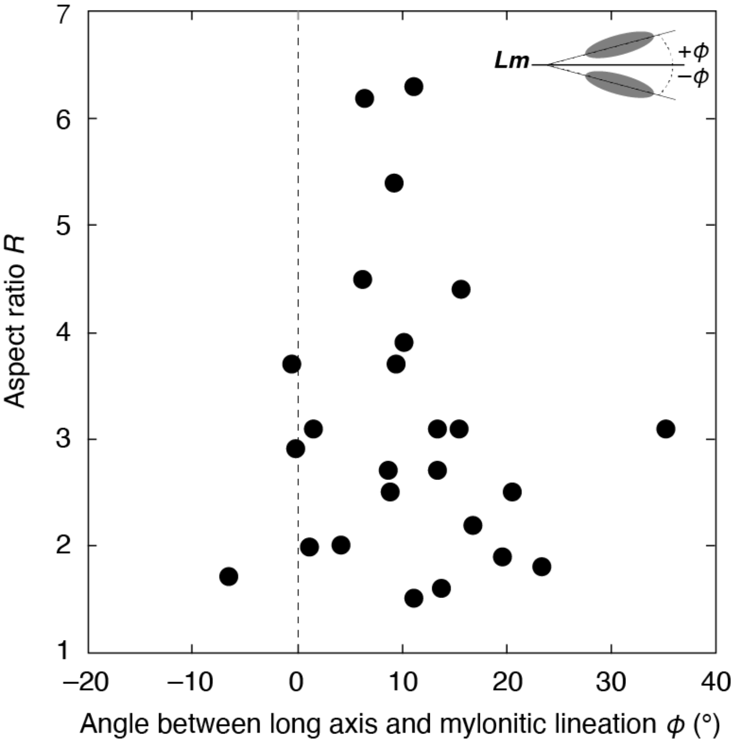

**Fig. 4.1.** Aspect ratios (*R*) versus long-axis orientations ($\varphi$) in the *XZ* section (Wang et al., 2024).

**Table 4.1.** Summary of the microstructural characteristics of quartz phenocrysts (Wang et al., 2024)

| Grain | Aspect ratio (*R*)[1] | $\varphi$[2] | *C*-axis orientation | Misorientation axis[3] | Dominant slip system | Group[4] |
|---|---|---|---|---|---|---|
| 3-01 | 6.3 | 11.2° | near *Y*-axis | parallel to [*c*] | prism <*a*> | A |
| 3-02 | 5.4 | 9.1° | in between *X*- and *Z*-axes | normal to {*m*} | basal <*a*> | B |
| 3-03 | 3.7 | 9.4° | in between *Y*- and *Z*-axes | parallel to [*c*] | prism <*a*> | A |
| 3-04A | 1.8 | 23.4° | in between *X*- and *Z*-axes | parallel to [*c*] | prism <*a*> | D |
| 3-04B | 2.0 | 1.1° | near *X*-axis | normal to {*z*} | rhomb <*a*> | C |
| 3-04C | 1.9 | 19.6° | in between *X*- and *Z*-axes | normal to {*z*} | rhomb <*a*> | C |
| 3-05 | 3.1 | 15.4° | in between *Y*- and *Z*-axes | parallel to [*c*] | prism <*a*> | A |
| 3-06A | 2.5 | 8.9° | in between *X*- and *Z*-axes | parallel to <*a*> + normal to {*m*} | prism [*c*] + basal <*a*> | B |
| 3-06B | 4.5 | 6.3° | near *Z*-axis | parallel to [*c*] ± parallel to <*a*+*c*> | prism <*a*> ± rhomb <*a*+*c*> | A |
| 3-08 | 1.7 | –6.5° | near *X*-axis | parallel to <*a*> | prism [*c*] | B |
| 3-09 | 3.1 | 35.1° | at equal angle to the three axes | parallel to [*c*] | prism <*a*> | A |
| 3-10 | 2.7 | 13.4° | in between *X*- and *Z*-axes | parallel to <*a*> | prism [*c*] | B |
| 3-12 | 2.9 | –0.1° | in between *X*- and *Z*-axes | parallel to <*a*> + normal to {*m*} | prism [*c*] + basal <*a*> | B |
| 3-13A | 3.9 | 10.2° | near *Z*-axis | parallel to [*c*] | prism <*a*> | A |
| 3-13B | 3.7 | –0.6 | near *Z*-axis | parallel to [*c*] | prism <*a*> | D |
| 3-14 | 4.4 | 15.6° | near *Z*-axis | parallel to [*c*] | prism <*a*> | A |
| 3-15 | 2.7 | 8.7° | in between *X*- and *Z*-axes | normal to {*m*} | basal <*a*> | B |
| 3-16A | 2.5 | 20.4° | near *Z*-axis | parallel to [*c*] | prism <*a*> | A |

| | | | | | | |
|---|---|---|---|---|---|---|
| 3-16B | 2.2 | 16.8° | in between *X*- and *Z*-axes | normal to {*m*} + parallel to <*a*> | basal <*a*> + prism [*c*] | B |
| 3-16C | 2.0 | 4.2° | in between *X*- and *Z*-axes | parallel to <*a*> + normal to {*m*} | prism [*c*] + basal <*a*> | B |
| 6-01A | 1.6 | 13.8° | near *Z*-axis | parallel to <*a*> + parallel to [*c*] | prism [*c*] + prism <*a*> | B |
| 6-01B | 3.1 | 13.3° | at equal angle to the three axes | parallel to [*c*] | prism <*a*> | A |
| 6-02 | 3.1 | 1.6° | near *Z*-axis | normal to {*m*} + parallel to <*a*> | basal <*a*> + prism [*c*] | B |
| 6-03 | 6.2 | 6.4° | near *Y*-axis | parallel to [*c*] | prism <*a*> | A |
| 6-04 | 1.5 | 11.2° | near *Z*-axis | parallel to [*c*] | prism <*a*> | A |

---

[1] The aspect ratio is the ratio of the length of the long axis to that of the short axis of the ellipse fitted to the quartz phenocryst.

[2] The angle between the orientation of the long axis of the ellipse fitted to the quartz phenocryst and the orientation of the stretching lineation (= bulk shear direction) on the *XZ*-sections (anticlockwise positive, see also **Fig. 4.1**).

[3] The distribution of the misorientation rotation axis is for misorientation angles with ≤4°.

[4] Groups A, B, and C are characterized by the distribution of the misorientation axis parallel to the *Y*-axis in the specimen coordinate, whereas Group D is characterized by the distribution of the misorientation axis near the *Z*-axis in the specimen coordinate. Furthermore, in the crystal coordinate, Groups A, B, and C are characterized by the maximum distribution of misorientation axis parallel to [*c*], parallel to <*a*> and/or normal to {*m*}, and normal to rhombohedral planes, respectively.

### *4.2. C-axes orientation of quartz phenocrysts and matrix grains*

The *c*-axis orientations of the 25 quartz phenocrysts and the matrix grains (945 grains) are plotted in the pole figures (**Fig. 4.2**). The *c*-axes distribution in the matrix is represented by a small-circle girdle with a large opening angle in the range of 70°–78°, which correspond to deformation temperatures of ~500–600 °C based on the quartz *c*-axis fabric opening-angle deformation thermometer of Faleiros et al. (2016). However, the matrix consists of multiple mineral phases, thus may not accurately reflects the deformation temperatures. For the phenocryst, some have *c*-axes scattered at the intermediate distances between the periphery of the pole figure and the *Y*-axis, while those scattered around the *Z*-axis distribute in the range with opening angles of ~60°–80°. Only one phenocryst (3-04C) has its *c*-axis plotted near the *X*-axis. Two phenocrysts (phenocrysts 3-01 and 6-03) with their *c*-axes aligned nearly parallel to *Y*-axis exhibit the highest aspect ratios (*R* = ~6, **Table 4.1**). The phenocrysts whose *c*-axes are located on the peripheral of the pole figure exhibit the lowest aspect ratios (*R* = ~1.5). The *R* values are moderate for the phenocrysts whose *c*-axes are located between the *Y*-axis and the peripheral. For the matrix quartz grains, the overall concentration (highest MUD) is weak, with maxima appearing mainly at the intermediate distances between the periphery of the pole figure and the *Y*-axis (**Fig. 4.2b**), which is similar to the *c*-axes distributions of the phenocrysts (**Fig. 4.2a**).

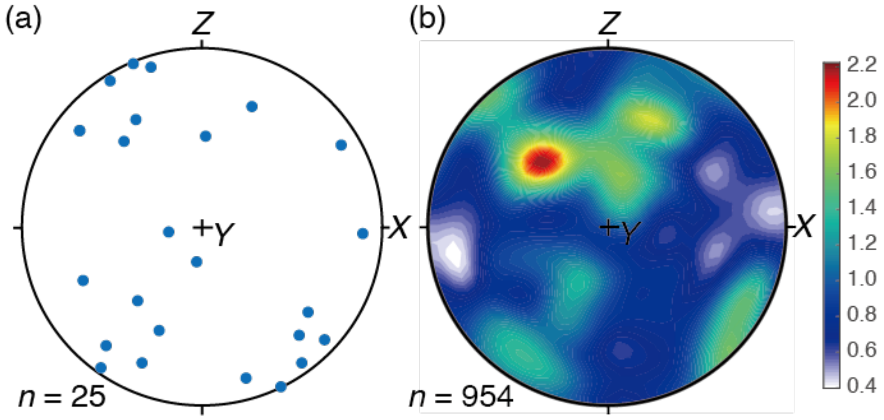

**Fig. 4.2.** *C*-axis crystallographic orientation of the quartz (Wang et al., 2024): (**a**) Phenocrysts (**b**) Matrix grains. The density of the distribution is shown by multiples of uniform distribution (MUD). Upper-hemisphere equal-area projection.

### *4.3. Misorientation analysis of subgrain boundary*

In almost all quartz phenocrysts, subgrain boundaries have developed in approximately two directions with different misorientation angles: one parallel to the long axis and the other parallel to the short axis of phenocrysts (**Figs. 2.2**, **4.3**, and **4.4**). **Figures 4.3** and **4.4** show intracrystalline deformation features related to the misorientation changes of the subgrain boundaries parallel to the long and short axes for phenocrysts 3-01 and 6-02; The red lines in the **Figs. 4.3c** and **4.3d** represents the subgrain boundaries. The misorientation angle profiles across the subgrain boundaries parallel to short and long axis of the phenocrysts illustrated in **Figs. 4.3b** and **4.4b**. They show the misorientation angle across the subgrain boundaries parallel to the short axis always below 4° (B–B' in **Figs 4.3b** and **4.4b**), while the misorientation angle across some subgrain boundaries parallel to the long axis above 4° (A–A' in **Figs. 4.3b** and **4.4b**). The subgrain boundaries with misorientation angles >4° are commonly parallel/subparallel to the long axis forming spaced arrays of planar structures (**Figs. 4.3d** and **4.4d**), whereas those with ≤4° show a marked preponderance for alignment parallel/subparallel to the short axis and nearly perpendicular to the shear plane, regardless of their crystallographic orientation (**Fig. 4.3c** and **4.4c**). The misorientation profiles across the subgrain boundaries parallel to the long axis (the left panel of **Figs. 4.3b** and **4.4b**) and across the subgrain boundaries parallel to the short axis (the right panel of **Figs. 4.3b** and **4.4b**) exhibit distinct characteristics. The misorientation profile across the subgrain boundaries parallel to the long axis is characterized by an alternation (increase and decrease) of misorientation values for the subgrains, whereas that across the subgrain boundaries parallel to the short axis shows progressive changes in orientation differences. The subgrain boundaries parallel to the long axis with misorientation angles >4° formed spaced arrays of planar structures. Thus, in this study, we will separately show the characteristics of the subgrain boundaries in the cases of ≤4° and >4°–10° in quartz phenocrysts in the following sections.

In almost all the quartz phenocrysts, the misorientation axes across subgrain boundaries are aligned either parallel or nearly parallel to the *Y*-axis in the specimen coordinate, i.e., the rotation axis of simple shear deformation (**Figs. 4.3e** and **4.4e**). The distributions of the misorientation axes of misorientation angles ≤4° and >4°are not significantly different in the specimen coordinates (**Figs. 4.3e** and **4.4e**). However, those are sometimes different in the crystal coordinate. In the example shown in **Fig. 4.4e,** the misorientation axes across subgrain boundaries for misorientation angles ≤4° are normal to the *m*-plane, while those for misorientation angles >4°are parallel to the *a*-axis.

In the quartz phenocrysts analyzed in this study, subgrain boundaries with misorientation angles ≤4° are found to be parallel to the short axis (i.e., perpendicular to the lineation, which indicates the slip direction) (**Figs. 4.3** and **4.4**). Based on the geometrical relationship between the subgrain boundaries and the slip direction (e.g., Neumann, 2000; Lloyd, 2004), we consider these subgrain boundaries to be tilt boundaries which predominantly comprise edge dislocations. **Figure 4.5** shows the GND of tilt and twist dislocations in the quartz phenocrysts 3-01, 6-01, and 6-02. The map represents the density of the entire EBSD data set for the phenocrysts, calculated using equation (3.1) In fact, the density of geometrically necessary dislocation (GND) of edge dislocations is higher than that of screw dislocations in deformed quartz phenocrysts (**Fig. 4.5**), indicating that edge dislocations predominate in quartz phenocryst. The energy minimization approach applied to estimate the GND density is used to choose a solution that favors screw dislocations with <*a*> Burgers vectors, and thus it remains possible that edge dislocations with <*a*> Burgers vectors may be present in greater densities than those revealed by the GND analysis (Wallis et al., 2019).

On the other hand, for subgrain boundaries with misorientation angles >4° aligning parallel to the long axis, the alternating misorientation angles from the initial reference orientation for the subgrains may suggest that the subgrain boundaries might be kink band boundaries (Nishikawa and Takeshita, 1999, 2000; Montagnat et al., 2011), pile-ups and an accumulation of screw dislocations (Hamann et al., 2007), or the subgrain boundaries just composed of dislocations with Burgers vectors of opposite sign. Therefore, our study did not focus on these subgrain boundaries.

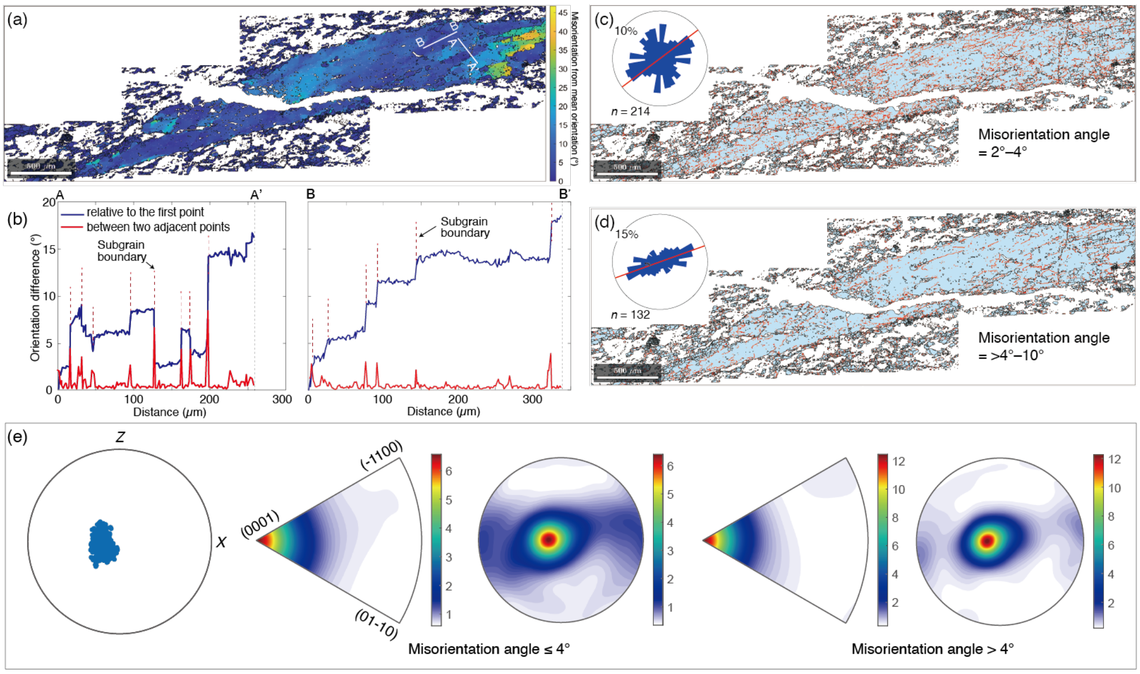

**Fig. 4.3.** Intracrystalline deformation features (phenocryst 3-01) (Wang et al., 2024). (**a**) Map showing the distribution of misorientation angles from the grain mean orientation. (**b**) The misorientation angle profiles along the lines indicated in (**a**). The red vertical dashed lines represent subgrain boundaries. (**c, d**) Map showing the distribution of the subgrain boundaries with misorientation angles: (**c**) 2°–4° (**d**) >4°–10°. Inset: The rose diagram shows the orientation distribution and the mean orientation (red line) of the subgrain boundaries. (**e**) Crystallographic orientation data for quartz phenocrysts. From left to right, pole figure showing the distributions of *c*-axes orientations within the phenocryst, inverse pole figure showing the distributions of the misorientation axes in the crystal coordinate, and pole figure showing the misorientation axes in the sample coordinate. The density of the distribution is shown by the multiples of uniform densities (MUD); the color indicates the uniform densities multiplied by the values on the scale bar. Upper hemisphere equal area projection.

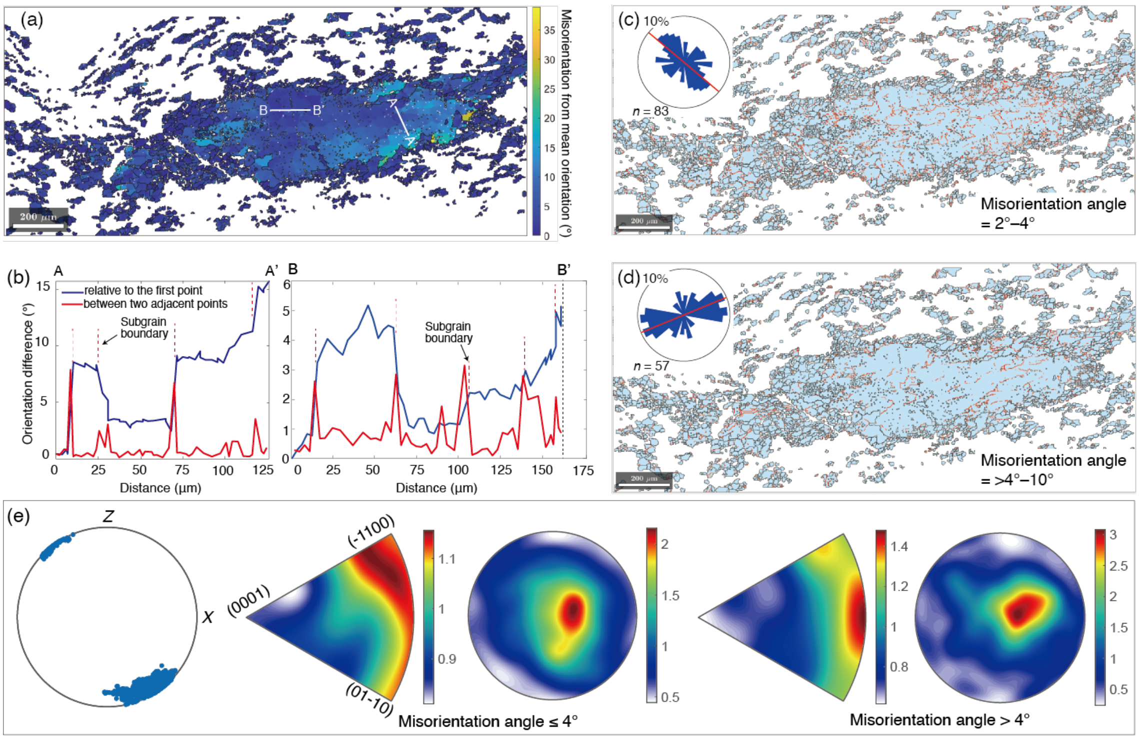

**Fig. 4.4.** Intracrystalline deformation features (phenocryst 6-02) (Wang et al., 2024). (**a**) Map showing the distribution of misorientation angles from the grain mean orientation. (**b**) The misorientation angle profiles along the lines indicated in (**a**). The red vertical dashed lines represent subgrain boundaries. (**c, d**) Map showing the distribution of subgrain boundaries with misorientation angles: (**c**) 2°–4° (**d**) >4°–10°. Inset: The rose diagram shows the orientation distribution and mean orientation (red line) of the subgrain boundaries. (**e**) Crystallographic orientation data for quartz phenocrysts. From left to right, pole figure showing the distributions of *c*-axes orientations within the phenocryst, inverse pole figure showing the distributions of the misorientation axes in the crystal coordinate, and pole figure showing the misorientation axes in the sample coordinate. The density of the distribution is shown by the MUD. Upper hemisphere equal area projection.

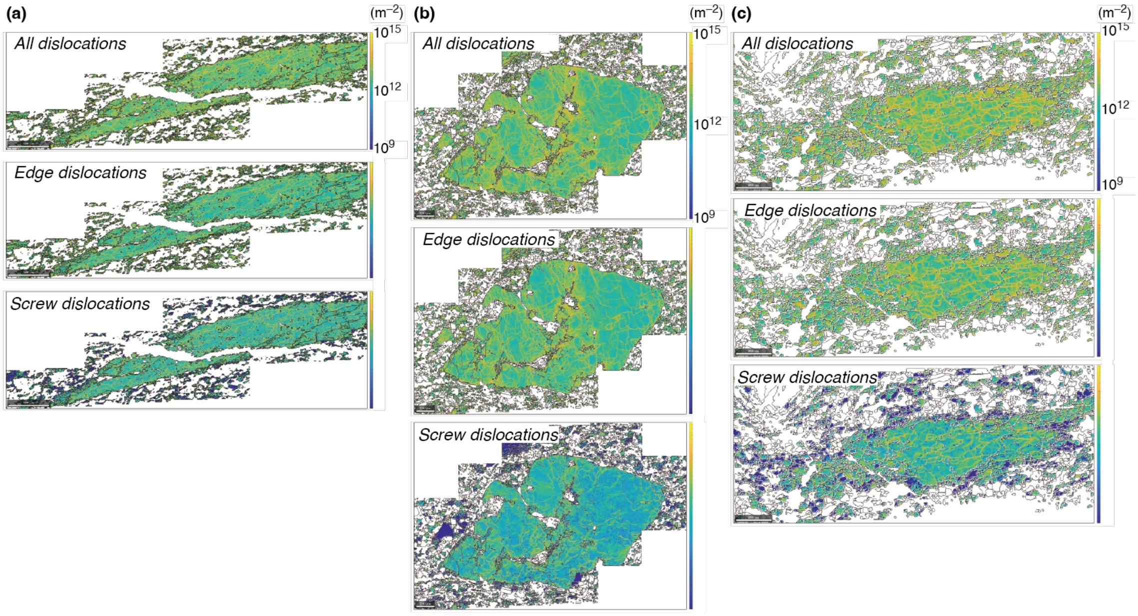

**Fig. 4.5.** Densities of geometrically necessary dislocations (GNDs) in some quartz phenocrysts (Wang et al., 2024). Results are presented as maps of the density of each type of dislocation, i.e., edge and screw dislocation, and also the sum of all dislocation types. Scale bars represent GND density ($m^{-2}$). (**a**) Phenocryst 3-01. (**b**) Phenocryst 6-01A. (**c**) Phenocryst 6-02. In the GND analysis, 19 dislocation types grouped into six families, i.e., (*c*) <*a*> edge, {*r*/*z*} <*a*> edge, {*m*} <*a*> edge, {*m*} [*c*] edge, <*a*> screw, and [*c*] screw.

### *4.4. Crystallographic orientations of the phenocryst and misorientation axes*

I divided the quartz phenocrysts into four groups from A to D, based on the distribution of misorientation axes mainly in the inverse pole figure (i.e., crystal coordinate) across subgrain boundaries for misorientation angles ≤4° (i.e., subgrain boundary parallel to the short axes) and their crystallographic orientations. Almost all *c*-axis orientations of Group B, C, and D phenocrysts are at the periphery of the pole figures, whereas most of the *c*-axis orientations of Group A phenocrysts are around the *Y*-axis (**Figs. 4.6**, **4.7,** and **4.8**; **Table 4.1**). Groups A and D are characterized by the misorientation axes in crystal coordinate that are parallel to the *c*-axis (**Figs. 4.6** and **4.8**), while Group B are characterized by those that are normal to *m*-planes and/or parallel to *a*-axes (**Fig. 4.7**). Some phenocrysts belonging to Group B also show the concentration of the misorientation axes parallel to the *c*-axis. (**Fig. 4.7**). Group C is characterized by the misorientation axes normal to rhombohedral planes (Group C of **Fig. 4.8**). For Groups A, B, and C, the misorientation axes are almost parallel/subparallel to the *Y*-axis in the specimen coordinate, whereas those for Group D locate near the *Z*-axis (**Figs. 4.6**, **4.7**, and **4.8**; **Table 4.1**).

### *4.5. Active slip systems*

The activation of a slip system results in the rotation of the crystallographic orientations around a rotation axis defined by the slip system. In the case of subgrain boundaries with characteristics of tilt boundaries, the misorientation axis is normal to both the slip plane normal and slip direction (e.g., Lloyd, 2004). Based on these concepts, the misorientation axes across the subgrain boundaries can be plotted in an inverse pole figure for tilt boundaries (**Fig. 3.5b**; Neumann, 2000; Kilian and Heilbronner, 2017). In **Fig. 3.5b**, although systems with slip directions oblique to the [*c*] and <*a*> directions are relatively hard to activate (Morales et al., 2014), the location of the misorientation axis indicative of an activity of <*a*+*c*> slip systems is also illustrated.

The comparison between the misorientation axes of quartz phenocrysts across each group (**Figs. 4.6**, **4.7**, and **4.8**) with **Fig. 3.5b** revealed that the prism <*a*> slip system is active in Groups A and D phenocrysts, and that the basal <*a*> and prism [*c*] slip systems is predominant in Group B phenocrysts. Although the phenocrysts in Group B differ from the monomineralic aggregates used in numerical simulations (e.g., Lister et al., 1978; Hobbs, 1985), our observations indicate that the activity of the basal <*a*> slip system can lead to the formation of quartz CPO with peripheral *c*-axes, offering natural sample evidence for the conclusions derived from these numerical simulations. The misorientation axes in Group C phenocrysts normal to the rhombohedral planes suggest the activity of rhomb <*a*> slip, especially acute rhomb {*π*'} <*a*>.

In instances of dextral shear deformation, I observe a relationship between the dominant slip systems and the crystallographic orientations of the phenocryst. **Figure 4.9** shows the *c*-axis distribution of phenocrysts and shape preferred orientation, along with the inferred slip system and aspect ratios. For phenocrysts exhibiting a dominant prism <*a*> slip system, their *c*-axes align around the *Y*-axis or lie moderately between the *Y* and *Z* axes within the pole figure (**Fig. 4.9a**). Those with a dominant basal <*a*> slip system typically present their *c*-axes at the periphery of the fourth quadrant of the pole figure (**Fig. 4.9a**), whereas those with dominant prism [*c*] generally locate their *c*-axes at the periphery within the first and third quadrants (**Fig. 4.9a**). The orientation of the inferred slip plane is positive (anticlockwise as positive) angles to the shear direction (0°≤ $\theta$ <90°) after the dextral shear deformation (**Figs. 4.6**, **4.7**, and **4.8**). Notably, for the two dominant rhomb <*a*> slip system phenocrysts, one positions its *c*-axis at the periphery of the pole figure around the *X*-axis, while the other is located near the *Z*-axis.

Most phenocrysts with dominant prism <*a*> slip system (Groups A and D) exhibit high aspect ratios (*R* >~3) (**Fig. 4.9b**). The *c*-axes of the phenocrysts with the highest aspect ratio (*R* = ~6) are located near the *Y* axis. Some phenocrysts with *c*-axes plotted between the *Y* and *Z* axis, also exhibit high aspect ratios (*R* =~4), while some others show smaller aspect ratios (*R* <~3). Some phenocrysts with dominant basal <*a*> (Group B) also exhibit high aspect ratio (*R* =~5), while others show small aspect ratio (*R* <~3) (**Fig. 4.9b**). Phenocrysts with dominant prism [*c*] (Group B) and rhomb <*a*> (Group C) slip systems always show low aspect ratio values ranges from 1.6 to 2.9 (**Fig. 4.9b**).

Group A

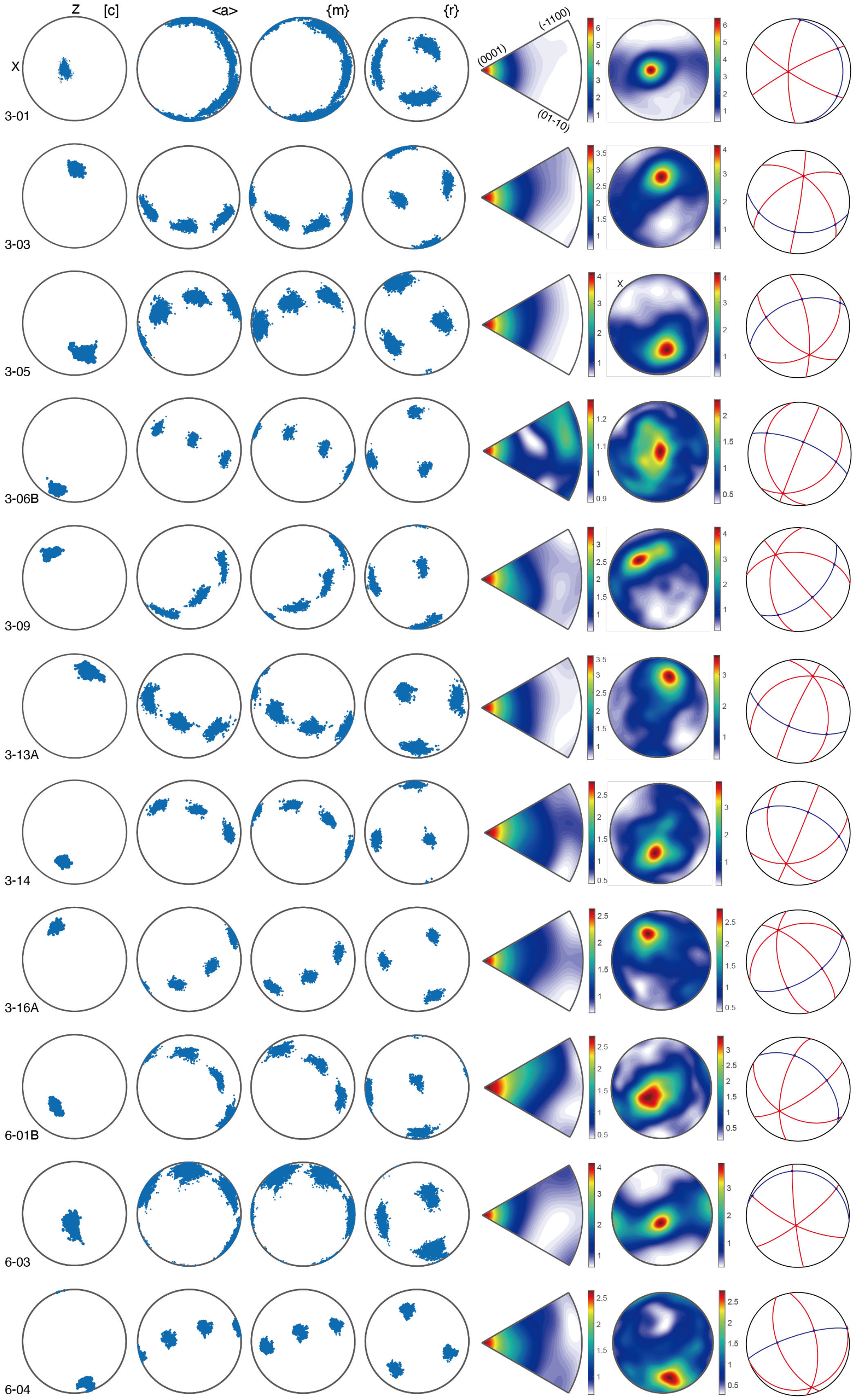
Z
[c]
<a>
{m}
{r}
X
(0001)
(-1100)
(01-10)
3-01
3-03
3-05
3-06B
3-09
3-13A
3-14
3-16A
6-01B
6-03
6-04

**Fig. 4.6.** Crystallographic orientation data for Group A phenocrysts (Wang et al., 2024). From left to right for each phenocryst, the pole figures show the distributions of crystallographic orientations within a phenocryst, inverse pole figure shows the distributions of the misorientation axes in the crystal coordinate, the pole figure shows the misorientation axes in the sample coordinate, and the pole figure shows the crystallographic plane (red is prismatic plane, blue is the basal plane). The density of the distribution is shown by the MUD. Upper hemisphere equal area projection.

Group B

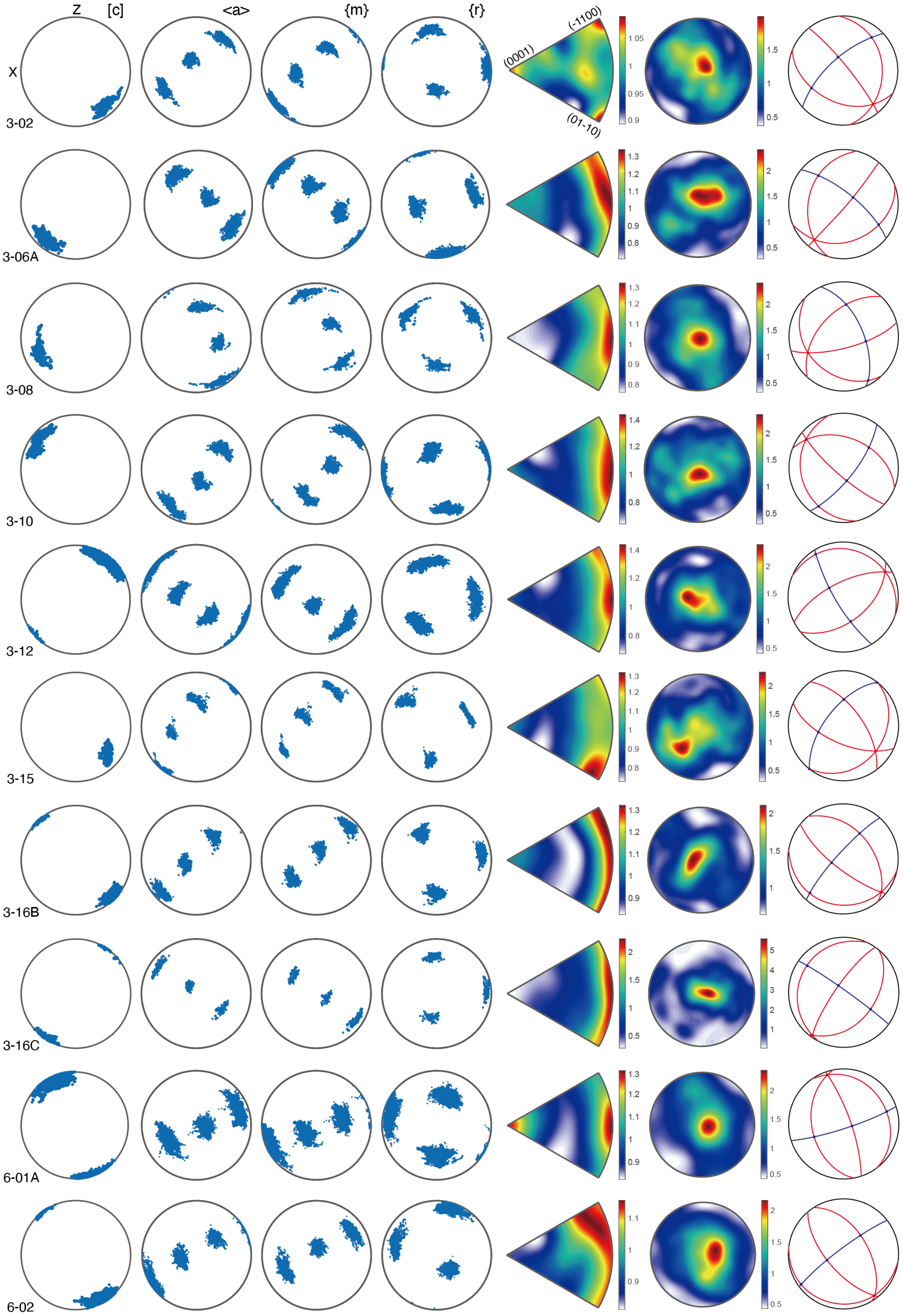
Z
[c]
<a>
{m}
{r}
X
(0001)
(-1100)
(01-10)
1.05
1
0.95
0.9
1.5
1
0.5
3-02
1.3
1.2
1.1
1
0.9
0.8
2
1.5
1
0.5
3-06A
1.3
1.2
1.1
1
0.9
0.8
2
1.5
1
0.5
3-08
1.4
1.2
1
0.8
2
1.5
1
0.5
3-10
1.4
1.2
1
0.8
2
1.5
1
0.5
3-12
1.3
1.2
1.1
1
0.9
0.8
2
1.5
1
0.5
3-15
1.3
1.2
1.1
1
0.9
2
1.5
1
3-16B
2
1.5
1
0.5
5
4
3
2
1
3-16C
1.3
1.2
1.1
1
0.9
2
1.5
1
0.5
6-01A
1.1
1
0.9
2
1.5
1
0.5
6-02

**Fig. 4.7.** Crystallographic orientation data for Group B phenocrysts (Wang et al., 2024). From left to right for each phenocryst, the pole figures show the distributions of crystallographic orientations within a phenocryst, the inverse pole figure shows the distributions of the misorientation axes in the crystal coordinate, the pole figure shows the misorientation axes in the sample coordinate, and the pole figure shows the crystallographic plane (red is prismatic plane, blue is the basal plane). The density of the distribution is shown by the MUD. Upper hemisphere equal area projection.

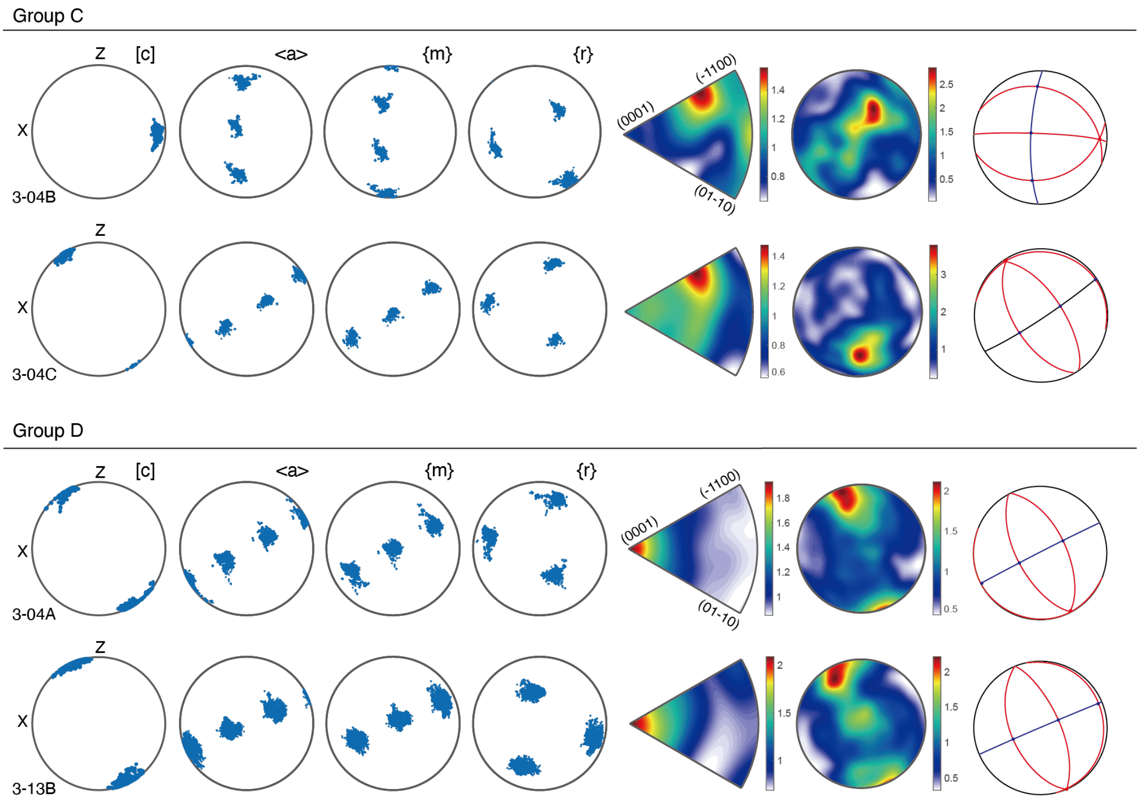

**Fig. 4.8.** Crystallographic orientation data for phenocrysts of Groups C and D (Wang et al., 2024). From left to right for each phenocryst, the pole figures show the distribution of crystallographic orientations within a phenocryst, the inverse pole figure show the distributions of the misorientation axes in the crystal coordinate, the pole figure shows the misorientation axes in the sample coordinate, and the pole figure shows the crystallographic plane (red is prismatic plane, blue is the basal plane). The density of the distribution is shown by the MUD. Upper hemisphere equal area projection.

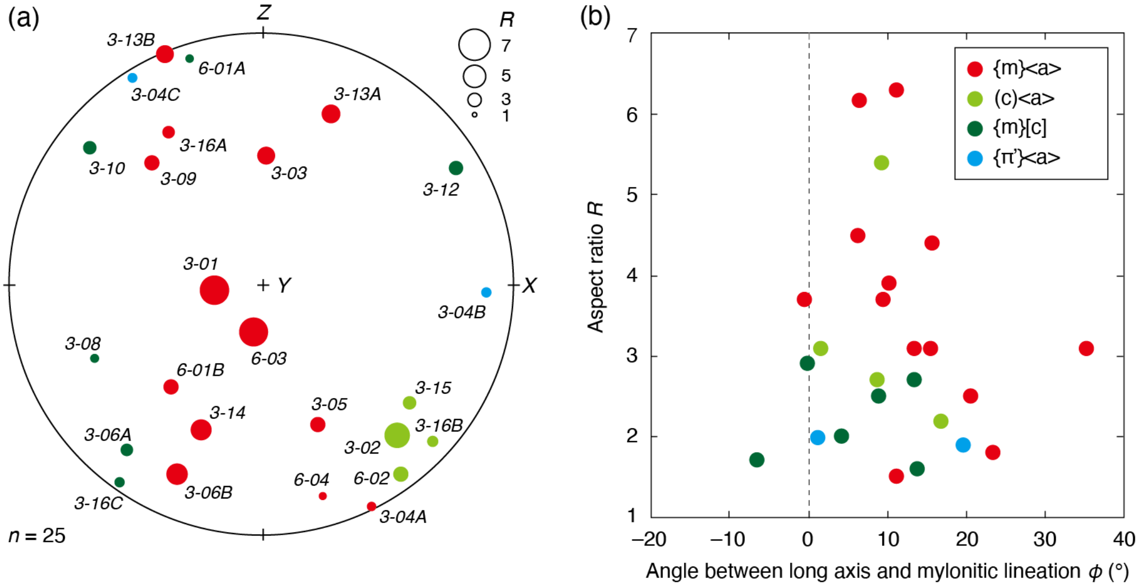

**Fig. 4.9.** Relationship between the inferred slip systems and the shape preferred orientations and the *c*-axis distributions (Wang et al., 2024). (**a**) The *c*-axis distributions. Red circles are prism <*a*> phenocrysts; Light green circles are basal <*a*> phenocrysts; Dark green circles are prism [*c*] phenocrysts; blue circles are rhomb <*a*> phenocrysts. The diameter of the solid circles represents the values of their aspect ratios. Phenocryst numbers are also presented. Projected in the upper-hemisphere, equal-area projection. (**b**) The shape preferred orientations in the *XZ* section. {*m*}<*a*> is prism <*a*>, (*c*)<*a*> is basal<*a*>, {*m*}[*c*] is prism [*c*], {*π'*}<*a*> is rhomb <*a*>.

# 5. Discussion

## *5.1. Dominant quartz slip systems inferred from the relationship between strain and active slip system*

In my observations, the relationship between aspect ratios and dominant slip systems shows that phenocrysts with dominant basal <*a*> and prism <*a*> slip system exhibit higher aspect ratios (**Fig. 4.9b**). This finding has also been reported in experimentally deformed samples (e.g., Tokle et al., 2023); grains with dominant prism <*a*> and basal <*a*> slip systems in high-strain samples exhibit higher aspect ratios. The Group D phenocrysts show little deformation, because they are not favorably oriented for any slip systems, except for some minor activation of the prism <*a*> slip system (see some of the A-grains in Takeshita et al., 1999). The differences in the aspect ratios within each group can be attributed to the initial orientation of active slip plane(s); phenocrysts oriented favorably are highly deformed, while those oriented unfavorably are weakly deformed (e.g., Takeshita et al., 1999). The model of Ishii and Sawaguchi (2002) can explain variable aspect ratios of quartz phenocrysts with prism <*a*> and basal <*a*> slip systems (**Fig. 5.1**). **Figure 5.1** shows the model for variable development of aspect ratios in quartz phenocrysts within deformed granite porphyries, attributed to the initial orientations of slip plane. Assuming an easy slip plane under the dextral simple shear, the initial orientation of the slip plane ($\theta_0$) relative to the shear direction ($\theta = 0°$) controls both the aspect ratio and the orientation of the long axis of phenocrysts ($\varphi$). With increasing deformation, (1) the orientation $\varphi$ is concentrated around 10°–30°, and (2) the slip planes with an initial orientation of $0° < \theta_0 \leq 90°$ or $-90° \leq \theta_0 \leq -30°$ rotate clockwise, whereas those with an initial orientation of $-30° < \theta_0 < 0°$ rotate anticlockwise. As the results, the orientation of the easy slip plane becomes positive angles to the shear direction ($0° \leq \theta < 90°$) after the sufficient dextral simple shear. As shown in **Fig. 4.9a**, phenocrysts with dominant basal <*a*> and prism [*c*] slip systems present their *c*-axes at the periphery of the pole figure, located within distinct quadrants. The derived slip planes from these phenocrysts form positive angles (~30°–60°) to the dextral sense of shear direction, consistent with expectations of the proposed model.

In case of quartz phenocrysts with prism <*a*> and basal <*a*> slip systems, the symmetry of prism <*a*> and basal <*a*> need to be considered (**Fig. 5.1**). When one of the slip planes of prism <*a*> system or the basal <*a*> system is parallel to the bulk shear plane ($\theta_0 = 0°$ in **Fig. 5.1**), the deformed quartz undergoes only simple shear deformation without any rotation on the glide plane. However, when the basal plane is highly oblique to the bulk shear plane ($\theta_0 = 60°$ and $-60°$ for basal <*a*> in **Fig. 5.1**), the quartz phenocryst initially is deformed through the basal <*a*> slip system and the prism [*c*] system becomes favorable for deformation after the glide plane rotation. In the case of an initial orientation is $\theta_0 = 90°$ for the basal <*a*> slip system, the activation of prism [*c*] slip system is suitable, or the phenocryst may deform initially by prism [*c*] slip and subsequently by basal <*a*> slip as a progressive rigid-body rotation. If the strength of the prism [*c*] slip system is higher than that of basal <*a*>, the aspect ratios of these phenocrysts would be small. Consequently, the aspect ratios would be highly variable for phenocrysts with a favorable orientation for basal <*a*> and prism [*c*] slip systems. In contrast, for phenocrysts with a favorable orientation for prism <*a*> slip system (Group

A), they can make one of the prism planes parallel or subparallel to the bulk shear plane due to its high symmetry, resulting in similar aspect ratios. The smaller aspect ratios are also expected in some cases ($\theta_0$ = 90° and –30° for prism <*a*> in **Fig. 5.1**).

Considering an initial condition where phenocrysts of different active slip systems having the respective active slip plane oriented similarly, the aspect ratios of the deformed phenocrysts is indicative of the relative strength (i.e., critical resolved shear stress CRSS) of the active slip systems. The aspect ratio of phenocryst 3-02 (with basal <*a*>, Group B) is as high (*R* = 5.4) as the highest values (*R* = 6.3, 6.2) of phenocrysts with prism <*a*> slip system **(Fig. 4.9**), implying that the relative strength of basal <*a*> slip system is similar to that of prism <*a*>. Furthermore, the aspect ratios of all phenocrysts with prism [*c*] slip system and rhomb <*a*> are smaller than those with basal <*a*> and prism <*a*> slip system, suggesting that the relative strength of prism [*c*] and rhomb <*a*> slip systems are higher than that of basal <*a*> and prism <*a*>slip system. It also implies that prism <*a*> and basal <*a*> slip systems are dominant slip systems, rather than prism [*c*] and rhomb <*a*> slip systems at temperature conditions of ~400–500 °C (lower amphibolite-facies conditions) in the upper to middle crust. The relative strength of prism <*a*> and basal <*a*> slip systems is possibly similar because their maximum aspect ratios are not significantly different.

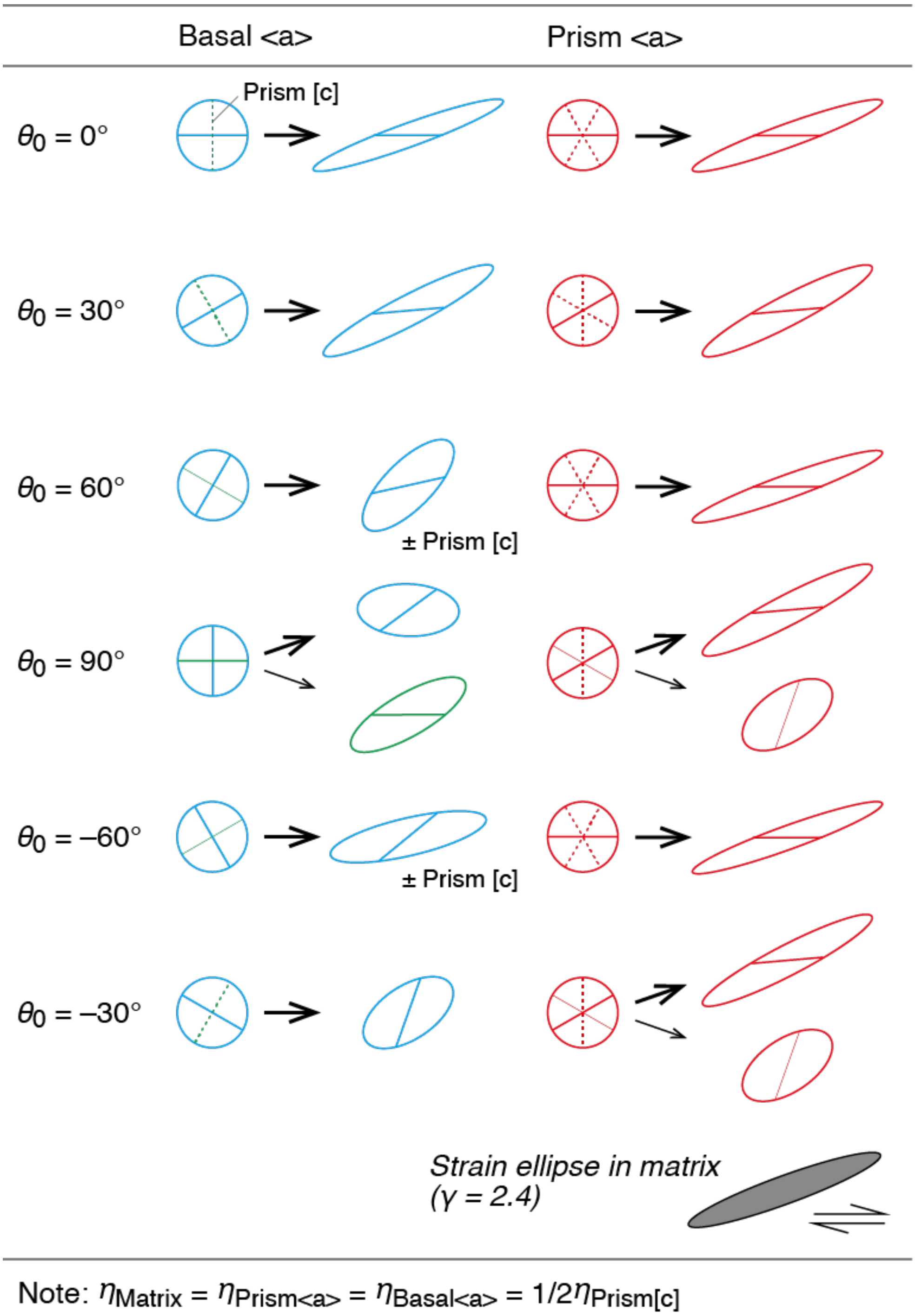

**Fig. 5.1.** A model for the variable development of shape-preferred orientations of the quartz phenocrysts in the deformed granite porphyries (Wang et al., 2024). The circles represent the initial grains before the deformation. The ellipses represent the resultant grains after deformation. The dotted lines indicate the orientations of the inactive glide

planes. Solid lines show the orientations of active glide planes. Blue, green, and red dotted/solid lines represent glide planes of basal <*a*>, prism [*c*], and prism <*a*> slip systems, respectively. $\theta_0$ is the initial orientation of the glide plane. The final shapes of particles are at a simple shear strain of the matrix of 2.4. The ductility of particles with basal <*a*> or prism <*a*> is assumed to be the same as the matrix, but that with prism [*c*] to be half the matrix.

### *5.2. Basal <a> and prism <a> as co-active slip systems at lower amphibolite-facies conditions*

Kilian and Heilbronner (2017) proposed a model of initial oriented nucleation and growth, forming textures with peripheral *c*-axis in pole figures, based on the observations on grain-shape fabric and the intragranular deformation intensity (i.e., mean grain kernel average misorientation) for the experimentally deformed Black Hills Quartzite of Heilbronner and Tullis (2002, 2006). Kilian and Heilbronner (2017) revealed that the increasing density of *c*-axes in the pole figure is moved away from the periphery to the center. The development and strengthening of a girdle component, and/or the formation of a central maximum can all be related to dislocation glide along multiple slip systems (**Fig. 1.6**). Furthermore, they summarized TEM observations from many previous studies (Kilian and Heilbronner, 2017 and references therein) and suggested that basal <*a*> related dislocation systems are not dominant or have very limited mobility. Thus, they concluded that the textures with peripheral *c*-axis in pole figures cannot be attributed to the activity of the basal <*a*> slip system. This model was supported by comparing their observations with other experimental works (e.g., Gleason et al., 1993; Trepmann and Stöckhert, 2013) where the grains with peripheral *c*-axis seem to be the first formed at high-stresses conditions. Gleason et al. (1993) conducted coaxial deformation experiments on quartz aggregates. They suggested that in the recrystallization mechanism regime at low temperatures and fast strain rates (i.e., regime 1 of Hirth and Tullis, 1992), strain-induced grain boundary migration recrystallization favors the growth of grains oriented poorly for basal slip. As a result, a

CPO developed with *c*-axes parallel to the $\sigma_1$ direction. Because it does not indicate low activity of basal <*a*> for peripheral grains, but the orientation of basal slip is not favorable for slip, their experimental results did not deny the activity of the basal slip system in the deforming quartz aggregates. Morales et al. (2011) also suggested that the presence of peripheral *c*-axes does not necessarily require the dominant activity of basal <*a*> slip system based on their numerical analysis, but their simulation results could not deny the activity of basal <*a*> slip system in the deforming quartz aggregates.

This study reveals that the basal <*a*> and prism <*a*> slip systems are activated as “easy” slip systems in naturally deformed quartz at temperature conditions of ~400–500 °C in the upper to middle crustal conditions. Therefore, the peripheral *c*-axes are indicative of the basal <*a*> slip system as the dominant slip system, as demonstrated by numerical simulation studies, and the interpretation of the activity of basal <*a*> slip based on their quartz *c*-axis fabrics is appropriate. This interpretation is supported by recent studies on experiments and natural samples (e.g., Muto et al., 2011; Halfpenny et al., 2012; Stünitz et al., 2017; Bestmann et al., 2021).

In this study, we analyzed quartz phenocrysts from a quartz porphyry deformed at temperature conditions of ~400–500 °C in the upper to middle crust, and revealed that the basal <*a*> and prism <*a*> slip systems are activated as “easy” slip systems in naturally deformed quartz. The activities of both slip systems do not significantly differ, and hence, they may be co-active slip systems in the samples analyzed in this study. This interpretation is consistent with that of the previous studies (e.g., Hobbs, 1985; Takeshita, 1996; Toy et al., 2008; Law, 2014; Bui et al., 2023).

### *5.3. Implications for rheology of the continental crust*

In this study we reveal that basal <*a*> and prism <*a*> are co-active as easy slip systems in naturally deformed quartz under lower-amphibolite facies conditions. To illustrate the strength and rheology of the mid-crust are significantly influenced by the co-activation of basal <*a*> and prism <*a*> slip systems, we calculated the strength under mid-crustal conditions (i.e., ~400–500 °C) based on the dislocation creep flow laws expressed as:

$$\dot{\varepsilon} = A\sigma^{n} f_{H_2O}^{r} e^{\left(\frac{-Q}{RT}\right)} \tag{5.1}$$

where $\dot{\varepsilon}$ is strain rate, $\sigma$ is differential stress, $n$ is the stress exponent, $f_{H_2O}$ is the water fugacity, $r$ is the water fugacity exponent, $Q$ is the activation enthalpy, $R$ is the ideal gas constant, $T$ is absolute temperature, and $A$ is a material parameter. Water fugacity was calculated using Wither's fugacity calculator following Shinevar et al. (2015) (https://publish.uwo.ca/~awither5/fugacity/index.htm).

I applied the two laboratory-fit flow laws proposed by Tokle et al. (2019): one with a stress exponent $n \approx 4$ at lower stresses, and another with $n \approx 2.7$ at higher stresses. The associated *c*-axis fabrics indicate the importance of easy slip systems, with the former applying to quartz aggregates dominated by prism <*a*> slip and the latter suitable where basal <*a*> slip is rate-limiting. I constructed plots of log strain rate versus log stress comparing the laboratory-fit flow laws at 400 °C and 500 °C (**Fig. 5.2**). The results indicate that at strain rate of $10^{-15}$ $s^{-1}$, the stress for dominant basal <*a*> slip system is 7 MPa at 400 °C and 2 MPa 500 °C, whereas for dominant prism <*a*> slip system it is 18 MPa and 7 MPa. As the strain rate increases, the difference in stress becomes more pronounced. At $10^{-12}$ $s^{-1}$ strain rate, the stress for dominant basal <*a*> slip system is 91 MPa at 400 °C and 26 MPa at 500 °C, whereas for dominant prism <*a*> slip system it is 101 MPa and 36 MPa. This demonstrates that at ~400–500 °C temperature conditions, the crustal strength controlled by prism <*a*> slip system is significantly different from that controlled by basal <*a*> slip system.

I also referenced a plot of stress versus depth with two laboratory-fit flow laws for a strain rate of $10^{-13}$ $s^{-1}$ from Tokle et al. (2019) (**Fig. 5.3**). The flow strength of quartz aggregates with a dominant basal <*a*> slip system is lower than that with a dominant prism <*a*> slip system by tens of megapascals under mid-crustal conditions. This is consistent with observations of natural samples, which the CRSS of basal <*a*> slip system is weaker than the prism <*a*> slip system. The flow law with $n = 4$ proposed by Tokle et al. (2019) suggested that the quartz aggregate may have been deforming through dislocation-accommodated grain boundary sliding. They adjust the parameters of the flow law and proposed extrapolated fit flow laws. The strength profile generated using this extrapolated fit flow laws suggests that under middle crustal temperature conditions, the basal <*a*> slip system is harder than the prism <*a*> slip system, which is inconsistent with natural observations (**Fig. 1.2**). This discrepancy could be attributed to the fact that the $n = 4$ extrapolated fit flow law, which reflects prism <*a*> slip-accommodated grain boundary sliding, does not represent the strength of dislocation creep by prism <*a*>. In mid-crustal conditions, the dominant slip system for quartz is neither exclusively prism <*a*> nor basal <*a*>, but rather their co-activation. The combined activation of these slip systems can lead to complex influences on the flow strength of quartz aggregates. The actual stress may differ substantially from the stress predicted by the laboratory-fit quartz flow laws assuming single active slip systems.

Currently, the mechanisms of co-activation in quartz slip systems are not well understood. Therefore, we hypothesize a model assumes that the total strain rate is proportionally contributed by both basal <*a*> and prism <*a*> slip systems, suggesting an interdependent relationship where the activation of one slip system can replace the activity of the other. In this situation, the total strain rate is expressed as:

$$\dot{\varepsilon} com = \alpha \dot{\varepsilon} basal + (1 - \alpha) \dot{\varepsilon} prism \qquad (5.2)$$

where the $\dot{\varepsilon} com$ represents the combination strain rate of the basal <*a*> and prism <*a*> quartz flow law; $\dot{\varepsilon} basal$ represents the strain rate of basal <*a*> quartz flow law; $\dot{\varepsilon} prism$ represents the strain rate of prism <*a*> quartz flow law; $\alpha$ represents the proportion of basal <*a*> slip systems,. $\alpha$ ranges from 0−100 %. This study has shown that the CRSS for basal <*a*> and prism <*a*> are nearly equal. It is widely accepted that basal <*a*> is the dominant slip system at lower temperatures. Therefore, the ratio $\alpha$ of the slip systems is not constant. Thus, we assume an equal activity ratio ($\alpha$ = 0.5) for basal <*a*> slip system at 450 °C (depth = ~15 km). Here we assume the value of $\alpha$ are constant 0.5 from 20 to 15 km, and it changes from 15 km to 10 km increasing by 0.1 for every 1 km decrease in depth. Based on this model, the strength profile lies between the strength profiles of prism <*a*> and basal <*a*> slip systems at a strain rate $10^{-13}$ $s^{-1}$. The predicted strength profile can be compared to the experimental sample with a mixture *c*-axis fabrics plotted between the basal <*a*> and prism <*a*> flow laws (**Fig. 5.3**). Therefore, the co-activation of basal <*a*> and prism <*a*> slip systems is crucial under mid-crustal conditions. Although, the hypotheses require experimental data and observations from natural samples for validation, the impact of the co-activation of basal <*a*> and prism <*a*> slip systems must be considered when discussing the mid-crustal strength. Regardless of the model, these findings underscore the importance of determining the dominant slip systems in quartz for accurate predictions of crustal strength.

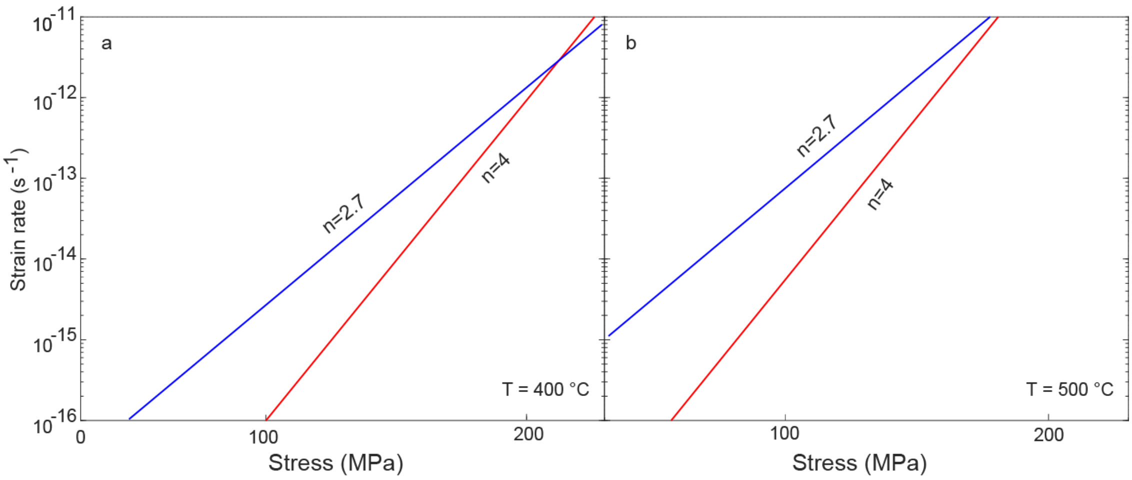

**Fig. 5.2.** Log strain rate versus log stress for the laboratory-fit quartz flow laws at (**a**) 400 °C; (**b**) 500 °C. Red and blue lines are applied for prism <*a*> slip and basal <*a*> slip, respectively.

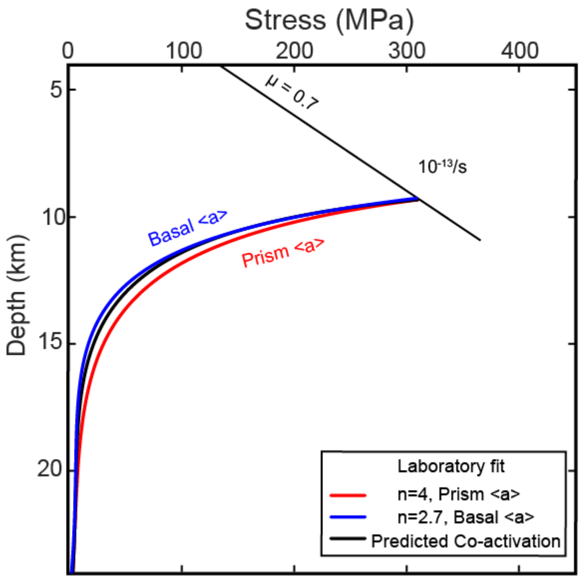

**Fig. 5.3.** The strength profile (stress versus depth) for a continental crust consistent with the laboratory-fit quartz flow laws for a strain rate of $10^{-13}$ $s^{-1}$ and the predicted strength profile for combination of basal <*a*> and prism <*a*> slip systems. The black curve represents the combination of basal <*a*> and prism <*a*> slip systems.

### *5.4. Limitation and remaining question: Formation processes of subgrain boundaries parallel to long axis*

While this research has provided significant insights into the dominant slip systems of naturally deformed quartz under mid-crustal conditions, several limitations and unanswered questions remain, and future research directions proposed to address these limitations. One key issue is the formation processes and mechanisms of subgrain boundaries parallel to the long axis of phenocrysts. The inference of slip systems in this study primarily relied on the misorientation axes of subgrain boundaries parallel to the short axis of phenocrysts. However, many subgrain boundaries developed parallel to the long axis of phenocrysts. This could suggest several potential formation mechanisms, such as kink band boundaries, pile-ups and accumulation of screw dislocations, or dislocations with Burgers vectors of opposite signs. However, the exact formation processes and mechanisms of these subgrain boundaries parallel to the long axis remain unclear. Further research is needed to understand their development and potential impact on the overall deformation mechanism.

I attempted to use GNDs analysis to characterize the dislocation combinations within subgrain boundaries. However, the analysis was conducted using EBSD data based on the Hough transform method. The resolution of Hough transform-based EBSD data is relatively low, leading to significant errors in the GNDs data. Moreover, the dislocation types determined by GNDs are based on minimum energy calculations and are related to the crystallographic orientation of the grains (Wallis et al., 2019). This may differ from the actual dislocation combinations present in the quartz phenocrysts, which contain not only GNDs but also statistically stored dislocations (SSDs).

Future studies should aim to investigate the formation processes and mechanisms of subgrain boundaries parallel to the long axis of phenocrysts. This could involve detailed crystallographic analysis and modeling to understand the formation and evolution of these boundaries. Employing high-angular resolution EBSD (HR-EBSD) can significantly improve the accuracy of GND analysis by providing higher spatial resolution and more precise measurement of dislocation densities and types, reducing errors associated with Hough transform-based EBSD data. Additionally, using techniques like Transmission Electron Microscopy (TEM) can provide high-resolution observations and characterization of these subgrain boundaries. By performing in-situ TEM observations, researchers can observe the real-time formation and evolution of subgrain boundaries under controlled deformation conditions, providing dynamic insights into the mechanisms involved. Additionally, applying computational models to simulate the formation and evolution of these subgrain boundaries can help understand the stress and strain distributions that promote their development and predict their behavior under different deformation conditions.

## 6. Conclusions

I analyzed the crystallographic orientation and shape of quartz phenocryst in a granitic porphyry in the Cretaceous Ryoke granitoids of the Awaji Island, SW Japan, to clarify the dominant slip systems in naturally deformed quartz under crustal conditions. The relationship between the aspect ratios of phenocrysts deformed by the dominant prism <*a*> and basal <*a*> slip systems are higher than that between the aspect ratios of phenocrysts deformed by prism [*c*] and rhomb <*a*> slip systems. This implies that prism <*a*> and basal <*a*> slip systems are dominant slip systems, rather than prism [*c*] and rhomb <*a*> slip systems at temperature conditions of ~400–500 °C in the upper to middle crust. The *c*-axis orientations of quartz phenocrysts, where basal <*a*> is inferred to be the dominant slip system from the misorientation analysis, are distributed at a high angle to the bulk shear plane (*XY*-plane) in pole figures. In contrast, those where prism <*a*> slip system is inferred to be dominant are located normal to the bulk shear direction on the *XY*-plane. The observation supports the traditional view that peripheral *c*-axis fabrics indicate an activation of basal <*a*> slip system rather than the oriented nucleation and growth model for the peripheral fabrics. Based on the flow laws of Tokle et al. (2019), the flow strength of quartz aggregates with a dominant basal <*a*> slip system is lower than that with a dominant prism <*a*> slip system by tens of megapascals under mid-crustal conditions, where crustal strength is at its maximum. We proposed a proportional model of the combination of basal <*a*> and prism <*a*> slip systems, suggesting that middle crustal strength would be influenced by the co-activity slip systems.

## References

Adams, B., Wrights, S., Kunze, K., 1993. Orientation imaging: The emergence of a new microscopy. Metall. Trans. A24. 819–831. https://doi.org/10.1007/BF02656503.

Ashby, M. F., 1972. A first report on deformation-mechanism maps. Acta Metall. 20, 887–897. https://doi.org/10.1016/0001-6160(72)90082-X.

Baëta, R.D., Ashbee, K.H.G., 1969. Slip systems in quartz: I. Experiments. Am. Mineral. 54, 1551–1573.

Behr, W.M., Platt, J.P., 2011. A naturally constrained stress profile through the middle crust in an extensional terrane. Earth Planet. Sci. Lett. 303, 181–192. https://doi.org/10.1016/j.epsl.2010.11.044

Bestmann, M., Pennacchioni, G., Grasemann, B., Huet, B., Jones, M.W.M., Kewish, C.M., 2021. Influence of deformation and fluids on Ti exchange in natural quartz. J. Geophys. Res. Solid Earth 126, e2021JB022548. https://doi.org/10.1029/2021JB022548

Bouchez, J.L., Duval, P., 1982. The fabric of polycrystalline ice deformed in simple shear: Experiments in torsion, natural deformation and geometrical interpretation. Texture, Stress, Microstruct. 5, 171–190. https://doi.org/10.1155/TSM.5.171.

Bui, D.V., Takeshita, T., Ando, J., Yamamoto, T., Huang, W., Yeo, T., Czertowicz, T.A., 2023. Development of the Median Tectonic Line-related shear zone, southwest Japan: An analysis of strain localization processes. Tectonophysics 850, 229751. https://doi.org/10.1016/j.tecto.2023.229751.

Ceccato, A., Menegon, L., Pennacchioni, G., Morales, L.F.G., 2018. Myrmekite and strain weakening in granitoid mylonites. Solid Earth 9, 1399–1419. https://doi.org/10.5194/se-9-1399-2018.

Etchecopar, A., 1977. A plane kinematic model of progressive deformation in a polycrystalline aggregate. Tectonophysics 39, 121–139. https://doi.org/10.1016/0040-1951(77)90092-0.

Evans, B., 2005. Creep constitutive laws for rocks with evolving structures. Geol. Soc., London, Spec. Pub. 245, 329–346. https://doi.org/10.1144/GSL.SP.2005.245.01.16.

Faleiros, F.M., Moraes, R., Pavan, M., Campanha, G.A.C., 2016. A new empirical calibration of the quartz c-axis fabric opening-angle deformation thermometer. Tectonophysics 671, 173–182. https://doi.org/10.1016/j.tecto.2016.01.014.

Flinn, D., 1962. On folding during three-dimensional progressive deformation. Quart. J. Geol. Soc. London, 118, 385–428.

Fossen, H., 2010. Structural Geology, Cambridge University Press, Cambridge.

Gao, H.J., Huang, Y.G., 2003. Geometrically necessary dislocation and size-dependent plasticity. Scr. Mater. 48, 113–118. https://doi.org/10.1016/S1359-6462(02)00329-9.

Gleason, G. C., Tullis, J., Heidelbach, F., 1993. The role of dynamic recrystallization in the development of lattice preferred orientations in experimentally deformed quartz aggregates. J. Struct. Geol. 15, 1145–1168. https://doi.org/10.1016/0191-8141(93)90161-3.

Halfpenny, A., Prior, D.J., Wheeler, J., 2012. Electron backscatter diffraction analysis to determine the mechanisms that operated during dynamic recrystallisation of quartz-rich rocks. J. Struct. Geol. 36, 2–15. https://doi.org/10.1016/j.jsg.2012.01.001.

Hamann, I., Weikusat, C., Azuma, N., Kipfstuhl, S., 2007. Evolution of ice crystal microstructure during creep experiments. J. Glaciol. 53, 479–489. https://doi.org/10.3189/002214307783258341.

Heilbronner, R., Tullis, J., 2002. The effect of static annealing on microstructure and crystallographic preferred orientations of quartzites experimentally deformed in axial compression and shear, in: De Meer, S., Drury, M.R., De Bresser, J.H.P., Pennock, G.M. (Eds.). Deformation Mechanisms, Rheology and Tectonics: Current Status and Future Perspectives. Geol. Soc. Spec. Publ. 200, 191–218. https://doi.org/10.1144/GSL.SP.2001.200.01.12.

Heilbronner, R., Tullis, J., 2006. Evolution of c axis pole figures and grain size during dynamic recrystallization: Results from experimentally sheared quartzite. J. Geophys. Res. 111, B10202. https://doi.org/10.1029/2005JB004194.

Hielscher, R., Schaeben, H., 2008. A novel pole figure inversion method: specification of the MTEX algorithm. J. Appl. Crystal. 41, 1024–1037. https://doi.org/10.1107/S0021889808030112

Hirth, G., Tullis, J., 1992. Dislocation creep regimes in quartz aggregates. J. Struct. Geol. 14, 145–159. https://doi.org/10.1016/0191-8141(92)90053-Y.

Hobbs, B.E., 1985. The geological significance of microfabric analysis, in: Wenk, H.R. (Ed.). Preferred Orientation in Deformed Metals and Rocks: An Introduction to Modern Texture Analysis. Academic Press, New York, pp. 463–484.

Humphreys, F.J., 2001. Review Grain and subgrain characterisation by electron backscatter diffraction. J. Mater. Sci., 36, 3833–3854. https://doi.org/10.1023/A:1017973432592.

Ishii, K., Sawaguchi, T., 2002. Lattice- and shape-preferred orientation of orthopyroxene porphyroclasts in peridotites: An application of two-dimensional numerical modeling. J. Struct. Geol. 24, 517–530. https://doi.org/10.1016/S0191-8141(01)00078-5.

Kano, H., Takagi, H., 2013. Mylonitization of older dikes in the Ryoke Belt, Awaji Island, SW Japan. J. Geol. Soc. Japan 119, 776–793. https://doi.org/10.5575/geosoc.2013.0054.

Kilian, R., Heilbronner, R., 2017. Analysis of crystallographic preferred orientations of experimentally deformed Black Hills Quartzite. Solid Earth 8, 1095–1117. https://doi.org/10.5194/se-8-1095-2017.

Kilian, R., Heilbronner, R., Stünitz, H., 2011. Quartz grain size reduction in a granitoid rock and the transition from dislocation to diffusion creep. J. Struct. Geol. 33, 1265–1284. https://doi.org/10.1016/j.jsg.2011.05.004.

Kohlstedt, D.L., Evans, B., Mackwell, S.J., 1995. Strength of the lithosphere: Constraints imposed by laboratory experiments. J. Geophys. Res. 100, 17587–17602. https://doi.org/10.1029/95JB01460.

Kruhl, J.H., 1998. Reply: Prism- and basal-plane parallel subgrain boundaries in quartz: a microstructural geothermobarometer. J. Metamorph. Geol. 16, 142–146. https://doi.org/10.1046/j.1525-1314.1996.00413.x.

Law, R.D., 2014. Deformation thermometry based on quartz *c*-axis fabrics and recrystallization microstructures: A review. J. Struct. Geol. 66, 129–161. https://doi.org/10.1016/j.jsg.2014.05.023.

Lister, G.S., Dornsiepen, U.F., 1982. Fabric transitions in the Saxony granulite terrain. J. Struct. Geol. 4, 81–92. https://doi.org/10.1016/0191-8141(82)90009-8.

Lister, G.S., Paterson, M.S., Hobbs, B.E., 1978. The simulation of fabric development in plastic deformation and its application to quartzite: The model. Tectonophysics 45, 107–158. https://doi.org/10.1016/0040-1951(78)90004-5.

Lloyd, G.E., 2004. Microstructural evolution in a mylonitic quartz simple shear zone: The significant roles of dauphine twinning and misorientation. Geol. Soc., Spec. Pub. 224, 39–61.

Lloyd, G.E., Farmer, A.B., Mainprice, D.,1997. Misorientation analysis and the formation and orientation of subgrain and grain boundaries. Tectonophysics 279, 55–78. https://doi.org/10.1016/S0040-1951(97)00115-7.

Lloyd, G.E., Freeman, B.,1994. Dynamic recrystallization of quartz under greenschist conditions. J. Struct. Geol. 14, 145–159. https://doi.org/10.1016/0191-8141(94)90151-1.

Mainprice, D., Nicolas, A., 1989. Development of shape and lattice preferred orientations: Application to the seismic anisotropy of the lower crust. J. Struct. Geol. 11, 175–189. https://doi.org/10.1016/0191-8141(89)90042-4.

Mainprice, D., Bachmann, F., Hielscher, R., Schaeben, H., 2014. Descriptive tools for the analysis of texture projects with large datasets using MTEX: Strength, symmetry and components. Geol. Soc., Spec. Pub. 409, 251–271. https://doi.org/10.1144/SP409.8.

Montagnat, M., Blackford, J.R., Piazolo, S., Arnaud, L., Lebensohn, R.A., 2011. Measurements and full-field predictions of deformation heterogeneities in ice. Earth Planet. Sci. Lett. 305, 153–160. https://doi.org/10.1016/j.epsl.2011.02.050.

Morales, L.F.G., Mainprice, D., Lloyd, G.E., Law, R.D., 2011. Crystal fabric development and slip systems in a quartz mylonite: An approach via transmission electron microscopy and viscoplastic self-consistent modelling. Geol. Soc., London, Spec. Pub. 360, 151–174. https://doi.org/10.1144/SP360.9.

Morales, L.F.G., Lloyd, G.E., Mainprice, D., 2014. Fabric transitions in quartz via viscoplastic self-consistent modeling part I: Axial compression and simple shear under constant strain. Tectonophysics 636, 52–69. https://doi.org/10.1016/j.tecto.2014.08.011.

Muto, J., Hirth, G., Heilbronner, R., Tullis, J., 2011. Plastic anisotropy and fabric evolution in sheared and recrystallized quartz single crystals. J. Geophys. Res. Solid Earth 116, B02206. https://doi.org/10.1029/2010JB007891.

Neumann, B., 2000. Texture development of recrystallised quartz polycrystals unravelled by orientation and misorientation characteristics. J. Struct. Geol. 22, 1695–1711. https://doi.org/10.1016/S0191-8141(00)00060-2.

Nishikawa, O., Takeshita, T., 1999. Dynamic analysis and two types of kink bands in quartz veins deformed under subgreenschist conditions. Tectonophysics 301, 21–34. https://doi.org/10.1016/S0040-1951(98)00219-4.

Nishikawa, O., Takeshita, T., 2000. Progressive lattice misorientation and microstructural development in quartz veins deformed under subgreenschist conditions. J. Struct. Geol. 22, 259–276. https://doi.org/10.1016/S0191-8141(99)00147-9.

Passchier, C.W., Trouw, R.A.J., 2005. Microtectonics, second ed. Springer-Verlag, Berlin.

Prior, D.J., Boyle, A.P., Brenker, F., Cheadle, M.C., Day, A., Lopez, G., Peruzzol, L., Potts, G.J., Reddy, S., Spiess, R., 1999. The application of electron backscatter diffraction and orientation contrast imaging in the SEM to textural problems in rocks. Am. Mineral. 84, 1741–1759. https://doi.org/10.2138/am-1999-11-1204.

Prior, D.J., Rutter, E.H., Tatham, D.J.,2011. Deformation mechanisms, rheology and tectonics: microstructures, mechanics and anisotropy: introduction. Geol. Soc., London, Spec. Pub. 360, 1–5. https://doi.org/10.1144/SP360.1.

Schmid, S.M., Casey, M., 1986. Complete fabric analysis of some commonly observed quartz c-axis patterns, in: Geophys. Monogr. S. Hobbs, B.E., Heard, H.C. (Eds.), Mineral and Rock Deformation: Laboratory Studies–The Paterson Volume. 36, 263–286.

Schneider, C.A., Rasband, W.S., Eliceiri, K.W., 2012. NIH Image to ImageJ: 25 years of image analysis. Nat. Method. 9, 671–675.

Scholz, C.H., 1998. Earthquakes and friction laws. Nature 391, 37–42.

Schwartz, A.J., Kumar, M., Adams, B.L., Field, D.P., 2009. Electron Backscatter Diffraction in Materials Science. Springer.

Shigematsu, N., Prior, D.J., Wheeler, J., 2006. First combined electron backscatter diffraction and transmission electron microscopy study of grain boundary structure of deformed quartzite. J. Microscopy. 224, 306–321. https://doi.org/10.1111/j.1365-2818.2006.01697.x.

Shinevar, W.J., Behn, M.D., Hirth, G., 2015. Compositional dependence of lower crustal viscosity. Geophys. Res. Lett. 42, 8333–8340. https://doi.org/10.1002/2015GL065459.

Simpson, G.D.H., Thompson, A.B., Connolly, J.A.D., 2000. Phase relations, singularities and thermobarometry of metamorphic assemblages containing phengite, chlorite, biotite, K-feldspar, quartz and $H_2O$. Contrib. Mineral. Petrol. 139, 555–569. https://doi.org/10.1007/s004100000154.

Spear, F.S., 1993. Metamorphic Phase Equilibria and Pressure-Temperature-Time Paths. Mineral. Soc. Am., Washington D.C.

Stipp, M., Tullis, J., 2003. The recrystallized grain size piezometer for quartz. Geophys. Res. Lett. 30, 2088. https://doi.org/10.1029/2003GL018444.

Stünitz, H., Thust, A., Heilbronner, R., Behrens, H., Kilian, R., Tarantola, A., Fitz Gerald, J.D., 2017. Water redistribution in experimentally deformed natural milky quartz single crystals–Implications for $H_2O$-weakening processes. J. Geophys. Res. Solid Earth 122, 866–894. https://doi.org/10.1002/2016JB013533

Takahashi, Y., Hattori, H., 1992. Granitic rocks in Awaji Island—with an emphasis on the foliated granites. Bull. Geol. Surv. Japan 43, 355–357.

Takeshita, T., 1996. Estimate of the physical conditions for deformation based on c-axis fabric transitions in naturally deformed quartz. J. Geol. Soc. Japan 102, 211–222.

Takeshita, T., Wenk, H.-R., 1988. Plastic anisotropy and geometrical hardening in quartzites. Tectonophysics 149, 345–361. https://doi.org/10.1016/0040-1951(88)90183-7.

Takeshita, T., Wenk, H.-R., Lebensohn, R., 1999. Development of preferred orientation and microstructure in sheared quartzite: comparison of natural data and simulated results. Tectonophysics 312, 133–155. https://doi.org/10.1016/S0040-1951(99)00173-0.

Thomas, J.B., Bruce Watson, E.B., Spear, F.S., Shemella, P.T., Nayak, S.K., Lanzirotti, A., 2010. TitaniQ under pressure: The effect of pressure and temperature on the solubility of Ti in quartz. Contrib. Mineral. Petrol. 160, 743–759. https://doi.org/10.1007/s00410-010-0505-3.

Tokle, L., Hirth, G., Behr, W.M., 2019. Flow laws and fabric transitions in wet quartzite. Earth Planet. Sci. Lett. 505, 152–161. https://doi.org/10.1016/j.epsl.2018.10.017.

Tokle, L., Hirth, G., 2021. Assessment of quartz grain growth and the application of the wattmeter to predict quartz recrystallized grain sizes. J. Geophys. Res. Solid Earth 126, e2020JB021475. https://doi.org/10.1029/2020JB021475.

Tokle, L., Hirth, G., Stünitz, H., 2023. The effect of muscovite on the microstructural evolution and rheology of quartzite in general shear. J. Struct. Geol. 169, 104835. https://doi.org/10.1016/j.jsg.2023.104835.

Toy, V.G., Prior, D.J., Norris, R.J., 2008. Quartz fabrics in the Alpine Fault mylonites: Influence of pre-existing preferred orientations on fabric development during progressive uplift. J. Struct. Geol. 30, 602–621. https://doi.org/10.1016/j.jsg.2008.01.001.

Trepmann, C.A., Stöckhert, B., 2013. Short-wavelength undulatory extinction in quartz recording coseismic deformation in the middle crust–an experimental study. Solid Earth 4, 263–276. https://doi.org/10.5194/se-4-263-2013.

Wallis, D., Parsons, A.J., Hansen, L.N., 2019. Quantifying geometrically necessary dislocations in quartz using HR-EBSD: Application to chessboard subgrain boundaries. J. Struct. Geol. 125, 235–247. https://doi.org/10.1016/j.jsg.2017.12.012.

Wang, Q., Okudaira, T., Shigematsu, N., 2024. Dominant slip systems of quartz under lower amphibolite-facies conditions identified from microstructures and CPOs in quartz phenocrysts. J. Struct. Geol. 182, 105106. https://doi.org/10.1016/j.jsg.2024.105106.

Wheeler, J., Prior, D.J., Jiang, Z., Spiess, R., Trimby, P.W., 2001. The petrological significance of misorientations between grains. Contrib. Mineral. Petrol. 141, 109–124. https://doi.org/10.1007/s004100000225.

Wilkinson, A.J., Randman, D., 2010. Determination of elastic strain fields and geometrically necessary dislocation distributions near nanoindents using electron back scatter diffraction. Philos. Mag. 90, 1159–1177. https://doi.org/10.1080/14786430903304145

Wilkinson, A.J., Meaden, G., Dingley, D.J., 2006. High-resolution elastic strain measurement from electron backscatter diffraction patterns: New levels of sensitivity. Ultramicroscopy 106, 307–313. https://doi.org/10.1016/j.ultramic.2005.10.001.

# Appendix

The following are the MATLAB scripts for analyzing crystallographic preferred orientation (CPO), misorientation, and geometrically necessary dislocation (GND) analyses for trigonal quartz. These scripts, originally written by David Mainprice and David Wallis, were modified by the author to analyze quartz phenocrysts.

## *A.1. MATLAB script for CPO analysis*

```
%%
% ****************************************************************************
% MTEX Script for EBSD Data
% Script set for ploting crystallographic preferred orientation (CPO)
%
% written by David Mainprice    31/10/2014 (MTEX ver.4.5.0)
% modified for Qtz 3/2/2022 (MTEX ver.5.8.0) on Matlab 2019b
% modified for Qtz 10/3/2022 (MTEX ver.5.8.0) on Matlab 2022a
% ****************************************************************************
% Import of Oxford/HKL *.ctf (ASCII) file
% ****************************************************************************
% clear memory and close plots - for new analysis of EBSD data
clear
close all
clc
% Specify Crystal and Specimen Symmetries
% crystal symmetry
CS = {...
  'notIndexed',...
  crystalSymmetry('-3m1', [4.9 4.9 5.5], 'X||a*', 'Y||b', 'Z||c*', 'mineral', 'Quartz', 'color', [0.53 
0.81 0.98]),...
  crystalSymmetry('12/m1', [8.6 13 7.2], [90,116.07,90]*degree, 'X||a*', 'Y||b*', 'Z||c', 'mineral', 
'Orthoclase', 'color', [0.56 0.74 0.56]),...
```

```
  crystalSymmetry('-1', [8.1 13 7.2], [94.19,116.61,87.68]*degree, 'X||a*', 'Z||c', 'mineral', 'Low albite', 'color', [0.85 0.65 0.13])};

% specimen symmetry : the MTEX4 default is triclinic so do not need this line
SS = specimenSymmetry('triclinic');

% plotting convention
setMTEXpref('xAxisDirection','east'); % 'west'
setMTEXpref('zAxisDirection','intoPlane'); % 'outOfPlane'

% Specify File Names
% path to files
pname = 'C:\Users\henry\Desktop\EBSD\EBSD\AWI_6_003';
% which files to be imported
fname = [pname '\AWI_006_003x.ctf''];

% Import the Data
% create an EBSD variable containing the data
ebsd = EBSD.load(fname,CS,'interface','ctf'','convertEuler2SpatialReferenceFrame','wizard');

% take only those measurements with MAD (Mean Angular Deviation) smaller then 1.0
ebsd = ebsd(ebsd.mad<1);

% **************************************************************************
% Calculate an ODF
% **************************************************************************
% Generate simple Crystal Symmetry variables for all phases
fprintf(' \n');
fprintf(' Crystal Symmetry (CS) : names of variables \n');
fprintf(' \n');

% phase names
Phase_names = ebsd.mineralList;
```

```
for i=1:length(CS)
% indexed point for mineral
    N_Points = length(ebsd(Phase_names(i)));
% print only indexed phases
   if((~strcmpi(Phase_names{i},'notIndexed')) && (N_Points > 0))
% retain first part of mineral name
     P_Name = strtok(char(Phase_names{i}),' ');
% make variables for CS with mineral names
     myvariable = strcat(P_Name,'_CS');
     datavalues = CS{i};
% print variable names for CS
     eval([sprintf(myvariable) ' = CS{i};'])
     fprintf(' %s %s \n','Variable name =',myvariable);
   end
end

disp(' ')
disp(' Use mineral_CS to defined your CS in m-file ')
disp(' ')

% Calculate an ODF
odf_Quartz = calcDensity(ebsd('Quartz').orientations,'halfwidth',10*degree);

% Texture index
Jindex_Quartz = textureindex(odf_Quartz)
Mindex_Quartz = calcMIndex(odf_Quartz)

% Create list of pole figures with hkls 100,010,001
% MTEX cannot mix hkls and uvws
% pole to planes can be specified by the option 'pole' or 'hkl'
% directions are specified by the option 'uvw'
```

```
PFs_Quartz_hkil = [ ...
   Miller(0,0,0,1,Quartz_CS,'hkil','phase','Quartz'), ...
   Miller(1,1,-2,0,Quartz_CS,'hkil','phase','Quartz'), ...
   Miller(1,0,-1,0,Quartz_CS,'hkil','phase','Quartz'), ...
   Miller(1,0,-1,1,Quartz_CS,'hkil','phase','Quartz'), ...
   Miller(0,1,-1,1,Quartz_CS,'hkil','phase','Quartz'), ...
   Miller(-1,1,0,2,Quartz_CS,'hkil','phase','Quartz'), ...
   Miller(0,1,-1,2,Quartz_CS,'hkil','phase','Quartz')]
PFs_Quartz_uvtw = [ ...
   Miller(0,0,0,1,Quartz_CS,'uvtw','phase','Quartz'),...
   Miller(1,1,-2,0,Quartz_CS,'uvtw','phase','Quartz')]

% <0001> (c-axis), <11-20> (a-axis), {10-10} (prism {m}),
% {10-11}(positive rhomb {r}), {01-11} (negative rhomb {z}),
% {10-12} (positive acute rhomb {pi}), {01-12} (negative acute rhomb {pi'})

%%
% ***************************************************************************
% Plot Quartz Pole Figures (PFs) for (hkls) in Sample co-ordinates (X,Y,Z)
% One colorbar for all pole figures : use CLim(gcm,'equal')
% ***************************************************************************
close all
setMTEXpref('FontSize',14)

figure % upper hemisphere
plotPDF(ebsd('Quartz').orientations,PFs_Quartz_hkil,'antipodal',...
   'points','all', 'color','r','MarkerSize',4,'figSize','small')

figure % upper hemisphere
plotPDF(odf_Quartz,PFs_Quartz_hkil,'antipodal','resolution',5*degree,'figSize','small');
CLim(gcm,'equal') % single colorbar for all pole figures
colorbar
```

```
% add labels for X,Y and Z sample directions on PFs
% annotate([xvector,yvector,-
zvector],'label',{'X','Y','Z'},'backgroundcolor','w','MarkerSize',12,'FontSize',18);

% gray for publications
% colormap(white2blackColorMap)

% *************************************************************************
% Plot Quartz Pole Figures (PFs) for [uvws] in Sample co-ordinates (X,Y,Z)
% One colorbar for all pole figures : use CLim(gcm,'equal')
% *************************************************************************
setMTEXpref('FontSize',14)

figure % complete
plotPDF(ebsd('Quartz').orientations,PFs_Quartz_uvtw,'complete',...
   'points','all','MarkerSize',4,'figSize','small')

figure % complete
plotPDF(odf_Quartz,PFs_Quartz_uvtw,'complete','resolution',5*degree,'figSize','small');
CLim(gcm,'equal');colorbar

%%
% *************************************************************************
% Grain modelling
% *************************************************************************
% disp(' ')
% disp(' Grain segmentation angle option ')
% disp(' Choose a high angle typically between 15 to 10 degrees for geological samples')
% disp(' OR choose low angle of 2 degrees if you want to detect sub-grains')
% segmentation_angle = input('The segmentation angle (e.g. 2-15):');
segmentation_angle = 10;
segAngle = segmentation_angle*degree;
```

```
% disp(' ')
% disp(' Keep non-indexed points option ')
% disp('*1= Scientifically correct, not extrapolating raw indexed data')
% disp('    model grains BUT keep non-index points : Default in MTEX 4')
% disp(' 2= May be more geologically correct in some cases, use with care')
% disp('    model grains AND include non-index points within grains boundaries')
% disp('    N.B. this option does NOT ADD map pixels with neighbouring ORIENTATIONS')
% non_indexed_option = input('Option an integer  (1-2):');
non_indexed_option = 1;

% keep non-indexed in now default in MTEX4
if(non_indexed_option == 1)
   [grains,ebsd.grainId,ebsd.mis2mean] = calcGrains(ebsd,'angle',segAngle)
end

% remove non-indexed points, restrict to indexed points only
if(non_indexed_option == 2)
   [grains,ebsd.grainId,ebsd.mis2mean] = calcGrains(ebsd('indexed'),'angle',segAngle)
end

% number of grains all phases
number_of_calcGrains = grains.length

% plot 'grain' phase map
close all
figure
setMTEXpref('FontSize',12)
% Correct MatLab problem with colour buffer
set(gcf,'renderer','zbuffer')
plot(grains,'figSize','medium')

% Removing small grains - not representative small grains, may be errors
% disp(' ')
```

```
% disp(' Small grains option ')
% disp(' Remove small grains containing less than a critical')
% disp(' number of indexed points as they error prone or ')
% disp(' If you require an accurate grain size and shape analysis')
% disp(' the recommended minimum number indexed points per grain size is 10')
% disp(' You can decide to keep all grain by accepting all grains with 0')
% small_grains_option = input('Indexed points per grain an integer (e.g. 0-10):');
small_grains_option = 5;

% remove grains containing less than critical number of indexed points,
selected_grains = grains(grains.grainSize > small_grains_option)

% number of small grains removed from all phase
number_of_small_grains_removed = number_of_calcGrains - selected_grains.length

n_Quartz_grains = selected_grains('Quartz').length

figure
setMTEXpref('FontSize',12)
set(gcf,'renderer','zbuffer')
plot(selected_grains,'figSize','medium')

%%
% *************************************************************************
% Plot 'selected' Quartz Pole Figures (PFs) for [hkil] per grain
% in Sample co-ordinates (X,Y,Z)
% One colorbar for all pole figures : use CLim(gcm,'equal')
% *************************************************************************
% Calculate an ODF
odf_Quartz = calcDensity(selected_grains('Quartz').meanOrientation,'halfwidth',10*degree);

% Texture index
Jindex_Quartz = textureindex(odf_Quartz)
```

```
Mindex_Quartz = calcMIndex(odf_Quartz)

number_of_grains = length(selected_grains('Quartz'))

PFs_Quartz_hkil = [ ...
   Miller(0,0,0,1,Quartz_CS,'hkil','phase','Quartz'), ...
   Miller(1,1,-2,0,Quartz_CS,'hkil','phase','Quartz'), ...
   Miller(1,0,-1,0,Quartz_CS,'hkil','phase','Quartz'), ...
   Miller(1,0,-1,1,Quartz_CS,'hkil','phase','Quartz'), ...
   Miller(0,1,-1,1,Quartz_CS,'hkil','phase','Quartz'), ...
   Miller(-1,1,0,2,Quartz_CS,'hkil','phase','Quartz'), ...
   Miller(0,1,-1,2,Quartz_CS,'hkil','phase','Quartz')];
PFs_Quartz_uvtw = [ ...
   Miller(0,0,0,1,Quartz_CS,'uvtw','phase','Quartz'),...
   Miller(1,1,-2,0,Quartz_CS,'uvtw','phase','Quartz')];

% <0001> (c-axis), <11-20> (a-axis), {10-10} (prism {m}),
% {10-11}(positive rhomb {r}), {01-11} (negative rhomb {z}),
% {10-12} (positive acute rhomb {pi}), {01-12} (negative acute rhomb {pi'})

setMTEXpref('FontSize',14)
figure % upper hemisphere
plotPDF(selected_grains('Quartz').meanOrientation,PFs_Quartz_hkil,...
   'antipodal','points','all','MarkerSize',4,'figSize','small')

figure % upper hemisphere
plotPDF(odf_Quartz,PFs_Quartz_hkil,'antipodal','resolution',5*degree,'figSize','small');
CLim(gcm,'equal');colorbar

%%
% ***************************************************************************
% Select EBSD region of interest with your mouse: Polygonal region
% ***************************************************************************
```

```
figure
setMTEXpref('FontSize',15)
plot(selected_grains,'figSize','medium')

% selecting data points (not grains) by x,y coordinates
% Instructions for using the mouse
disp(' ')
disp('Define selected region of map using the curse and mouse')
disp('The last point does not need to exactly the first point')
disp('as the program ensures the polygon is closed')
disp('Left mouse button picks points')
disp('Right mouse button picks last point somewhere near the first point')
disp(' ')
region = selectPolygon;

% select region of polygon with condition

condition = inpolygon(ebsd,region);

% select EBSD data within region and printout to command window
ebsd_subregion = ebsd(condition)

% plot whole EBSD Orientation map with region of interest marked in red
% figure
plot(selected_grains,'figSize','medium')
hold on
plot(region(:,1),region(:,2),'r--','linewidth',2)
hold off

%%
% *************************************************************************
% Select EBSD region of interest with your mouse: Rectangle region
% *************************************************************************
```

```
figure
setMTEXpref('FontSize',15)
plot(selected_grains,'figSize','large')

% selecting data points (not grains) by x,y coordinates
% Instructions for using the mouse
disp(' ')
disp('Rubberband selection rectangle region')
disp('Drag mouse from top right corner with mouse')
disp('button pressed (down), release (up) button to define botton right corner')
disp(' ')
k = waitforbuttonpress; % Wait for key press or mouse-button click
point1 = get(gca,'CurrentPoint');    % button PRESS (down) detected
finalRect = rbbox;                   % return figure units
point2 = get(gca,'CurrentPoint');    % button RELEASE (up) detected
point1 = point1(1,1:2);              % extract x
point2 = point2(1,1:2);              %     and y
p1 = min(point1,point2);             % calculate locations
offset = abs(point1-point2);         % and dimensions
% EBSD map subregion
xy_subregion(1,:) = [p1(1) p1(1)+offset(1) p1(1)+offset(1) p1(1) p1(1)];
xy_subregion(2,:) = [p1(2) p1(2) p1(2)+offset(2) p1(2)+offset(2) p1(2)];
hold on
axis manual

% region = rectangle, N.B. transpose of xy_subregion
region = xy_subregion';

% draw selection rectangle
plot(region(:,1),region(:,2),'r--','linewidth',2)
hold off

% select region of rectangle with condition
```

```
condition = inpolygon(ebsd,region);

% select EBSD data within region and printout to command window
ebsd_subregion = ebsd(condition)

%%
% ************************************************************************
% Plot CPOs of data points (not grains!) in selected polygonal or rectangle subregion
% for (hkls) and [uvw] in Sample co-ordinates (X,Y,Z)
% One colorbar for all pole figures : use CLim(gcm,'equal') for subregion
% ************************************************************************
% Calculate an ODF
odf_Quartz = calcDensity(ebsd_subregion('Quartz').orientations,'halfwidth',10*degree);

% Texture index
Jindex_Quartz = textureindex(odf_Quartz)
Mindex_Quartz = calcMIndex(odf_Quartz)

number_of_dataPoints = length(ebsd_subregion('Quartz'))

PFs_Quartz_hkil = [ ...
   Miller(0,0,0,1,Quartz_CS,'hkil','phase','Quartz'), ...
   Miller(1,1,-2,0,Quartz_CS,'hkil','phase','Quartz'), ...
   Miller(1,0,-1,0,Quartz_CS,'hkil','phase','Quartz'), ...
   Miller(1,0,-1,1,Quartz_CS,'hkil','phase','Quartz'), ...
   Miller(0,1,-1,1,Quartz_CS,'hkil','phase','Quartz'), ...
   Miller(-1,1,0,2,Quartz_CS,'hkil','phase','Quartz'), ...
   Miller(0,1,-1,2,Quartz_CS,'hkil','phase','Quartz')];
PFs_Quartz_uvtw = [ ...
   Miller(0,0,0,1,Quartz_CS,'uvtw','phase','Quartz'),...
   Miller(1,1,-2,0,Quartz_CS,'uvtw','phase','Quartz')];

% <0001> (c-axis), <11-20> (a-axis), {10-10} (prism {m}),
```

```
% {10-11}(positive rhomb {r}), {01-11} (negative rhomb {z}),
% {10-12} (positive acute rhomb {pi}), {01-12} (negative acute rhomb {pi'})

setMTEXpref('FontSize',14)
figure % upper hemisphere
plotPDF(ebsd_subregion('Quartz').orientations,PFs_Quartz_hkil,'antipodal',...
    'points','all','MarkerSize',4,'figSize','small')

figure % upper hemisphere
plotPDF(odf_Quartz,PFs_Quartz_hkil,'antipodal','resolution',5*degree,'figSize','small');
CLim(gcm,'equal');colorbar

%%
% **************************************************************************
% Plot CPOs of grains (not data points!) in selected polygonal or rectangle subregion
% for (hkls) and [uvw] in Sample co-ordinates (X,Y,Z)
% One colorbar for all pole figures : use CLim(gcm,'equal') for subregion
% **************************************************************************
% remove all not indexed pixels
ebsd_subregion = ebsd_subregion('indexed');
% reconstruct grains
[grains,ebsd_subregion.grainId,ebsd_subregion.mis2mean] =
calcGrains(ebsd_subregion('indexed'),'angle',10*degree);
% remove two pixel grains (less than 5 pixels)
ebsd_subregion(grains(grains.grainSize<=5)) = [];
[grains,ebsd_subregion.grainId,ebsd_subregion.mis2mean] =
calcGrains(ebsd_subregion('indexed'),'angle',10*degree);
% smooth them
grains = grains.smooth

% Calculate an ODF
odf_Quartz = calcDensity(grains('Quartz').meanOrientation,'halfwidth',10*degree);
```

```
% Texture index
Jindex_Quartz = textureindex(odf_Quartz)
Mindex_Quartz = calcMIndex(odf_Quartz)

number_of_grains = length(grains('Quartz'))

PFs_Quartz_hkil = [ ...
   Miller(0,0,0,1,Quartz_CS,'hkil','phase','Quartz'), ...
   Miller(1,1,-2,0,Quartz_CS,'hkil','phase','Quartz'), ...
   Miller(1,0,-1,0,Quartz_CS,'hkil','phase','Quartz'), ...
   Miller(1,0,-1,1,Quartz_CS,'hkil','phase','Quartz'), ...
   Miller(0,1,-1,1,Quartz_CS,'hkil','phase','Quartz'), ...
   Miller(-1,1,0,2,Quartz_CS,'hkil','phase','Quartz'), ...
   Miller(0,1,-1,2,Quartz_CS,'hkil','phase','Quartz')];
PFs_Quartz_uvtw = [ ...
   Miller(0,0,0,1,Quartz_CS,'uvtw','phase','Quartz'),...
   Miller(1,1,-2,0,Quartz_CS,'uvtw','phase','Quartz')];

% <0001> (c-axis), <11-20> (a-axis), {10-10} (prism {m}),
% {10-11}(positive rhomb {r}), {01-11} (negative rhomb {z}),
% {10-12} (positive acute rhomb {pi}), {01-12} (negative acute rhomb {pi'})

setMTEXpref('FontSize',14)
figure % upper hemisphere
plotPDF(grains('Quartz').meanOrientation,PFs_Quartz_hkil,'antipodal',...
   'points','all','MarkerSize',4,'figSize','small')

figure % upper hemisphere
plotPDF(odf_Quartz,PFs_Quartz_hkil,'antipodal','resolution',5*degree,'figSize','small');
CLim(gcm,'equal');colorbar
```

### *A.2. MATLAB script for misorientation analysis*

```
%%
% ************************************************************************
% MTEX Script for EBSD Data
% Script set for misorientation analysis
%
% written by David Mainprice    31/10/2014 (MTEX ver.4.5.0)
% modified for Qtz 3/2/2022 (MTEX ver.5.8.0) on Matlab 2019b
% modified for Qtz 10/3/2022 (MTEX ver.5.8.0) on Matlab 2022a
% ************************************************************************
% Import of Oxford/HKL *.ctf (ASCII) file
% ************************************************************************

% clear memory and close plots - for new analysis of EBSD data
clear
close all

% Specify Crystal and Specimen Symmetries
% crystal symmetry
CS = {...
  'notIndexed',...
  crystalSymmetry('-3m1', [4.9 4.9 5.5], 'X||a*', 'Y||b', 'Z||c*', 'mineral', 'Quartz', 'color', [0.53
0.81 0.98])};

% specimen symmetry : the MTEX4 default is triclinic so do not need this line
SS = specimenSymmetry('triclinic');

% plotting convention
setMTEXpref('xAxisDirection','east'); % 'west'
setMTEXpref('zAxisDirection','intoPlane'); % 'outOfPlane'

% Specify File Names
% path to files
```

```
pname = '/C:\Users\henry\Desktop\EBSD\EBSD\AWI_3_001';
% which files to be imported
fname = [pname '\AWI_3_001.ctf'];

% Import the Data
% create an EBSD variable containing the data
ebsd = EBSD.load(fname,CS,'interface','ctf','convertEuler2SpatialReferenceFrame','wizard');

% take only those measurements with MAD (Mean Angular Deviation) smaller then 1.0
ebsd = ebsd(ebsd.mad<1)

% ******************************************************************************
% Calculate an ODF
% ******************************************************************************
% Generate simple Crystal Symmetry variables for all phases
fprintf(' \n');
fprintf(' Crystal Symmetry (CS) : names of variables \n');
fprintf(' \n');

% phase names
Phase_names = ebsd.mineralList;

for i=1:length(CS)
% indexed point for mineral
    N_Points = length(ebsd(Phase_names(i)));
% print only indexed phases
   if((~strcmpi(Phase_names{i},'notIndexed')) && (N_Points > 0))
% retain first part of mineral name
     P_Name = strtok(char(Phase_names{i}),' ');
% make variables for CS with mineral names
     myvariable = strcat(P_Name,'_CS');
     datavalues = CS{i};
% print variable names for CS
```

```
   eval([sprintf(myvariable) ' = CS{i};'])
   fprintf(' %s %s \n','Variable name =',myvariable);
  end
end

disp(' ')
disp(' Use mineral_CS to defined your CS in m-file ')
disp(' ')

% Calculate an ODF
odf_Quartz = calcDensity(ebsd('Quartz').orientations,'halfwidth',10*degree);

% Texture index
% Jindex_Quartz = textureindex(odf_Quartz)
% Mindex_Quartz = calcMIndex(odf_Quartz)

% Create list of pole figures with hkls 100,010,001
% MTEX cannot mix hkls and uvws
% pole to planes can be specified by the option 'pole' or 'hkl'
% directions are specified by the option 'uvw'

PFs_Quartz_hkil = [ ...
  Miller(0,0,0,1,Quartz_CS,'hkil','phase','Quartz'), ...
  Miller(1,1,-2,0,Quartz_CS,'hkil','phase','Quartz'), ...
  Miller(1,0,-1,0,Quartz_CS,'hkil','phase','Quartz'), ...
  Miller(1,0,-1,1,Quartz_CS,'hkil','phase','Quartz'), ...
  Miller(0,1,-1,1,Quartz_CS,'hkil','phase','Quartz'), ...
  Miller(-1,1,0,2,Quartz_CS,'hkil','phase','Quartz'), ...
  Miller(0,1,-1,2,Quartz_CS,'hkil','phase','Quartz')]
PFs_Quartz_uvtw = [ ...
  Miller(0,0,0,1,Quartz_CS,'uvtw','phase','Quartz'),...
  Miller(1,1,-2,0,Quartz_CS,'uvtw','phase','Quartz')]
```

```
% <0001> (c-axis), <11-20> (a-axis), {10-10} (prism {m}),
% {10-11}(positive rhomb {r}), {01-11} (negative rhomb {z}),
% {10-12} (positive acute rhomb {pi}), {01-12} (negative acute rhomb {pi'})

%%
% ************************************************************************
% Grain modelling
% ************************************************************************

% set angles of low- and high-angle boundaries
% low-abgle subgrain boundary=1; high-angle grain boundary=10

% disp(' ')
% disp(' Keep non-indexed points option '
% disp('*1= Scientifically correct, not extrapolating raw indexed data')
% disp('    model grains BUT keep non-index points : Default in MTEX 4')
% disp(' 2= May be more geologically correct in some cases, use with care')
% disp('    model grains AND include non-index points within grains boundaries')
% disp('    N.B. this option does NOT ADD map pixels with neighbouring ORIENTATIONS')
% non_indexed_option = input('Option an integer  (1-2):');
non_indexed_option = 1;

% keep non-indexed in now default in MTEX4
if(non_indexed_option == 1)
   [grains,ebsd.grainId,ebsd.mis2mean] = calcGrains(ebsd,'threshold',[1*degree,10*degree])
   % [grains,ebsd.grainId,ebsd.mis2mean] = calcGrains(ebsd,'angle',10*degree)
end

% remove non-indexed points, restrict to indexed points only
if(non_indexed_option == 2)
   [grains,ebsd.grainId,ebsd.mis2mean] =
calcGrains(ebsd('indexed'),'threshold',[1*degree,10*degree])
   % [grains,ebsd.grainId,ebsd.mis2mean] = calcGrains(ebsd('indexed'),'angle',10*degree)
```

```
end

% number of grains all phases
number_of_calcGrains = grains.length

% plot 'grain' phase map
close all
figure
% Correct MatLab problem with colour buffer
set(gcf,'renderer','zbuffer')
plot(grains,'figSize','medium')

% Removing small grains - not representative small grains, may be errors
% disp(' ')
% disp(' Small grains option ')
% disp(' Remove small grains containing less than a critical')
% disp(' number of indexed points as they error prone or ')
% disp(' If you require an accurate grain size and shape analysis')
% disp(' the recommended minimum number indexed points per grain size is 10')
% disp(' You can decide to keep all grain by accepting all grains with 0')
% small_grains_option = input('Indexed points per grain an integer (e.g. 0-10):');
small_grains_option = 5;

% remove grains containing less than critical number of indexed points,
selected_grains = grains(grains.grainSize > small_grains_option);

% number of small grains removed from all phase
number_of_small_grains_removed = number_of_calcGrains - selected_grains.length

%n_Quartz_grains = selected_grains('Quartz').length
% close all
figure
% Correct MatLab problem with colour buffer
```

```
set(gcf,'renderer','zbuffer')
plot(selected_grains,'figSize','medium')

%%
% ************************************************************************
% Orientation, misorientation of grains
% ************************************************************************
% Rotation ANGLE of mean orientation of each grain from reference orientation
% Uniform colour for each grain mean orientation
% get all rotations of mean rotation from the reference orientation
% using all ebsd indexed points inside grains

Mean_rotations = selected_grains('Quartz').meanRotation;
figure
plot(selected_grains('Quartz'),angle(Mean_rotations)/degree,'figSize','large')
colorbar

%% Misorientation ANGLE from mean within a grain
% get all misorientations from the mean orientation
% using all ebsd indexed points inside grains
% error message non-existent field 'mis2meanRotation' if you have not used
% new syntax [grains ebsd] = calcGrains(ebsd)

% ignore grain boundary misorientations
% [grains,ebsd.grainId] = calcGrains(ebsd)
% selected_grains = grains(grains.grainSize > small_grains_option);

figure
plot(ebsd(selected_grains('Quartz')),...
   ebsd(selected_grains('Quartz')).mis2mean.angle./degree,'figSize','medium')

% caxis - allows you focus the scale of the angle range of interest
% example 0 to 5 degrees
```

```
% caxis([0 10])
% mtexColorbar

hold on
plot(selected_grains.boundary)

%% Misorientation AXIS from mean within a grain
% get all misorientations from the mean orientation using all ebsd indexed points inside grains
oM = ipfHSVKey(ebsd(selected_grains('Quartz')))

figure
plot(ebsd(selected_grains('Quartz')),...
   oM.Miller2Color(ebsd(selected_grains('Quartz')).mis2mean.axis),'figSize','medium')

hold on
plot(selected_grains.boundary)

% caxis - allows you focus the scale of the range of interest
% does not work with this plot, must be normalied colour scale caxis([0 30])

% Orientation IPF colourbar plot
% Orthorhombic with Quartz symmetry and r = x = 1,0,0
figure
plot(oM,'figSize','small')

%% Kernel Average Misorientation (KAM)
% Intragranular average misorientation angle per orientation
% plot(ebsd('Quartz'),ebsd('Quartz').KAM./ degree)

% ignore grain boundary misorientations
% [grains,ebsd.grainId] = calcGrains(ebsd)
% selected_grains = grains(grains.grainSize > small_grains_option);
```

```
% ignore misorientation angles > threshold
% consider also second order neigbors
kam = KAM(ebsd(selected_grains('Quartz')),'threshold',10*degree,'order',2);

figure
plot(ebsd(selected_grains('Quartz')),kam./degree,'figSize','medium')
mtexColorbar
% setColorRange([0 2],'zerowhite')

hold on
plot(selected_grains.boundary)

%% Grain Orientation Spread (GOS)
% Intragranular average of misorientation angles to grain mean orientation
% plot(ebsd('Quartz'),ebsd('Quartz').GOS./ degree)

% ignore grain boundary misorientations
% [grains,ebsd.grainId] = calcGrains(ebsd)
% selected_grains = grains(grains.grainSize > small_grains_option);

% take the avarage of the misorientation angles for each grain
gos=selected_grains('Quartz').GOS/degree;

figure
plot(selected_grains('Quartz'),gos,'figSize','medium')
mtexColorbar
setColorRange([0 10],'zerowhite')

hold on
plot(selected_grains.boundary)


%%
```

```
% ************************************************************************
% Plot all grains and select a grain using the a curser on the phase map and plot all pixels
% ************************************************************************

% set angles of low- and high-angle boundaries
% low-abgle subgrain boundary=1; high-angle grain boundary=10

% disp(' ')
% disp(' Keep non-indexed points option ')
% disp('*1= Scientifically correct, not extrapolating raw indexed data')
% disp('    model grains BUT keep non-index points : Default in MTEX 4')
% disp(' 2= May be more geologically correct in some cases, use with care')
% disp('    model grains AND include non-index points within grains boundaries')
% disp('    N.B. this option does NOT ADD map pixels with neighbouring ORIENTATIONS')
% non_indexed_option = input('Option an integer  (1-2):');
non_indexed_option = 1;

% keep non-indexed in now default in MTEX4
if(non_indexed_option == 1)
   [grains,ebsd.grainId,ebsd.mis2mean] = calcGrains(ebsd,'threshold',[1*degree,10*degree])
end

% remove non-indexed points, restrict to indexed points only
if(non_indexed_option == 2)
   [grains,ebsd.grainId,ebsd.mis2mean] =
calcGrains(ebsd('indexed'),'threshold',[1*degree,10*degree])
end

% number of grains all phases
number_of_calcGrains = grains.length

% plot 'grain' phase map
close all
```

```
% figure
% Correct MatLab problem with colour buffer
% set(gcf,'renderer','zbuffer')
% Default phase map
% plot(grains,'figSize','small')

% Removing small grains - not representative small grains, may be errors
close all
% disp(' ')
% disp(' Small grains option ')
% disp(' Remove small grains containing less than a critical')
% disp(' number of indexed points as they error prone or ')
% disp(' If you require an accurate grain size and shape analysis')
% disp(' the recommended minimum number indexed points per grain size is 10')
% disp(' You can decide to keep all grain by accepting all grains with 0')
% small_grains_option = input('Indexed points per grain an integer (e.g. 0-10):');
small_grains_option = 5;

% remove grains containing less than critical number of indexed points,
selected_grains = grains(grains.grainSize > small_grains_option);
% number of small grains removed from all phase
number_of_small_grains_removed = number_of_calcGrains - selected_grains.length
%n_Quartz_grains = selected_grains('Quartz').length
figure
% Correct MatLab problem with colour buffer
set(gcf,'renderer','zbuffer')
% MTEX 4 default map is phase map
plot(selected_grains,'figSize','medium')

% selecting a single grain by x,y coordinates
disp(' ')
disp('Select grain with cursor and one mouse click')
disp(' ')
```

```
% Displays a cursor over the map and waits for one click on the selected grain
[xgg, ygg] = ginput(1)
% select single grain
%selected_single_grain = findByLocation(grains,[xgg  ygg])
selected_single_grain = selected_grains(xgg,ygg);
% grain id
grain_id = selected_single_grain.id
% grain centroid
[centroid_x,centroid_y] = centroid(selected_single_grain)

% plot selected grain : boundary and misorientation from mean orientation
close all
% plot grain boundary outline
plot(selected_single_grain.boundary,'linewidth',2,'figSize','medium')
hold on
% plot ebsd orientation pixels
plot(ebsd(selected_single_grain),ebsd(selected_single_grain).mis2mean.angle./degree,...
   'figSize','small')
% plot grain centroid
% plot(centroid_x,centroid_y,'MarkerEdgeColor','k','MarkerFaceColor','r','MarkerSize',10)
hold off
mtexColorbar
% mean orientation of selected single grain
grain_mean_orientation = selected_single_grain.meanOrientation

% plot crystallographic axes
figure
plotPDF(ebsd(selected_single_grain).orientations,PFs_Quartz_hkil,'antipodal',...
   'points','all','MarkerSize',4,'figSize','small')
figure
plotPDF(ebsd(selected_single_grain).orientations,PFs_Quartz_hkil,'antipodal',....
   'lower','points','all','MarkerSize',4,'figSize','small')
figure
```

```
plotPDF(ebsd(selected_single_grain).orientations,PFs_Quartz_uvtw,'antipodal',...
   'points','all','MarkerSize',4,'figSize','small')
figure
plotPDF(ebsd(selected_single_grain).orientations,PFs_Quartz_uvtw,'antipodal',...
   'lower','points','all','MarkerSize',4,'figSize','small')
% bnd_Quartz=grains.boundary(selected_single_grain,'Quartz','Quartz')
% figure
% plotAxisDistribution(bnd_Quartz.misorientation,'antipodal','points','all','MarkerSize',5)

%%
%orientation map one mineral with Euler RGB colormap: uses colours in ODF sections
% define the RGB to Bunge Euler angles to RGB orientation colormap
oM = BungeColorKey(ebsd(selected_single_grain))

figure
plot(ebsd(selected_single_grain),oM.orientation2color(ebsd(selected_single_grain).orientations),
'figSize','medium')
title('All Euler','FontSize',14)

% Orientation colour bar plot - euler angle ODF sections
% figure
% plot(oM)

%%
% ************************************************************************
% Misorientation line profile in a grain
% ************************************************************************
% plot selected grain : boundary and misorientation from mean orientation
close all

% plot grain boundary outline
plot(selected_single_grain.boundary,'linewidth',2,'figSize','large')
hold on
```

```
% plot ebsd orientation pixels
plot(ebsd(selected_single_grain),ebsd(selected_single_grain).mis2mean.angle./degree,...
    'figSize','large')
hold on

% Define profile
disp(' ')
disp('Define misorientation profile: Two mouse clicks, one at each end of the profile')
disp('NB!!: Misorientation profile should be along horizonttal or vertical line')
disp(' ')

% Displays a cursor over the map and waits for 2 mouse clicks for the start
% and for the end of the line, respectively
[X_line, Y_line] = ginput(2);

% profile line
XYprofile =  [X_line(1) Y_line(1); X_line(2)  Y_line(2)];
line(XYprofile(:,1),XYprofile(:,2),'linewidth',2,'color','white')
hold off

% Plot orientation difference profile
% extract orientations along XYprofile
ebsd_line = spatialProfile(ebsd(selected_single_grain),XYprofile)

% Calcluate misorientation angle along XYprofile and plot results
% NB!!: We can only plot for X1-X2 or Y1-Y2 profile
Figure
% Misorientation with respect the first point along profile
plot(ebsd_line.x,...
  angle(ebsd_line(1).orientations,ebsd_line.orientations)/degree,'color','b') % for horozontal line
%plot(ebsd_line.y,...
  angle(ebsd_line(1).orientations,ebsd_line.orientations)/degree,'color','b') % for vertical line
```

```
% Misorientation with respect the neighbouring point along profile (orientation gradient)
hold all
plot(0.5*(ebsd_line.x(1:end-1)+ebsd_line.x(2:end)),...
   angle(ebsd_line(1:end-1).orientations,ebsd_line(2:end).orientations)/degree,'color','r') % for
horozontal line
%plot(0.5*(ebsd_line.y(1:end-1)+ebsd_line.y(2:end)),...
%  angle(ebsd_line(1:end-1).orientations,ebsd_line(2:end).orientations)/degree,'color','r') % for
vertical line
xlabel('Position (microns)','FontSize',12)
ylabel('Orientation difference in degrees','FontSize',12)
title('Orientation difference profile','FontSize',12)
legend('to reference orientation','orientation gradient','Location','northwest')
hold off

%%
% ************************************************************************
% Plot the orientations along this line into inverse pole figures and
% colorize them according to their y (or x)-coordinate
% ************************************************************************
ori_1 = ebsd_line(1:end-1).orientations
ori_2 = ebsd_line(2:end).orientations

% misorientation axis with respect to crystal coordinate system
% mori_cc = axis(inv(ori_1).*ori_2,crystalSymmetry('trigonal'))
% mori_cc = axis(inv(ori_1).*ori_2,crystalSymmetry('triclinic'))
mis12 = inv(ori_1).*ori_2,crystalSymmetry('trigonal')
mori_cc = mis12.axis
length(mori_cc)

mis12_angle=angle(ori_1,ori_2)./degree
length(mis12_angle)
```

```
mis12_angle_L=4


% misorientation axis with respect to sample coordinate system
mori_sc = axis(ori_1,ori_2)
length(mori_sc)


figure
density = calcDensity(mori_cc,'halfwidth',10*degree);
plot(density,'fundamentalRegion','figSize','small')
mtexColorbar


hold on
plot(mori_cc,'markersize',6,'antipodal','figSize','small')
hold on
plot(mori_cc(mis12_angle > mis12_angle_L),'markersize',8,'antipodal','figSize','small')
% title('crystal coordinate','FontSize',10)


cs = crystalSymmetry('-3m1', [4.913 4.913 5.504],[90,90,120]*degree,...
  'X||a*','Y||b','Z||c','mineral','Quartz')
cd_Quartz_hkil = ...
  [Miller(0,0,0,1,cs,'hkil'),Miller(-2,2,0,1,cs,'hkil'),Miller(-1,1,0,1,cs,'hkil'),...
  Miller(-1,1,0,0,cs,'hkil'),Miller(-1,2,-1,2,cs,'hkil'),Miller(-1,2,-1,0,cs,'hkil'),...
  Miller(0,1,-1,1,cs,'hkil'),Miller(0,2,-2,1,cs,'hkil'),Miller(0,1,-1,0,cs,'hkil'),...
  Miller(-1,1,0,2,cs,'hkil'),Miller(0,1,-1,2,cs,'hkil'),Miller(-1,0,1,0,cs,'hkil'),...
  Miller(-2,0,2,1,cs,'hkil'),Miller(-1,0,1,1,cs,'hkil'),Miller(-2,1,1,2,cs,'hkil'),...
  Miller(-2,1,1,0,cs,'hkil'),Miller(-1,0,1,2,cs,'hkil')]
hold on
plot(cd_Quartz_hkil,'markersize',4,'labeled','MarkerFaceColor','k')


figure
plot(mori_sc,'markersize',6,'antipodal','figSize','small')
hold on
plot(mori_sc(mis12_angle > mis12_angle_L),'markersize',8,'antipodal','figSize','small')
```

```
% title('sample coordinate','FontSize',10)

%%
% ****************************************************************************************
% Misorientation analysis for a selected single grain below *degrees
% ****************************************************************************************

figure
% plot the ebsd data (IPF)
plot(ebsd(selected_single_grain),ebsd(selected_single_grain).orientations,'faceAlpha',0.5,'figSize','medium')
hold on
% plot grain boundaries
plot(selected_single_grain.boundary,'linewidth',2,'linecolor','k')
% compute transparency from misorientation angle
alpha=selected_single_grain.innerBoundary.misorientation.angle/(5*degree);
% plot the subgrain boundaries
plot(selected_single_grain.innerBoundary,'linewidth',1.5,'edgeAlpha',alpha,'linecolor','b');
hold off

% number of low-angle boundary segments inside each grain
% figure
% plot(selected_single_grain,selected_single_grain.subBoundarySize./selected_single_grain.grainSize)
% mtexColorbar

% density of low-angle boundaries per grain as the length of the subgrain boundaries divided by the grain area
% figure
% plot(grains, grains.subBoundaryLength ./ grains.area)
% mtexColorbar
```

```
% extract all subgrain boundary misorientation below * degrees
mori =
selected_single_grain.innerBoundary(selected_single_grain.innerBoundary.misorientation.angle
/degree<10,selected_single_grain.innerBoundary.misorientation.angle/degree>=2).misorientati
on;

figure
% and visualize the distribution of the misorientation axes
% plot(mori.axis,'fundamentalRegion','contourf','LineStyle','none','figSize','medium')
density = calcDensity(mori.axis,'halfwidth',10*degree);
plot(density,'fundamentalRegion','figSize','medium')
mtexColorbar

hold on
% plot crystal direction
% cs=crystalSymmetry('-3m1',[4.913 4.913 5.504],[90,90,120]*degree,...
% 'X||a*','Y||b','Z||c','mineral','Quartz')
cs=crystalSymmetry('-3m1',[4.9 4.9 5.5],'X||a*','Y||b','Z||c*',...
    'mineral','Quartz')

cd_Quartz_hkil = ...
  [Miller(0,0,0,1,cs,'hkil'),Miller(-2,2,0,1,cs,'hkil'),Miller(-1,1,0,1,cs,'hkil'),...
  Miller(-1,1,0,0,cs,'hkil'),Miller(-1,2,-1,2,cs,'hkil'),Miller(-1,2,-1,0,cs,'hkil'),...
  Miller(0,1,-1,1,cs,'hkil'),Miller(0,2,-2,1,cs,'hkil'),Miller(0,1,-1,0,cs,'hkil'),...
  Miller(-1,1,0,2,cs,'hkil'),Miller(0,1,-1,2,cs,'hkil')]
plot(cd_Quartz_hkil,'labeled','MarkerFaceColor','red')

% <0001> (c-axis), <11-20> (a-axis), {10-10} (prism {m}),
% {10-11}(positive rhomb {r}), {01-11} (negative rhomb {z}),
% {10-12} (positive acute rhomb {pi}), {01-12} (negative acute rhomb {pi'})

%%
% ************************************************************************
```

```
% Misorientation analysis for a selected single grain: Tilt and twist boundaries
% ************************************************************************
% extract subgrain boundaries
subGB =
selected_single_grain.innerBoundary(selected_single_grain.innerBoundary.misorientation.angle
/degree<=10,selected_single_grain.innerBoundary.misorientation.angle/degree>=2);

% plot the misorientation axes in the fundamental sector
figure
plot(subGB.misorientation.axis,'fundamentalRegion','figSize','small')

% compute and plot the density distribution of misorientation axes
figure
density = calcDensity(subGB.misorientation.axis,'halfwidth',10*degree);
plot(density,'figSize','small')
mtexColorbar

% find the two prefered misorientation axes
[~,hkil] = max(density,'numLocal',2); round(hkil)

% compute and plot the misorientation axis in specimen coordinates
oriGB = ebsd('id',subGB.ebsdId).orientations
axS = axis(oriGB(:,1),oriGB(:,2),'antipodal')

figure
plot(axS,'MarkerAlpha',0.2,'MarkerSize',2,'figSize','small')

density = calcDensity(axS,'halfwidth',10*degree);
figure
plot(density,'figSize','small')
mtexColorbar

[~,pos] = max(density)
```

```
annotate(pos)

% We colorize in the following plot all subgrain boundaries according to the angle between
% the boundary trace and the misorientation axis. Blue subgrain boundaries are
% very likely tilt boundaries, while red subgrain boundaries are can be either tilt or twist boundaries.
figure
plot(ebsd(selected_single_grain),'faceAlpha',0.5,'figSize','large')

% init override mode
hold on

% plot grain boundares
% plot(grains.boundary,'linewidth',2)

% colorize the subgrain boundaries according the angle between boundary
% trace and misorientation axis
plot(subGB,angle(subGB.direction,axS)./degree,'linewidth',2)
mtexColorMap blue2red
mtexColorbar

hold off

%%
% ***************************************************************************
% Misorientation analysis for all area of the specimen
% ***************************************************************************
% set angles of low- and high-angle boundaries
% low-abgle subgrain boundary=1; high-angle grain boundary=10
[grains,ebsd.grainId,ebsd.mis2mean]=calcGrains(ebsd('indexed'),'threshold',[1*degree,10*degree]);

% get the misorientations to mean
```

```
mori=ebsd('Quartz').mis2mean

% plot a histogram of the misorientation angles
close all
plotAngleDistribution(mori,'figSize','medium')
xlabel('Misorientation angles in degree')

plot(ebsd('Quartz'),ebsd('Quartz').mis2mean.angle./degree,'figSize','medium')
mtexColorMap WhiteJet
mtexColorbar
hold on
plot(grains.boundary,'edgecolor','k','linewidth',.5,'figSize','medium')
hold off

%% Correlated misorientation angle distribution between two adjacent pixels in a selected
single grain
figure
plotAngleDistribution(selected_single_grain.innerBoundary.misorientation,...
   'DisplayName','Misorientation angle between two adjacent pixels','figSize','small')
legend('show','Location','northeast')



%% Boundary misorientation map
figure
plot(grains,'figSize','medium')
hold on

bnd_Quartz=grains.boundary('Quartz','Quartz')
plot(bnd_Quartz,'linecolor','r','figSize','medium')
hold off

%% Correlated misorientation angle distribution between two adjacent grains
figure
```

```
plotAngleDistribution(grains.boundary('Quartz','Quartz').misorientation,...
    'DisplayName','Quartz-Quartz','figSize','small')
legend('show','Location','northwest')

%% Uncorrelated misorientation angle distribution
% compute uncorrelated misorientations
mori=calcMisorientation(ebsd('Quartz'),ebsd('Quartz'));

figure
% plot the angle distribution
plotAngleDistribution(mori,'DisplayName','Quartz-Quartz','figSize','small')

hold on
plotAngleDistribution(odf_Quartz.CS,odf_Quartz.CS,'DisplayName','untextured')
hold off
legend('-dynamicLegend','Location','northwest') % update legend

%% Axis distribution
close all
mori=calcMisorientation(ebsd('Quartz'));
number_of_mori = length(mori)

figure
mtexFig=newMtexFigure;
plotAxisDistribution(mori,'smooth','parent',mtexFig.gca)
mtexTitle('uncorrelated axis distribution')
mtexFig.drawNow('figSize','normal')
mtexColorbar

% figure
% plotAxisDistribution(mori,'antipodal','points','all','MarkerSize',2)
% title('uncorrelated axis distribution','FontSize',12)
```

```
% selected misorientation angle intervals
selected_mori_a = mori(angle(mori) > 1/360*(2*pi) & angle(mori) <= 10/360*(2*pi));
number_of_selected_mori_a = length(selected_mori_a)

selected_mori_b = mori(angle(mori) > 10/360*(2*pi) & angle(mori) <= 20/360*(2*pi));
number_of_selected_mori_b = length(selected_mori_b)

selected_mori_c = mori(angle(mori) > 20/360*(2*pi) & angle(mori) <= 30/360*(2*pi));
number_of_selected_mori_c = length(selected_mori_c)

selected_mori_d = mori(angle(mori) > 30/360*(2*pi) & angle(mori) <= 90/360*(2*pi));
number_of_selected_mori_d = length(selected_mori_d)

selected_mori_e = mori(angle(mori) > 175/360*(2*pi) & angle(mori) <= 180/360*(2*pi));
number_of_selected_mori_e = length(selected_mori_e)

figure
plotAxisDistribution(selected_mori_a,'antipodal','points','all','MarkerSize',8,...
   'MarkerFaceColor','red')
mtexTitle('uncorrelated axis distribution 2-10:R 11-20:G 21-30:B')
hold on
plotAxisDistribution(selected_mori_b,'antipodal','points','all','MarkerSize',4,...
   'MarkerFaceColor','green')
mtexColorbar
hold off

bnd_Quartz=grains.boundary('Quartz','Quartz')

figure
mtexFig = newMtexFigure;
plotAxisDistribution(bnd_Quartz.misorientation,'antipodal','points','all','MarkerSize',2)
mtexTitle('boundary axis distribution','FontSize',12)
mtexFig.drawNow('figSize','normal')
```

```
hold on

mtexFig.nextAxis
plotAxisDistribution(bnd_Quartz.misorientation,'smooth','parent',mtexFig.gca)
mtexTitle('boundary axis distribution')
mtexColorbar

%%
% **********************************************************************************
% Axis distribution of uncorrelated and correlated misorientation
% for selected_grains
% **********************************************************************************
% close all

grains = calcGrains(ebsd,'angle',10*degree)

bnd_Quartz = grains.boundary('Quartz','Quartz')

bnd_Quartz.misorientation

figure
plot(ebsd('Quartz'),'figsize','medium')

hold on
plot(bnd_Quartz,'figsize','medium','linecolor','red')
plot(bnd_Quartz,bnd_Quartz.misorientation.angle./degree,'figsize','medium','linewidth',2)
mtexColorMap blue2red
mtexColorbar
hold off

%%
% input specific angle intervals
disp('Input the angle intergals for misorientation analysis')
```

```
angle_lower_limit = input('Angle intervals lower limit (>10):');
angle_upper_limit = input('Angle intervals upper limit (<180):');

selected_bnd_Quartz = bnd_Quartz(bnd_Quartz.misorientation.angle >
angle_lower_limit*degree &...
    bnd_Quartz.misorientation.angle < angle_upper_limit*degree);

figure
mtexFig = newMtexFigure;
mori = calcMisorientation(ebsd('Quartz'),ebsd('Quartz'));
selected_mori = mori(angle(mori) > angle_lower_limit/360*(2*pi) & angle(mori) <
angle_upper_limit/360*(2*pi));
%plotAxisDistribution(selected_mori,'smooth','parent',mtexFig.gca)
plotAxisDistribution(selected_mori,'antipodal','smooth','parent',mtexFig.gca)
mtexTitle('uncorrelated axis distribution')
mtexFig.drawNow('figSize','normal')
hold on

% plot crystal direction
  cs = crystalSymmetry('-3m1', [4.913 4.913 5.504],[90,90,120]*degree,...
  'X||a*','Y||b','Z||c','mineral','Quartz')

% cd_Quartz_uvtw = ...
%  [Miller(0,0,0,1,cs,'uvtw'),Miller(1,1,-2,0,cs,'uvtw')] % <0001> (c-axis), <11-20> (a-axis)
cd_Quartz_hkil = ...
  [Miller(0,0,0,1,cs,'hkil'),Miller(-2,2,0,1,cs,'hkil'),Miller(-1,1,0,1,cs,'hkil'),...
  Miller(-1,1,0,0,cs,'hkil'),Miller(-1,2,-1,2,cs,'hkil'),Miller(-1,2,-1,0,cs,'hkil'),...
  Miller(0,1,-1,1,cs,'hkil'),Miller(0,2,-2,1,cs,'hkil'),Miller(0,1,-1,0,cs,'hkil'),...
  Miller(-1,1,0,2,cs,'hkil'),Miller(0,1,-1,2,cs,'hkil')]

% plot(cd_Quartz_uvtw,'labeled','MarkerFaceColor','black')
plot(cd_Quartz_hkil,'labeled','MarkerFaceColor','red')
% hold on
```

```
% plot(cd_Quartz_hkil,'plane','linecolor','red','linewidth',1)

mtexFig.nextAxis
plotAxisDistribution(selected_bnd_Quartz.misorientation,'smooth','parent',mtexFig.gca)
%
plotAxisDistribution(selected_bnd_Quartz.misorientation,'antipodal','points','all','MarkerSize',2)
mtexTitle('boundary axis distribution')
mtexColorbar
hold on
% plot(cd_Quartz_uvtw,'labeled','MarkerFaceColor','black')
% plot(cd_Quartz_hkil,'plane','linecolor','red','linewidth',1)
plot(cd_Quartz_hkil,'labeled','MarkerFaceColor','red')

%%

%%
% ************************************************************************
% plot crystal direction (full)
% Considering the common slip systems of quartz, the following directions
% and planes have been plotted:
% <0001> (c-axis), <11-20> (a-axis), {10-10} (prism {m}),
% {10-11}(positive rhomb {r}), {01-11} (negative rhomb {z}),
% {10-12} (positive acute rhomb {pi}), {01-12} (negative acute rhomb {pi'})
% *************************************************************************
cs = crystalSymmetry('-3m1', [4.913 4.913 5.504],[90,90,120]*degree,...
  'X||a*','Y||b','Z||c','mineral','Quartz')

cd_Quartz_uvtw = ...
  [Miller(0,0,0,1,cs,'uvtw'),Miller(1,1,-2,0,cs,'uvtw')]
cd_Quartz_hkil = ...
  [Miller(0,0,0,1,cs,'hkil'),Miller(-2,2,0,1,cs,'hkil'),Miller(-1,1,0,1,cs,'hkil'),...
  Miller(-1,1,0,0,cs,'hkil'),Miller(-1,2,-1,2,cs,'hkil'),Miller(-1,2,-1,0,cs,'hkil'),...
  Miller(0,1,-1,1,cs,'hkil'),Miller(0,2,-2,1,cs,'hkil'),Miller(0,1,-1,0,cs,'hkil'),...
```

```
  Miller(-1,1,0,2,cs,'hkil'),Miller(0,1,-1,2,cs,'hkil')]

figure
plot(cd_Quartz_uvtw,'labeled','MarkerFaceColor','black')
hold on
plot(cd_Quartz_hkil,'labeled','MarkerFaceColor','red')

figure
plot(cd_Quartz_uvtw,'upper','labeled','MarkerFaceColor','black')
hold on
plot(cd_Quartz_hkil,'upper','labeled','MarkerFaceColor','red')

figure
plot(cd_Quartz_uvtw,'antipodal','labeled','MarkerFaceColor','black')
hold on
plot(cd_Quartz_hkil,'antipodal','labeled','MarkerFaceColor','red')

%%
% *************************************************************************
% plot crystal direction (selected)
% **************************************************************************
  cs = crystalSymmetry('-3m1', [4.913 4.913 5.504],[90,90,120]*degree,...
  'X||a*','Y||b','Z||c','mineral','Quartz')

cd_Quartz_uvtw = ...
  [Miller(0,0,0,1,cs,'uvtw'),Miller(1,1,-2,0,cs,'uvtw')]
cd_Quartz_hkil = ...
  [Miller(0,0,0,1,cs,'hkil'),Miller(-2,2,0,1,cs,'hkil'),Miller(-1,1,0,1,cs,'hkil'),...
  Miller(-1,1,0,0,cs,'hkil'),Miller(-1,2,-1,2,cs,'hkil'),Miller(-1,2,-1,0,cs,'hkil'),...
  Miller(0,1,-1,1,cs,'hkil'),Miller(0,2,-2,1,cs,'hkil'),Miller(0,1,-1,0,cs,'hkil'),...
  Miller(-1,1,0,2,cs,'hkil'),Miller(0,1,-1,2,cs,'hkil')]

figure
```

```
% plot(cd_Quartz_uvtw,'labeled','MarkerFaceColor','black')
plot(cd_Quartz_uvtw,'upper','antipodal','labeled','MarkerFaceColor','black')
% hold on
plot(cd_Quartz_hkil,'upper','plane','linecolor','red','linewidth',1)
hold on

% plot(cd_Quartz_hkil,'plane','linecolor','red','linewidth',1)
plot(cd_Quartz_uvtw,'upper','antipodal','labeled','MarkerFaceColor','black')
plot(cd_Quartz_hkil,'upper','antipodal','labeled','MarkerFaceColor','red')

%%
% *************************************************************************
% plot crystal direction (use for checking)
% *************************************************************************
  cs = crystalSymmetry('-3m1', [4.913 4.913 5.504],[90,90,120]*degree,...
  'X||a*','Y||b','Z||c','mineral','Quartz')

m_1 = Miller(0,0,0,1,cs,'uvtw')
m_2 = Miller(1,1,-2,0,cs,'uvtw')
% m_3 = Miller(1,0,-1,0,cs,'uvtw')
% m_4 = Miller(1,0,-1,1,0,cs,'uvtw')
m_5 = Miller(0,0,0,1,cs,'hkil')
m_6 = Miller(1,1,-2,0,cs,'hkil')
m_7 = Miller(1,0,-1,0,cs,'hkil')
m_8 = Miller(1,0,-1,1,cs,'hkil')

figure
plot(m_1,'upper','antipodal','labeled','MarkerFaceColor','black')
hold on
plot(m_2,'upper','antipodal','labeled','MarkerFaceColor','black')
hold on
% plot(m_3,'upper','antipodal','labeled','MarkerFaceColor','black')
% hold on
```

```
% plot(m_4,'upper','antipodal','labeled','MarkerFaceColor','black')
% hold on
plot(m_5,'upper','plane','linecolor','r','linewidth',1)
hold on
plot(m_6,'upper','plane','linecolor','r','linewidth',1)
hold on
plot(m_7,'upper','plane','linecolor','r','linewidth',1)
hold on
plot(m_8,'upper','plane','linecolor','r','linewidth',1)
```

## *A.3. MATLAB script for GND analysis*

```
%%
% ************************************************************************
% MTEX Script for EBSD Data
% Script set for GND analysis
%
% ************************************************************************
% Import of Oxford/HKL *.ctf (ASCII) file
% ************************************************************************

% clear memory and close plots - for new analysis of EBSD data
clear
close all

% Specify Crystal and Specimen Symmetries
% crystal symmetry
% crystal symmetry
CS = {...
  'notIndexed',...
  crystalSymmetry('-3m1', [4.9 4.9 5.5], 'X||a*', 'Y||b', 'Z||c*', 'mineral', 'Quartz', 'color', [0.53 0.81 0.98])};

% specimen symmetry : the MTEX4 default is triclinic so do not need this line
SS = specimenSymmetry('triclinic');

% plotting convention
setMTEXpref('xAxisDirection','east'); % 'west'
setMTEXpref('zAxisDirection','intoPlane'); % 'outOfPlane'

% Specify File Names
% path to files
pname = 'C:\Users\henry\Desktop\EBSD\EBSD\AWI_3_001'
% which files to be imported
```

```
fname = [pname '\AWI_3_001.ctf'];

% Import the Data
% create an EBSD variable containing the data
ebsd = EBSD.load(fname,CS,'interface','ctf','convertEuler2SpatialReferenceFrame','wizard');

% take only those measurements with MAD (Mean Angular Deviation) smaller then 1.3
ebsd = ebsd(ebsd.mad<1)

%%
% reconstruct grains, remove all grains with less then
% 5 pixels and smooth the grain boundaries.

% reconstruct grains
[grains,ebsd.grainId] = calcGrains(ebsd,'angle',15*degree);

% remove small grains
ebsd(grains(grains.grainSize<=5)) = [];

% redo grain reconstruction
[grains,ebsd.grainId] = calcGrains(ebsd,'angle',10*degree);

% smooth grain boundaries
grains = smooth(grains,5);

hold on
plot(grains.boundary,'linewidth',1)
hold off

%%
%a key the colorizes according to misorientation angle and axis
ipfKey = axisAngleColorKey(ebsd('Quartz'));
```

```
% set the grain mean orientations as reference orinetations
ipfKey.oriRef = grains(ebsd('Quartz').grainId).meanOrientation;

% plot the orientation data
plot(ebsd('Quartz'),ipfKey.orientation2color(ebsd('Quartz').orientations),'micronBar','off','figSize','medium')

hold on
plot(grains.boundary,'linewidth',1)
hold off

%% denoise orientation data
F = halfQuadraticFilter;

ebsd = smooth(ebsd('Quartz'),F,'fill',grains);

% plot the denoised data
ipfKey.oriRef = grains(ebsd('Quartz').grainId).meanOrientation;
plot(ebsd('Quartz'),ipfKey.orientation2color(ebsd('Quartz').orientations),'micronBar','off','figSize','medium')

hold on
plot(grains.boundary,'linewidth',1)
hold off

%%GND density map
% The incomplete curvature tensor
% consider only the Quartz phase
ebsd = ebsd('Quartz').gridify;

% compute the curvature tensor
kappa = ebsd.curvature;
```

```
% kappa(2,3)
% the components of the curvature tensor
kappa12 = kappa{1,2};
size(kappa12)
newMtexFigure('nrows',3,'ncols',3);

% cycle through all components of the tensor
for i = 1:3
  for j = 1:3

    nextAxis(i,j)
    plot(ebsd,kappa{i,j},'micronBar','off')
    hold on; plot(grains.boundary,'linewidth',1); hold off

  end
end

% unify the color rage  - you may also use setColoRange equal
setColorRange([-0.005,0.005])
drawNow(gcm,'figSize','large')

%% The incomplete dislocation density tensor
alpha = kappa.dislocationDensity;
% sS=slipSystem.Quartz(Quartz_CS)
%  alpha(2,3)
% Cystallographic Dislocations
% dSbasalA = dislocationSystem.BasalA(Quartz_CS);
% dSprismA = dislocationSystem.PrismA(Quartz_CS);
% dS = [dSprismA dSbasalA]
dS = dislocationSystem.Quartz(Quartz_CS)
% size of the unit cell
a = norm(Quartz_CS.aAxis)
% in bcc and fcc the norm of the burgers vector is sqrt(3)/2*a
```

```
norm(dS().b)
%  The energy of dislocations
nu= 0.1;
% energy of the edge dislocations
dS(dS.isEdge).u = 1;
% energy of the screw dislocations
dS(dS.isScrew).u = 0.9;
% Question to verybody: what is the best way to set the enegry? I found
% different formulae
%
% E = 1 - poisson ratio
% E = c * G * |b|^2,  - G - Schubmodul / Shear Modulus Energy per (unit length)^2
%A single dislocation causes a deformation that can be represented by the rank one tensor
dS(1).tensor
%Note that the unit of this tensors is the same as the unit used for describing the
% length of the unit cell, which is in most cases Angstrom (au). Furthremore, we
% observe that the tensor is given with respect to the crystal reference frame while
% the dislocation densitiy tensors are given with respect to the specimen reference
% frame. Hence, to make them compatible we have to rotate the dislocation tensors
% into the specimen reference frame as well. This is done by
dSRot = ebsd.orientations * dS

%% Fitting dislocations to the incomplete dislocation denstiy tensor
%Now we are ready for fitting the dislocation tensors to the dislocation densitiy
% tensor in each pixel of the map. This is done by the command fitDislocationSystems.
[rho,factor] = fitDislocationSystems(kappa,dSRot);
% the restored dislocation density tensors
alpha = sum(dSRot.tensor .* rho,2);

% we have to set the unit manualy since it is not stored in rho
alpha.opt.unit = '1/um';

% the restored dislocation density tensor for pixel 2
```

```
% alpha(2)


% the dislocation density dervied from the curvature in pixel 2
% kappa(2).dislocationDensity


%we may also restore the complete curvature tensor with
kappa = alpha.curvature;
% plot it as before
newMtexFigure('nrows',3,'ncols',3);


% cycle through all components of the tensor
for i = 1:3
  for j = 1:3


    nextAxis(i,j)
    plot(ebsd,kappa{i,j},'micronBar','off')
    hold on; plot(grains.boundary,'linewidth',2); hold off


  end
end


setColorRange([-0.005,0.005])
drawNow(gcm,'figSize','large');


%% The total dislocation energy
% The unit of the densities h in our example is 1/um * 1/au where 1/um comes
% from the unit of the curvature tensor an 1/au from the unit of the Burgers
% vector. In order to transform h to SI units, i.e., 1/m^2 we have to multiply
% it with 10^16. This is exactly the values returned as the second output
% factor by the function fitDislocationSystems.
factor;


% Multiplying the densities rho with this factor and the individual energies
```

```
% of the the dislocation systems we end up with the total dislocation energy.
% Lets plot this at a logarithmic scale
close all

figure
plot(ebsd,factor*sum(abs(rho.* dSRot.u),2),'micronbar','off')
title('Total','FontSize',14)
% mtexColorMap('hot')
mtexColorbar
 set(gca,'ColorScale','log'); % this works only starting with Matlab 2018a
%  set(gca,'CLim',[10^13 10^14]);
  set(gca,'CLim',[10^9 10^15]);
 hold on
plot(grains.boundary,'linewidth',1)
hold off

figure
plot(ebsd,factor*sum(abs(rho.* dSRot.isEdge),2),'micronbar','off')
title('Edge','FontSize',14)
% mtexColorMap('hot')
mtexColorbar
 set(gca,'ColorScale','log'); % this works only starting with Matlab 2018a
%  set(gca,'CLim',[10^13 10^14]);
  set(gca,'CLim',[10^9 10^15]);
 hold on
plot(grains.boundary,'linewidth',1)
hold off

figure
plot(ebsd,factor*sum(abs(rho.* dSRot.isScrew),2),'micronbar','off')
title('Screw','FontSize',14)
% mtexColorMap('hot')
mtexColorbar
```

```
 set(gca,'ColorScale','log'); % this works only starting with Matlab 2018a
%  set(gca,'CLim',[10^13 10^14]);
  set(gca,'CLim',[10^9 10^15]);
 hold on
plot(grains.boundary,'linewidth',1)
hold off

figure
plot(ebsd,factor*sum(abs(rho(:,1:3) .* dSRot.u(:,1:3)),2),'micronbar','off')
title('Basal <a>','FontSize',14)
% mtexColorMap('hot')
mtexColorbar
 set(gca,'ColorScale','log'); % this works only starting with Matlab 2018a
%  set(gca,'CLim',[10^13 10^14]);
  set(gca,'CLim',[10^9 10^15]);
 hold on
plot(grains.boundary,'linewidth',1)
hold off

figure
plot(ebsd,factor*sum(abs(rho(:,4:6) .* dSRot.u(:,4:6)),2),'micronbar','off')
title('Prism <a>','FontSize',14)
% mtexColorMap('hot')
mtexColorbar
 set(gca,'ColorScale','log'); % this works only starting with Matlab 2018a
%  set(gca,'CLim',[10^13 10^14]);
 set(gca,'CLim',[10^9 10^15]);
hold on
plot(grains.boundary,'linewidth',1)
hold off

figure
plot(ebsd,factor*sum(abs(rho(:,7:12) .* dSRot.u(:,7:12)),2),'micronbar','off')
```

```
title('Rhomb <a>','FontSize',14)
% mtexColorMap('hot')
mtexColorbar
 set(gca,'ColorScale','log'); % this works only starting with Matlab 2018a
%  set(gca,'CLim',[10^13 10^14]);
  set(gca,'CLim',[10^9 10^15]);
hold on
plot(grains.boundary,'linewidth',1)
hold off

figure
plot(ebsd,factor*sum(abs(rho(:,13:15) .* dSRot.u(:,13:15)),2),'micronbar','off')
title('Prism [c]','FontSize',14)
% mtexColorMap('hot')
mtexColorbar
 set(gca,'ColorScale','log'); % this works only starting with Matlab 2018a
%  set(gca,'CLim',[10^13 10^14]);
  set(gca,'CLim',[10^9 10^15]);
hold on
plot(grains.boundary,'linewidth',1)
hold off

figure
plot(ebsd,factor*sum(abs(rho(:,16) .* dSRot.u(:,16)),2),'micronbar','off')
title('[c] screw','FontSize',14)
% mtexColorMap('hot')
mtexColorbar
 set(gca,'ColorScale','log'); % this works only starting with Matlab 2018a
%  set(gca,'CLim',[10^13 10^14]);
  set(gca,'CLim',[10^9 10^15]);
hold on
plot(grains.boundary,'linewidth',1)
hold off
```

```
figure
plot(ebsd,factor*sum(abs(rho(:,17:19) .* dSRot.u(:,17:19)),2),'micronbar','off')
title('<a> screw','FontSize',14)
% mtexColorMap('hot')
mtexColorbar
 set(gca,'ColorScale','log'); % this works only starting with Matlab 2018a
%  set(gca,'CLim',[10^13 10^14]);
  set(gca,'CLim',[10^9 10^15]);
hold on
plot(grains.boundary,'linewidth',1)
hold off
```

## *A.4. MATLAB script for GND analysis of selected region and summarize the ratio of the dislocation types*

```
%%
% ***************************************************************************
% MTEX Script for EBSD Data
% Script set for GND analysis of selected region
% and summarize the ratio of the dislocation types
%
% ***************************************************************************
% Import of Oxford/HKL *.ctf (ASCII) file
% ***************************************************************************

% clear memory and close plots - for new analysis of EBSD data
clear
close all

% Specify Crystal and Specimen Symmetries
% crystal symmetry
% crystal symmetry
CS = {...
  'notIndexed',...
  crystalSymmetry('-3m1', [4.9 4.9 5.5], 'X||a*', 'Y||b', 'Z||c*', 'mineral', 'Quartz', 'color', [0.53 0.81 0.98])};

% specimen symmetry : the MTEX4 default is triclinic so do not need this line
SS = specimenSymmetry('trigonal');

% plotting convention
setMTEXpref('xAxisDirection','east'); % 'west'
setMTEXpref('zAxisDirection','intoPlane'); % 'outOfPlane'

% Specify File Names
```

```
% path to files
pname = 'C:\Users\henry\Desktop\EBSD\EBSD\AWI_3_001';
% which files to be imported
fname = [pname '\AWI_3_001.ctf'];

% Import the Data
% create an EBSD variable containing the data
ebsd = EBSD.load(fname,CS,'interface','ctf','convertEuler2SpatialReferenceFrame','wizard');

% take only those measurements with MAD (Mean Angular Deviation) smaller then 1.0
ebsd = ebsd(ebsd.mad<1)

% *************************************************************************
% Calculate an ODF
% *************************************************************************
% Generate simple Crystal Symmetry variables for all phases
fprintf(' \n');
fprintf(' Crystal Symmetry (CS) : names of variables \n');
fprintf(' \n');

% phase names
Phase_names = ebsd.mineralList;

for i=1:length(CS)
% indexed point for mineral
    N_Points = length(ebsd(Phase_names(i)));
% print only indexed phases
   if((~strcmpi(Phase_names{i},'notIndexed')) && (N_Points > 0))
% retain first part of mineral name
     P_Name = strtok(char(Phase_names{i}),' ');
% make variables for CS with mineral names
     myvariable = strcat(P_Name,'_CS');
     datavalues = CS{i};
```

```
% print variable names for CS
      eval([sprintf(myvariable) ' = CS{i};'])
      fprintf(' %s %s \n','Variable name =',myvariable);
    end
end

disp(' ')
disp(' Use mineral_CS to defined your CS in m-file ')
disp(' ')

% Calculate an ODF
odf_Quartz = calcDensity(ebsd('Quartz').orientations,'halfwidth',10*degree);

% Texture index
% Jindex_Quartz = textureindex(odf_Quartz)
% Mindex_Quartz = calcMIndex(odf_Quartz)

% Create list of pole figures with hkls 100,010,001
% MTEX cannot mix hkls and uvws
% pole to planes can be specified by the option 'pole' or 'hkl'
% directions are specified by the option 'uvw'

PFs_Quartz_hkil = [ ...
    Miller(0,0,0,1,Quartz_CS,'hkil','phase','Quartz'), ...
    Miller(1,1,-2,0,Quartz_CS,'hkil','phase','Quartz'), ...
    Miller(1,0,-1,0,Quartz_CS,'hkil','phase','Quartz'), ...
    Miller(1,0,-1,1,Quartz_CS,'hkil','phase','Quartz'), ...
    Miller(0,1,-1,1,Quartz_CS,'hkil','phase','Quartz'), ...
    Miller(-1,1,0,2,Quartz_CS,'hkil','phase','Quartz'), ...
    Miller(0,1,-1,2,Quartz_CS,'hkil','phase','Quartz')]
PFs_Quartz_uvtw = [ ...
    Miller(0,0,0,1,Quartz_CS,'uvtw','phase','Quartz'),...
    Miller(1,1,-2,0,Quartz_CS,'uvtw','phase','Quartz')]
```

```
% <0001> (c-axis), <11-20> (a-axis), {10-10} (prism {m}),
% {10-11}(positive rhomb {r}), {01-11} (negative rhomb {z}),
% {10-12} (positive acute rhomb {pi}), {01-12} (negative acute rhomb {pi'})
%%
% ************************************************************************
% Grain modelling
% ************************************************************************

% set angles of low- and high-angle boundaries
% low-abgle subgrain boundary=1; high-angle grain boundary=10

% disp(' ')
% disp(' Keep non-indexed points option ')
% disp('*1= Scientifically correct, not extrapolating raw indexed data')
% disp('    model grains BUT keep non-index points : Default in MTEX 4')
% disp(' 2= May be more geologically correct in some cases, use with care')
% disp('    model grains AND include non-index points within grains boundaries')
% disp('    N.B. this option does NOT ADD map pixels with neighbouring ORIENTATIONS')
% non_indexed_option = input('Option an integer  (1-2):');
non_indexed_option = 1;

% keep non-indexed in now default in MTEX4
if(non_indexed_option == 1)
   [grains,ebsd.grainId,ebsd.mis2mean] = calcGrains(ebsd,'threshold',[2*degree,10*degree])
end

% remove non-indexed points, restrict to indexed points only
if(non_indexed_option == 2)
   [grains,ebsd.grainId,ebsd.mis2mean] =
calcGrains(ebsd('indexed'),'threshold',[2*degree,10*degree])
end
```

```
% number of grains all phases
number_of_calcGrains = grains.length

% plot 'grain' phase map
close all
figure
% Correct MatLab problem with colour buffer
set(gcf,'renderer','zbuffer')
plot(grains,'figSize','medium')

% Removing small grains - not representative small grains, may be errors
% disp(' ')
% disp(' Small grains option ')
% disp(' Remove small grains containing less than a critical')
% disp(' number of indexed points as they error prone or ')
% disp(' If you require an accurate grain size and shape analysis')
% disp(' the recommended minimum number indexed points per grain size is 10')
% disp(' You can decide to keep all grain by accepting all grains with 0')
% small_grains_option = input('Indexed points per grain an integer (e.g. 0-10):');
small_grains_option = 5;

% remove grains containing less than critical number of indexed points,
selected_grains = grains(grains.grainSize > small_grains_option);

% number of small grains removed from all phase
number_of_small_grains_removed = number_of_calcGrains - selected_grains.length

%n_Quartz_grains = selected_grains('Quartz').length
% close all
figure
% Correct MatLab problem with colour buffer
set(gcf,'renderer','zbuffer')
plot(selected_grains,'figSize','medium')
```

```
%%
% *************************************************************************
% Plot all grains and select a grain using the a curser on the phase map
% *************************************************************************

% set angles of low- and high-angle boundaries
% low-abgle subgrain boundary=1; high-angle grain boundary=10

% disp(' ')
% disp(' Keep non-indexed points option ')
% disp('*1= Scientifically correct, not extrapolating raw indexed data')
% disp('    model grains BUT keep non-index points : Default in MTEX 4')
% 1
% disp(' 2= May be more geologically correct in some cases, use with care')
% disp('    model grains AND include non-index points within grains boundaries')
% disp('    N.B. this option does NOT ADD map pixels with neighbouring ORIENTATIONS')
% non_indexed_option = input('Option an integer  (1-2):');
non_indexed_option = 1;

% keep non-indexed in now default in MTEX4
if(non_indexed_option == 1)
   [grains,ebsd.grainId,ebsd.mis2mean] = calcGrains(ebsd,'threshold',[1*degree,10*degree])
end
% remove non-indexed points, restrict to indexed points only
if(non_indexed_option == 2)
   [grains,ebsd.grainId,ebsd.mis2mean] =
calcGrains(ebsd('indexed'),'threshold',[1*degree,10*degree])
end
% number of grains all phases
number_of_calcGrains = grains.length
% plot 'grain' phase map
close all
% figure
```

```
% Correct MatLab problem with colour buffer
% set(gcf,'renderer','zbuffer')
% Default phase map
% plot(grains,'figSize','small')

% Removing small grains - not representative small grains, may be errors
close all
% disp(' ')
% disp(' Small grains option ')1
% disp(' Remove small grains containing less than a critical')
% disp(' number of indexed points as they error prone or ')
% disp(' If you require an accurate grain size and shape analysis')
% disp(' the recommended minimum number indexed points per grain size is 10')
% disp(' You can decide to keep all grain by accepting all grains with 0')
% small_grains_option = input('Indexed points per grain an integer (e.g. 0-10):');
small_grains_option = 5;

% remove grains containing less than critical number of indexed points,
selected_grains = grains(grains.grainSize > small_grains_option);
% number of small grains removed from all phase
number_of_small_grains_removed = number_of_calcGrains - selected_grains.length
%n_Quartz_grains = selected_grains('Quartz').length
figure
% Correct MatLab problem with colour buffer
set(gcf,'renderer','zbuffer')
% MTEX 4 default map is phase map
plot(selected_grains,'figSize','medium')

% selecting a single grain by x,y coordinates
disp(' ')
disp('Select grain with cursor and one mouse click')
disp(' ')
% Displays a cursor over the map and waits for one click on the selected grain
```

```
[xgg, ygg] = ginput(1)
% select single grain
%selected_single_grain = findByLocation(grains,[xgg  ygg])
selected_single_grain = selected_grains(xgg,ygg);
% grain id
grain_id = selected_single_grain.id
% grain centroid
[centroid_x,centroid_y] = centroid(selected_single_grain)

% plot selected grain : boundary and misorientation from mean orientation
close all
% subGB =
selected_single_grain.innerBoundary(selected_single_grain.innerBoundary.misorientation.angle
/degree<10,selected_single_grain.innerBoundary.misorientation.angle/degree>=2);
% plot grain boundary outline
plot(selected_single_grain.boundary,'linewidth',2,'figSize','medium')
hold on
% plot ebsd orientation pixels
plot(ebsd(selected_single_grain),ebsd(selected_single_grain).mis2mean.angle./degree,'figSize',
'small')
% plot(subGB)
% plot grain centroid
% plot(centroid_x,centroid_y,'MarkerEdgeColor','k','MarkerFaceColor','r','MarkerSize',10)
hold off
mtexColorbar
% mean orientation of selected single grain
grain_mean_orientation = selected_single_grain.meanOrientation

% plot crystallographic axes
figure
plotPDF(ebsd(selected_single_grain).orientations,PFs_Quartz_hkil,'antipodal',...
   'points','all','MarkerSize',4,'figSize','small')
```

```
figure
plotPDF(ebsd(selected_single_grain).orientations,PFs_Quartz_uvtw,'antipodal',...
    'points','all','MarkerSize',4,'figSize','small')
% bnd_Quartz=grains.boundary(selected_single_grain,'Quartz','Quartz')
% figure
% plotAxisDistribution(bnd_Quartz.misorientation,'antipodal','points','all','MarkerSize',5)

%% Subgrain boundaries in a selected single grain colorized by misorientation angle
figure
plot(ebsd(selected_single_grain));
subGB = selected_single_grain.innerBoundary(selected_single_grain.innerBoundary.misorientation.angle/degree<=10,selected_single_grain.innerBoundary.misorientation.angle/degree>=1);
hold on
% plot(subGB,'linewidth',1)
plot(subGB,subGB.misorientation.angle./degree,'linewidth',1)
mtexColorMap hot
mtexColorbar
hold off

%%
% *************************************************************************
% Select EBSD region of interest with your mouse: Rectangle region
% *************************************************************************
figure
setMTEXpref('FontSize',15)
plot(selected_single_grain,'figSize','large')
hold on
% plot grain boundaries
plot(selected_single_grain.innerBoundary(selected_single_grain.innerBoundary.misorientation.angle/degree<=4,selected_single_grain.innerBoundary.misorientation.angle/degree>=2),'linewidth',1.5,'linecolor','b','micronbar','off')
```

```
plot(selected_single_grain.innerBoundary(selected_single_grain.innerBoundary.misorientation.angle/degree<=10,selected_single_grain.innerBoundary.misorientation.angle/degree>4),'linewidth',1.5,'linecolor','r')
hold off
% selecting data points (not grains) by x,y coordinates
% Instructions for using the mouse
disp(' ')
disp('Rubberband selection rectangle region')
disp('Drag mouse from top right corner with mouse')
disp('button pressed (down), release (up) button to define botton right corner')
disp(' ')
k = waitforbuttonpress; % Wait for key press or mouse-button click
point1 = get(gca,'CurrentPoint');    % button PRESS (down) detected
finalRect = rbbox;                   % return figure units
point2 = get(gca,'CurrentPoint');    % button RELEASE (up) detected
point1 = point1(1,1:2);              % extract x
point2 = point2(1,1:2);              %     and y
p1 = min(point1,point2);             % calculate locations
offset = abs(point1-point2);         % and dimensions
% EBSD map subregion
xy_subregion(1,:) = [p1(1) p1(1)+offset(1) p1(1)+offset(1) p1(1) p1(1)];
xy_subregion(2,:) = [p1(2) p1(2) p1(2)+offset(2) p1(2)+offset(2) p1(2)];
hold on
axis manual

% region = rectangle, N.B. transpose of xy_subregion
region = xy_subregion';

% draw selection rectangle
plot(region(:,1),region(:,2),'r--','linewidth',2)
hold off

% select region of rectangle with condition
```

```
condition = inpolygon(ebsd,region);

% select EBSD data within region and printout to command window
ebsd_subregion = ebsd(condition);
%%
% **************************************************************************
% Select EBSD region of interest with your mouse: Polygonal region1
% **************************************************************************

[selected_single_grain1,ebsd_subregion.grainId,ebsd_subregion.mis2mean]=calcGrains(ebsd_subregion('Indexed'),'threshold',[1*degree,10*degree])
% plot the ebsd data (IPF)
plot(selected_single_grain1)
hold on
% plot grain boundaries
plot(selected_single_grain1.boundary,'linewidth',2,'linecolor','k')
%
plot(selected_single_grain1.innerBoundary(selected_single_grain1.innerBoundary.misorientation.angle/degree<=4,selected_single_grain1.innerBoundary.misorientation.angle/degree>=2),'linewidth',1.5,'linecolor','b','micronbar','off')
%
plot(selected_single_grain1.innerBoundary(selected_single_grain1.innerBoundary.misorientation.angle/degree<=10,selected_single_grain1.innerBoundary.misorientation.angle/degree>4),'linewidth',1.5,'linecolor','r')
plot(selected_single_grain1.innerBoundary,selected_single_grain1.innerBoundary.misorientation.angle./degree,'linewidth',2)
mtexColorMap hot
mtexColorbar
hold off
% selecting data points (not grains) by x,y coordinates
% Instructions for using the mouse
disp(' ')
disp('Define selected region of map using the curse and mouse')
```

```
disp('The last point does not need to exactly the first point')
disp('as the program ensures the polygon is closed')
disp('Left mouse button picks points')
disp('Right mouse button picks last point somewhere near the first point')
disp(' ')
region1 = selectPolygon;

% select region of polygon with condition

condition1 = inpolygon(ebsd,region1);

% select EBSD data within region and printout to command window
ebsd_subregion1 = ebsd(condition1)

% plot whole EBSD Orientation map with region of interest marked in red
% figure
plot(ebsd_subregion);
hold on
% plot grain boundaries
plot(selected_single_grain1.boundary,'linewidth',2,'linecolor','k')
%
plot(selected_single_grain1.innerBoundary(selected_single_grain1.innerBoundary.misorientation.angle/degree<=4,selected_single_grain1.innerBoundary.misorientation.angle/degree>=2),'linewidth',1.5,'linecolor','b','micronbar','off')
%
plot(selected_single_grain1.innerBoundary(selected_single_grain1.innerBoundary.misorientation.angle/degree<=10,selected_single_grain1.innerBoundary.misorientation.angle/degree>4),'linewidth',1.5,'linecolor','r')

plot(region1(:,1),region1(:,2),'r--','linewidth',2)
hold off
ebsd1=ebsd_subregion1;
```

```
%% a key the colorizes according to misorientation angle and axis
ipfKey = axisAngleColorKey(ebsd1('Quartz'));

% set the grain mean orientations as reference orinetations
ipfKey.oriRef = grains(ebsd1('Quartz').grainId).meanOrientation;

% plot the data
plot(ebsd1('Quartz'),ipfKey.orientation2color(ebsd1('Quartz').orientations),'micronBar','off','figSi
ze','medium')

% hold on
% plot(grains.boundary,'linewidth',2)
% hold off

%% denoise orientation data
F = halfQuadraticFilter;

ebsd1 = smooth(ebsd1('Quartz'),F,'fill',grains);

% plot the denoised data
ipfKey.oriRef = grains(ebsd1('Quartz').grainId).meanOrientation;
plot(ebsd1('Quartz'),ipfKey.orientation2color(ebsd1('Quartz').orientations),'micronBar','off','figSi
ze','medium')

% hold on
% plot(grains.boundary,'linewidth',2)
% hold off
%% GND density map
% The incomplete curvature tensor
% consider only the Quartz(alpha) phase
ebsd1=ebsd1('Quartz').gridify;
%compute the curvature
```

```
kappa = ebsd1.curvature;
% kappa(2,3)
% the components of the curvature tensor
kappa12 = kappa{1,2};
size(kappa12)
newMtexFigure('nrows',3,'ncols',3);
% cycle through all components of the tensor
for i = 1:3
  for j = 1:3


    nextAxis(i,j)
    plot(ebsd1,kappa{i,j},'micronBar','off')
%      hold on; plot(grains.boundary,'linewidth',2); hold off
  end
end

%unify the color rage - you may also use set ColoRange equal
setColorRange([-0.005,0.005])
drawNow(gcm,'figSize','large')

%% The incomplete dislocation density tensor
alpha = kappa.dislocationDensity;
% sS=slipSystem.Quartz(Quartz_CS)
%  alpha(2,3)
% Cystallographic Dislocations
% dSbasalA = dislocationSystem.BasalA(Quartz_CS);
% dSprismA = dislocationSystem.PrismA(Quartz_CS);
% dS = [dSprismA dSbasalA]
dS = dislocationSystem.Quartz(Quartz_CS)
% size of the unit cell
a = norm(Quartz_CS.aAxis)
% in bcc and fcc the norm of the burgers vector is sqrt(3)/2*a
norm(dS().b)
```

```
% The energy of dislocations
nu= 0.1;
% energy of the edge dislocations
dS(dS.isEdge).u = 1;
% energy of the screw dislocations
dS(dS.isScrew).u = 0.9;
% Question to verybody: what is the best way to set the enegry? I found
% different formulae
%
% E = 1 - poisson ratio
% E = c * G * |b|^2,  - G - Schubmodul / Shear Modulus Energy per (unit length)^2
%A single dislocation causes a deformation that can be represented by the rank one tensor
dS(1).tensor
%Note that the unit of this tensors is the same as the unit used for describing the
% length of the unit cell, which is in most cases Angstrom (au). Furthremore, we
% observe that the tensor is given with respect to the crystal reference frame while
% the dislocation densitiy tensors are given with respect to the specimen reference
% frame. Hence, to make them compatible we have to rotate the dislocation tensors
% into the specimen reference frame as well. This is done by
dSRot = ebsd1.orientations * dS
%% Fitting dislocations to the incomplete dislocation denstiy tensor
%Now we are ready for fitting the dislocation tensors to the dislocation densitiy
% tensor in each pixel of the map. This is done by the command fitDislocationSystems.
[rho,factor] = fitDislocationSystems(kappa,dSRot);
% the restored dislocation density tensors
alpha = sum(dSRot.tensor .* rho,2);

% we have to set the unit manualy since it is not stored in rho
alpha.opt.unit = '1/um';

% the restored dislocation density tensor for pixel 2
% alpha(2)
```

```
% the dislocation density dervied from the curvature in pixel 2
% kappa(2).dislocationDensity


%we may also restore the complete curvature tensor with
kappa = alpha.curvature;
% plot it as before
newMtexFigure('nrows',3,'ncols',3);


% cycle through all components of the tensor
for i = 1:3
  for j = 1:3


    nextAxis(i,j)
    plot(ebsd1,kappa{i,j},'micronBar','off')
%     hold on; plot(grains.boundary,'linewidth',2); hold off


  end
end


setColorRange([-0.005,0.005])
drawNow(gcm,'figSize','large');


%% The total dislocation energy
% The unit of the densities h in our example is 1/um * 1/au where 1/um comes
% from the unit of the curvature tensor an 1/au from the unit of the Burgers
% vector. In order to transform h to SI units, i.e., 1/m^2 we have to multiply
% it with 10^16. This is exactly the values returned as the second output
% factor by the function fitDislocationSystems.
factor;


% Multiplying the densities rho with this factor and the individual energies
% of the the dislocation systems we end up with the total dislocation energy.
% Lets plot this at a logarithmic scale
```

```
close all

figure
plot(ebsd1,factor*sum(abs(rho.* dSRot.u),2),'micronbar','off')
title('Total','FontSize',14)
% mtexColorMap('hot')
mtexColorbar
 set(gca,'ColorScale','log'); % this works only starting with Matlab 2018a
%  set(gca,'CLim',[10^13 10^14]);
  set(gca,'CLim',[10^9 10^15]);
 hold on
plot(selected_single_grain1.innerBoundary,'linewidth',1)
%
text(selected_single_grain1.innerBoundary.midPoint(:,1),selected_single_grain1.innerBoundary.
midPoint(:,2),sprintfc(' %d',Mangle))
hold off

figure
plot(ebsd1,factor*sum(abs(rho.* dSRot.isEdge),2),'micronbar','off')
title('Edge','FontSize',14)
% mtexColorMap('hot')
mtexColorbar
 set(gca,'ColorScale','log'); % this works only starting with Matlab 2018a
%  set(gca,'CLim',[10^13 10^14]);
  set(gca,'CLim',[10^9 10^15]);
%  hold on
% plot(grains.boundary,'linewidth',1)
% hold off

figure
plot(ebsd1,factor*sum(abs(rho.* dSRot.isScrew),2),'micronbar','off')
title('Screw','FontSize',14)
% mtexColorMap('hot')
```

```
mtexColorbar
 set(gca,'ColorScale','log'); % this works only starting with Matlab 2018a
%  set(gca,'CLim',[10^13 10^14]);
  set(gca,'CLim',[10^9 10^15]);
%  hold on
% plot(grains.boundary,'linewidth',1)
% hold off

figure
plot(ebsd1,factor*sum(abs(rho(:,1:3) .* dSRot.u(:,1:3)),2),'micronbar','off')
title('Basal <a>','FontSize',14)
% mtexColorMap('hot')
mtexColorbar
 set(gca,'ColorScale','log'); % this works only starting with Matlab 2018a
%  set(gca,'CLim',[10^13 10^14]);
  set(gca,'CLim',[10^9 10^15]);
%  hold on
% plot(grains.boundary,'linewidth',1)
% hold off

figure
plot(ebsd1,factor*sum(abs(rho(:,4:6) .* dSRot.u(:,4:6)),2),'micronbar','off')
title('Prism <a>','FontSize',14)
% mtexColorMap('hot')
mtexColorbar
 set(gca,'ColorScale','log'); % this works only starting with Matlab 2018a
%  set(gca,'CLim',[10^13 10^14]);
 set(gca,'CLim',[10^9 10^15]);
% hold on
% plot(grains.boundary,'linewidth',1)
% hold off

figure
```

```
plot(ebsd1,factor*sum(abs(rho(:,7:12) .* dSRot.u(:,7:12)),2),'micronbar','off')
title('Rhomb <a>','FontSize',14)
% mtexColorMap('hot')
mtexColorbar
 set(gca,'ColorScale','log'); % this works only starting with Matlab 2018a
%  set(gca,'CLim',[10^13 10^14]);
  set(gca,'CLim',[10^9 10^15]);
% hold on
% plot(grains.boundary,'linewidth',1)
% hold off

figure
plot(ebsd1,factor*sum(abs(rho(:,13:15) .* dSRot.u(:,13:15)),2),'micronbar','off')
title('Prism [c]','FontSize',14)
% mtexColorMap('hot')
mtexColorbar
 set(gca,'ColorScale','log'); % this works only starting with Matlab 2018a
%  set(gca,'CLim',[10^13 10^14]);
  set(gca,'CLim',[10^9 10^15]);
% hold on
% plot(grains.boundary,'linewidth',1)
% hold off

figure
plot(ebsd1,factor*sum(abs(rho(:,16) .* dSRot.u(:,16)),2),'micronbar','off')
title('[c] screw','FontSize',14)
% mtexColorMap('hot')
mtexColorbar
 set(gca,'ColorScale','log'); % this works only starting with Matlab 2018a
%  set(gca,'CLim',[10^13 10^14]);
  set(gca,'CLim',[10^9 10^15]);
% hold on
% plot(grains.boundary,'linewidth',1)
```

```
% hold off


figure
plot(ebsd1,factor*sum(abs(rho(:,17:19) .* dSRot.u(:,17:19)),2),'micronbar','off')
title('<a> screw','FontSize',14)
% mtexColorMap('hot')
mtexColorbar
 set(gca,'ColorScale','log'); % this works only starting with Matlab 2018a
%  set(gca,'CLim',[10^13 10^14]);
  set(gca,'CLim',[10^9 10^15]);
% hold on
% plot(grains.boundary,'linewidth',1)
% hold off



%% Summarize the GNDs ratio of different dislocation types in seleted region
rho=abs(rho);
% NaN=0
rho(isnan(rho))=0;
rhores=sum(rho.*dSRot.u);
% res summarize the 19 dislocation types (1*19)
res=sum(rhores,1)
%res normalization
nomalize=res./sum(res);
% summarize the 19 dislocation types into 6 families
Resratio=[sum(nomalize(:,1:3)),sum(nomalize(:,4:6)),sum(nomalize(:,7:12)),sum(nomalize(:,13:15)
),nomalize(:,16),sum(nomalize(:,17:19))]
```